Testing of different resistivity investigation methods for mapping permafrost

Syed Shakir Gilani

Master thesis in Geosciences
Discipline: Geo-hazards and Geo-Mechanics
60 Credits

Department of Geosciences
Faculty of Mathematics and Natural Sciences

UNIVERSITY OF OSLO

June, 2021

Supervisors: Sara Bazin, Bernd Etzelmüller

ABSTRACT

The following thesis is the study of permafrost while using different resistivity techniques. The main purpose of this project is to compare the resistivity models from ERT and CCR techniques and to evaluate the resolution, penetration depth and some geomorphological features in resistivity models that obtained from later techniques. The field work was conducted on UNIS East site and Adventdalen site at Svalbard.

CCR survey is performed by using OhmMapper device. The Ohm-Mapper can measure resistivity of ground that has high value of resistivity such as permafrost ground. The Ohm-Mapper is a device that can be pulled over the surface of the ground and can provide continuous resistivity profiling. After getting the profiles we can interpret the CCR data in term of thawed zone. Two types of acquisition were tested, 2-D as simple survey and 3-D as map survey. The 2-D profiling was carried out by several passages and successively increasing the distance between the dipoles. Depth of active layer was measured manually, in July 2019, during OhmMapper survey and the maximum depth was recorded as 60 cm for UNIS East site.

A map survey was also carried out by walking with the OhmMapper streamer along parallel lines separated by 5 m. 2-D and 3-D datasets are processed with Res2DInv and Res3DInv software, respectively.

DEM of the Adventdalen site is investigated with ArcMap software. The shading effect in topography reveals elongated geological features which are ice wedges.

Electrical resistivity tomography (ERT) is very effective in mapping frozen soils due to the strong resistivity contrast between ice and water. Traditional ERT surveys are conducted by using Terrameter instrument (method based on electrodes planted in the ground). The resistivity model obtained from Terrameter is also processed with Res2DInv software. Depth of active layer was measured in September 2017 during Terrameter survey and the average depth value was recorded as 79 cm.

CCR surveying is a suitable tool for the mapping the active layer thickness. The CCR method is flexible (2-D and 3-D acquisition modes) and relatively easy to deploy. The CCR method overcomes the problem of electrical coupling between the ground and the electrodes, which is a challenge in cold and resistive environments. This method is useful for the monitoring of climate changes by regular mapping of the active layer in permafrost area. CCR method is rapid in terms of data acquisition. ERT method has an advantage over CCR method in terms of larger depth of investigation and higher signal quality.

ACKNOWLEDGEMENTS

First, I need to thank the person who made this entire project possible, my supervisor, Dr Sara Bazin. Thank you for giving me this incredible opportunity and showing your trust on me while in the entire period of research. I would appreciate your patience and the way you always treated me. You introduced me to the fascinating world of permafrost, and gave me the chance to work at the most beautiful field site in the world. You gave me the means to design my own project, where anything I wanted to do was possible.

I also would like to thank my co-supervisor, Professor Bernd Etzelmüller, for his scientific expertise regarding permafrost. You always support me and encourage me and by your kind supervision, finally, I have achieved this milestone. You are true mentor for me.

Thank you to NGI to provide me this valuable and interesting topic for research in my master thesis.

I must thank all those who have helped me in the field and at UNIS, specially, Graham Gilbert. Thank you for providing me all related data from UNIS, whenever, I needed for my thesis project. I would like to thank my friend Saad ullah Nisar for the encouragement to apply for master's degree from UiO.

I am positive that no other graduate student has ever experienced luxury accommodation like I did while staying out at Longyearbyen, Svalbard. Thank you Sara Bazin for accommodating all of my needs throughout my thesis.

I also need to thank all the good people at the department of Geoscience for the moral support needed during the thesis, especially the IT guys.

Ali Wajdan, Waqas Iftikhar and Asad bin asif, there is no way I would have done any of this, if not for your constant source of support. Words cannot describe what yours friendship means to me.

Finally, thank you to my parents and family who have sent me love and support from the other side of the world over the past two and a half years. Your love means the world to me.

Table of Contents

List of Figures

List of tables

1. Introduction

The ground that remains at or below 0° C for at least two consecutive years is permafrost or frozen ground. Permafrost is a material of lithosphere and it is invisible as we cannot see it from the ground surface. It is a thermal phenomenon of subsurface, but some processes related to the water or ice can transform permafrost sites into very different landscapes (Oswald, 2009).

Recent studies has shown that 25% of the terrestrial area of the Earth is underlain by permafrost that includes Mountains, Arctic and Antarctic areas (French, 2007). There is a rough estimate that almost 5 to 8 million people are living in periglacial environment (French, 2007). Most of the permafrost is on the northern latitude and is present in different extent, it can be divided as continuous, discontinuous, isolated and sporadic, and totally depend on the thermal condition of the area (Cohen, 2013). Most of the areas of mountain in Norway have permafrost in their subsurface (Reusch, 1901).

Due to drastic change in climate, studies on permafrost are getting more attention because increase in temperature can degrade permafrost. The warming and degradation of permafrost can cause slope destabilization, structure failure, and release of greenhouse gas e.g. methane (Christensen et al. 2004) and can also trigger other thermal based disturbances such as melting of ground ice (Kneisel et al. 2007). Slope instability also depends on the subsurface material properties like porosity, crack size and orientation, hydraulic properties, presence of water or air in the pores and quantity of unfrozen water (Arenson et al. 2003).

It has been observed that the temperature of permafrost has increased in the last 20-30 years especially in Arctic lowlands (Romanovsky et al. 2010) and the data collected from boreholes in both hemispheres proved that there has been an increase in permafrost temperature range between 0.5-2° C during last two decades (Brown and Romanovsky, 2008).

The distribution and evolution of permafrost is sensitive to the climate condition. In mountain areas, the spatial heterogeneity of permafrost is due to the variability of ground thermal regimes that is dependent on many factors such as topography, ground surface characteristics and snow cover (Isaksen et al. 2011). In mountain areas, where people are living, it is essential to determine the location and extent of permafrost for engineering and construction reasons (Hauck et al. 2004).

There are different techniques, direct and indirect observation techniques that are used to monitor permafrost. Direct observation such as borehole monitoring, is popular as it is based on thermal measurement of the study area. Borehole monitoring, in remotely areas of mountain, is very expensive and it is site specific. So other observation techniques such as indirect observation techniques, like geophysical methods, are also applied to determine the condition and extent of permafrost (Hauck et al. 2004).

Geophysical methods or indirect observation techniques have more several advantages over direct observation methods. Geophysical investigations are non-invasive, economical and suitable for permafrost sites for determining the properties especially the composition of the subsurface material. Geophysical measurements do not affect the processes, composition and structures of the subsurface, which makes it more efficient methods for monitoring (Hilbich et al. 2008).

The geophysical method that is potentially more suitable and effective in permafrost long term monitoring is Electrical Resistivity Tomography (ERT) (Hauck, 2002) but other geophysical techniques such as Ground Penetration Radar (GPR) and Refraction Seismic Tomography are also studied on rock glaciers (Maurer and Hauck, 2007).

It is better to use a combination of different geophysical techniques to avoid ambiguities and to get reliable and more accurate results for interpretation (Vonder Mühll et al. 2002). For mountain permafrost monitoring, the most efficient and effective combination of geophysical techniques are ERT and Seismic refraction (Kneisel et al. 2008). ERT and Capacitively Coupled Resistivity (CCR) measure resistivity in subsurface materials. These techniques can detect and differentiate between frozen and unfrozen content present in ground. The frozen materials behave as electrically insulator and will have more resistivity.

The main objective of this thesis is to detect, to characterize and to map permafrost areas using OhmMapper. It works on a principle called Capacitively Coupled Resistivity (CCR) (Chen, 2020). After processing and interpretation of data from the OhmMapper, comparison is conducted with Terrameter's resistivity profiles. We used the OhmMapper for the first time in Svalbard during this geophysical investigation.

This instrument consists of a streamer that can be pulled over the ground surface and can acquire continuous resistivity profiling. After the survey, one can process and interpret the data collected in a permafrost area by differentiating frozen and unfrozen ground. The OhmMapper should be optimum to measure high resistivity of frozen ground as frozen materials have high resistivity values, which are challenging for methods using electrodes to transmit current into the ground, such as the Terrameter (Calvert, 2002).

The goal of this thesis is to get ground profiling that will elaborate the underground conditions of permafrost.

2. Theoretical background

2.1. Permafrost

Permafrost is an important topic in the field of geoscience and many papers and researches have been published and discussed about the impact of warming on permafrost due to climate change. S.W. Muller, a professor of geology from Stanford University, was the first person who came with the term "Permafrost" after world war II (French, 2007). Permafrost can be defined while considering the one physical parameter i.e. temperature. As the ground that maintains temperature of 0^{o} C or less for continuous two years. According to (French, 2007), there is possibility of unfrozen water in permafrost due to presence of salts that can decrease the freezing point of water. Therefore, it is not necessary that all permafrost is maintained frozen. There is a relation of moisture (solid/liquid) with the permafrost, so any substance in ground that is frozen for consecutive two years is part of permafrost (French, 2007). Freezing processes of ice is highly dependent on the indigenous material. The other factors that can also affect the freezing processes are: soil properties, heat conductivity, moisture content, grain size and nature of salt in water content (French, 2007).

The largest extent of permafrost is in Russia, Canada is on second rank and China is on third. Permafrost is also present in Scandinavia, European Alps, Antarctica and other parts of United States (French, 2007). The factor that controls the distribution and extent of the permafrost in any areas is mainly climate condition. The availability of permafrost in an area purely depends on altitude, air temperature, incoming solar radiation and ground and subsurface properties such as composition of active layer, properties of unconsolidated sediments (Kneisel et al. 2008). But there are other in situ factors such as vegetation, thickness of snow cover, thermal conductivity, topography of area, aspect and water bodies (French, 2007).

A permafrost layer consists of three different sections that can be separated by considering the temperature gradient with depth. The top most layer is called the "active layer" or supra permafrost layer and it is seasonal frozen layer of the ground. The middle layer is the permafrost table, below which is located the permafrost (French, 2007). Permafrost thickness can vary from few centimeters to hundreds of meters (French, 2007).

Up to 25% of land area in Northern hemisphere is underlain by permafrost (French, 2007). Distribution of permafrost is classified into three major areas; continuous permafrost area (>90%), discontinuous permafrost area (50-90%), sporadic permafrost area (10-50%). In continuous permafrost area, it is present everywhere except at the unfrozen sites of that area. In discontinuous permafrost zone, bodies of frozen ground are separated with bodies of unfrozen ground. In sporadic permafrost zone, frozen ground is scattered with irregular pattern (French, 2007). The percentages that is mentioned earlier are the quantity of permafrost in ground surface (French and Slaymaker, 2011).

Source: International Permafrost Association, 1998.
Circumpolar Active-Layer Permafrost System (CAPS), version 1.0.

Figure 2.1: *Map of permafrost: Dark purple shade indicates higher percentages of permanently frozen ground. (Figure from* **https://nsidc.org/cryosphere/sotc/permafrost.html***).*

Important studies on permafrost in the northern polar hemisphere were published during the International Polar Year (IPY) (Christiansen et al. 2010). More than 500 boreholes were identified in different countries such as North America, Russia and Nordic areas, are still being monitored under the project of IPY (Romanovsky et al. 2010). Various studies under IPY project revealed that in continuous permafrost zone the mean annual ground temperature (MAGT) has a range from -1° C to -15° C. Warming in permafrost has been observed in last three decades and still it is continued (Romanovsky et al. 2010). In northern hemisphere, due to the presence of land and sea, the ocean currents are influencing the distribution of energy and meteorological scheme and also responsible to influence the distribution of permafrost (Romanovsky et al. 2010).

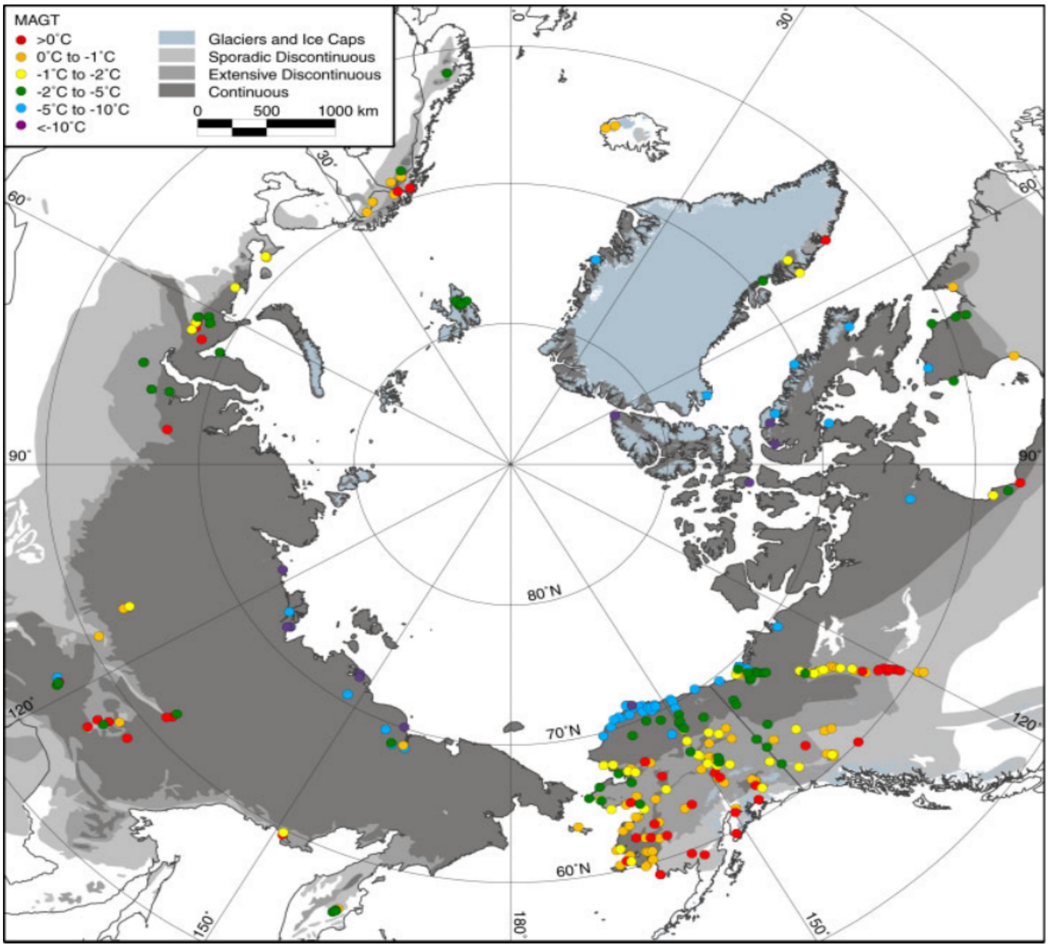

Figure 2.2: *Map is showing mean annual ground temperature (MAGT) of the Arctic and the points are representing bore holes where temperature is taken at a depth of zero. (Figure from IPY 2007-2009; from (Romanovsky et al. 2010)).*

Canada, Russia and some areas of Alaska have continental climates and their permafrost is of the continuous type. Scandinavia and some areas in southern part of Alaska have oceanic climate and are occupied with discontinuous permafrost zone (Romanovsky et al. 2010).

There are many factors that can influence the thermal regime of ground at a permafrost site. Relief is an important factor, as it can change direction of the incoming solar radiation on the ground. As a consequence, the thermal properties of ground can change (French, 2007). The rock type can change the albedo and thermal conductivity of ground, especially in continuous permafrost areas (French, 2007). Another factor is vegetation, which behaves as an insulator on the surface of ground and shield the ground from incoming solar radiation. Snow cover is also one factor that insulates the permafrost site (French, 2007).

Climate change due to global warming cause permafrost degradation and the consequences will be destabilization of slopes, construction failures and other thermal related hazards like melting of ground ice (Haeberli and Beniston 1998, Kååb et al. 2007). Frequent rock slides due to slope instability as seen in high Alpine areas, can disturb the infrastructure where people live (Gruber et al. 2004). The other problem associated with permafrost degradation is the release of greenhouse gas such as methane has observed in the arctic peat land (Christensen et al. 2004). These problems are considered to be related with the warming and degradation of permafrost.

In lowland areas of Periglacial landscapes underlain by continuous permafrost, the most frequent available feature is wedge (Dionne 1996, French and Williams 2007). These are resistive features and usually form in cold and dry environments with mean annual temperature below -5° C to -6°C (Sørbel and Tolgensbakk, 2002). Variety of features such as ice wedges, soil wedges or composite wedges are formed by filling of cracks produced by thermal contraction. Those cracks are controlled by the near surface condition and are filled with snow, ice, particles of different minerals and organic materials (Murton, 2007). It has also been observed that cracking due to thermal contraction in perennially frozen ground can produce polygon structures (Murton, 2013). There is a seasonal cycle of development of ice wedge polygons that are controlled by three main processes (figure 2.3). The first step is, frost heave and thaw settlement. The second step is, thermal expansion of thaw layer in summer. The last step in development of ice wedge is, thermal contraction of frozen layer in winter (Matsuoka et al. 2018).

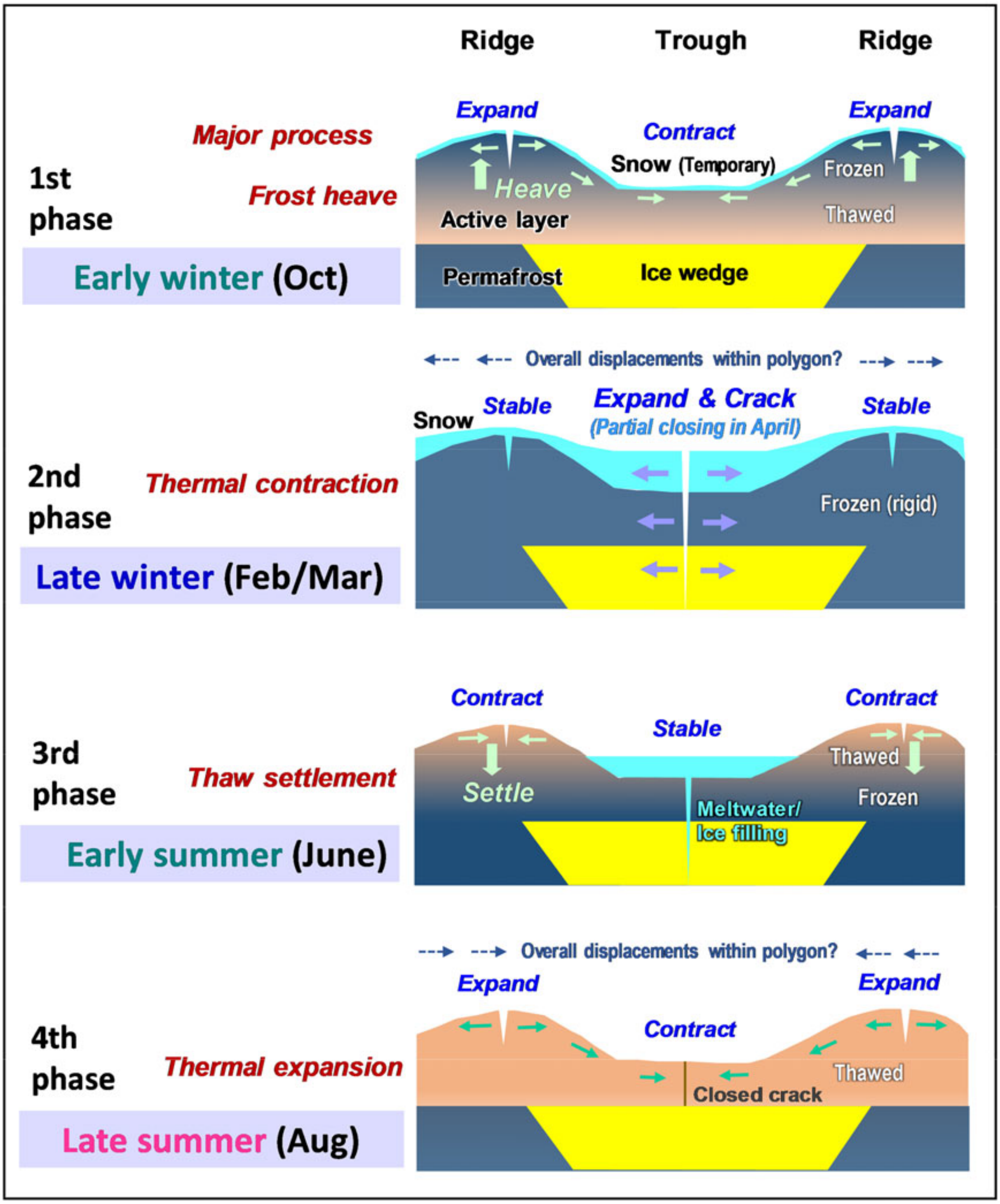

Figure 2.3: *Annual cycle of development of an ice wedge with margins of trough and ridge. The arrows are not showing any kind of magnitude of cracking or expansion, but these arrows are showing the movement. Figure from (Matsuoka et al. 2018).*

There are two main methods that are often used in the field. One is direct method and other is an indirect method. We usually use these methods to characterize permafrost spatially (Hauck et al. 2004). In direct method such as borehole monitoring, one collects data and samples and tests these samples in laboratory. In indirect investigations such as geophysical observation techniques, one uses different instruments such as the Terrameter or the OhmMapper on site for data acquisition. Geophysical investigations are more efficient and suitable for monitoring of permafrost due to several reasons, such as, they are easy to handle due to light weight, they even can be used in harsh environment, the instruments are portable and easy to operate. Finally, tomographic inversion of geophysical datasets can be obtained in 2 dimensional (2-D) or 3-dimensional (3-D) as representation of heterogeneous subsurface structures (Hauck, Isaksen et al. 2004). Geophysical methods also have a positive edge on direct method because of the cost effectiveness, suitability on permafrost ground as it does not affect the processes, characteristics and structure of the ground as well as the non-invasive nature (Hilbich, Hauck et al. 2008). Geophysical investigations are also popular for covering large vertical sections (2-D) or volumes (3-D) of the subsurface, which is not possible with direct method. It is also possible to repeat geophysical surveys for monitoring in the field (Hilbich, 2009).

Borehole monitoring, in remote areas in mountain is an expensive technique, that can be used to determine the extent and the type of permafrost (Hauck et al. 2004). The combination of direct and indirect methods are useful while monitoring permafrost. Application of geophysical techniques were started to solve the problems related to permafrost few decades ago (King et al. 1988), so, geophysical techniques are now widely used for detection, characterization, and mapping of mountain permafrost (Hauck and Kneisel, 2008). A detailed study of geophysics on permafrost has been published by (Scott et al. 1990). Comprehensive reports on the application of different geophysical techniques applied on specific engineering aspects in polar permafrost are provided by (Ingeman-Nielsen 2006, Yoshikawa et al. 2006). First attempt of tomographic inversion method for the detection, mapping and characterization of permafrost was given by (Hauck, 2001). An evaluation report on applicability of different geophysical techniques such as Electrical resistivity tomography (ERT), ground penetration radar (GPR), refraction seismic tomography (RST) for the use on rock glaciers was presented by (Maurer and Hauck, 2007). Applicability of ERT were studied on different features of land such as rock glaciers, scree slopes, etc. by (Kneisel 2004, Kneisel 2006). Electromagnetic induction method was used to measure deep sounding to determine the base of permafrost (Hauck, 2001).

2.2. Geophysical investigations

Geophysical research is only the key to provide the methods that can be helpful to determine the permafrost distribution and to describe the characterization of permafrost terrain (Mühll et al. 2001). The main theme of geophysical investigations is to find out the internal features by use of sounding techniques, to develop the optimum and ideal method to map permafrost and to establish the conditions for long term observation of permafrost to find out changes due to variation in climate (Mühll et al. 2001). Combination of different geophysical methods are useful to avoid ambiguities during interpretation of results, as the subsurface is complex and heterogeneous in nature (Maurer and Hauck, 2007). The best combination, among different geophysical methods for mountain permafrost monitoring is, considered so far to be ERT and refraction seismic (Kneisel et al. 2008).

2.2.1. Electrical Resistivity Tomography (ERT)

ERT monitoring for permafrost was first introduced by (Hauck, 2002). ERT is suitable for permafrost monitoring due to high sensitivity towards the unfrozen water content (Fortier et al. 1994). Resistivity contrast is large between frozen water (ice) and unfrozen water and it is small between insulating materials such as ice, air and some rocks, because all of them are electrically insulators. ERT is widely used to detect the ice content in ground of different layers of moraine and in rock glaciers. (Hauck and Kneisel, 2006). The values of apparent resistivity obtained from ERT is higher for areas that contain more ice content in the ground and less resistivity for low ice content in the ground. The apparent resistivity differences between freezing and non-freezing areas elaborates the distribution of ground ice (You et al. 2013). ERT is also used to investigate the structure of permafrost and its depth. It can also be used to detect the depth of the permafrost base and to identify the properties of the ground ice and to mark the variation in permafrost due to climate change (You et al. 2013).

Resistivity surveys are normally performed by injecting direct current in to the ground through two current electrodes while two potential electrodes are used to measure the voltage difference at the ground surface. The material in the subsurface resists the flow of current and is characterized by electrical resistivity. So, the main purpose of the survey is to determine and measure the resistivity distribution in subsurface.

$$\rho a = K\frac{\Delta V}{I}$$

In this formula, “K” is the geometric factor, it depends on the position of the four electrodes. “ρa” is the apparent resistivity of the subsurface and it is calculated as if the subsurface is a homogeneous half space. It is not the true resistivity of the subsurface when the subsurface is heterogeneous. The resistivity distribution can be derived from the apparent resistivity by using inversion methods. By increasing the distance between the current electrodes, one can increase the penetration depth and obtain deeper information on the subsurface (Hauck and Kneisel, 2008).

With resistivity surveys one can get information about the distribution of resistivity in subsurface which convey understanding about the material composition in subsurface. The resistivity value of any material depends on its water content, its porosity structure, its temperature and the chemical properties of water inside the pores (Hauck and Kneisel, 2008). But the main component that is responsible for varying resistivity value is water content. Resistivity value for frozen ground has a wide range between 1 and 5 kΩ.m to several hundred kΩ (Hoekstra 1973, Haeberli and Vonder Mühll 1996, Kneisel and Kääb 2007).

Most of the time in 20th Century, VES (Vertical Electrical Sounding) was dominantly used as resistivity method. The main three reason behind usage in whole world was geotechnical investigations, groundwater explorations and to explore the minerals. VES is performed using either the Wenner electrode configuration or using the Schlumberger electrode configuration. (The more common method is Schlumberger method that was used for exploration of minerals and groundwater and for this method we need less labor for installation). The main advantage of VES is that it is easy to operate and get better results, especially, when specific criteria related to survey is fulfilled. There are few limitations that is associated with the VES method. To interpret the data of VES, accurately, there should be some points that are under consideration such as, each layer in the subsurface should be homogeneous in terms of electrical resistivity and the geological layering in the ground should be horizontal with fixed thickness over the surveyed area. So, this method is not applicable everywhere in the field as the nature is not homogeneous.

It is assumed that, for interpretation the one-dimensional data obtained from the survey, the resistivity changes should be along the depth of the subsurface not along the horizontally. The survey geometry to measure lateral changes in resistivity is the Wenner array. All four electrodes have a fixed distance and are moved simultaneously for each reading. Advancements in technology of instruments and development of inversion methods have indeed made two dimensional (2-D) resistivity investigations more feasible and suitable for the study of permafrost (Kneisel et al. 2000, Marescot et al. 2003).

In ERT, there are three main geometries for measurements: Wenner, Wenner-Schlumberger and dipole-dipole arrays as shown in figure 2.4.

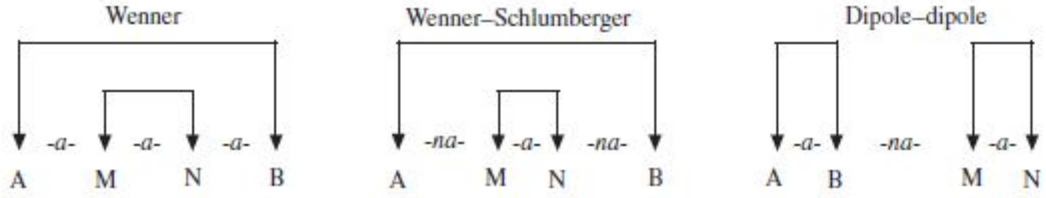

Figure 2.4: *Schematics of the most commonly used array geometries in ERT where "A, B" and "M, N" are the current and potential electrodes, respectively. The spacing between electrodes are mentioned as "a" (Hauck and Kneisel, 2008).*

In Wenner survey, the spacing between potential electrodes will increase as the spacing between current electrode increases with equal distance for all of four electrodes for each measurement. Wenner configuration has a good resolution along horizontal features that changes with depth and has medium investigation depth but completion time for survey is shorter with less information of the subsurface (Hauck and Kneisel, 2008).

Wenner-Schlumberger array is the combination of Wenner and Schlumberger array with constant spacing of potential electrodes but spacing between the current electrodes increases to get the better resolution along depth. This configuration is better for horizontal and vertical geomorphological features (Hauck and Kneisel, 2008). In dipole-dipole array configuration, the arrangements of current electrodes make two dipole on one side and two dipoles of potential electrodes on other side (Hauck and Kneisel, 2008). The spacing of current and potential electrodes are the same but in between them are the integer multiple (n) of the distance (a) between the current and potential electrodes (figure 2.4). This array type has a better horizontal resolution and cover shallow depth of investigation (Hauck and Kneisel, 2008).

2.2.2. OhmMapper

The OhmMapper is an instrument made by Geometrics which relies on the principle of Capacitively Coupled Resistivity (CCR). This instrument is used to measure the electrical properties of the subsurface without penetration of electrodes into the ground like in other direct current resistivity investigation systems such as ERT (Timofeev et al. 1994). It is a streamer which contains one transmitter and one receiver or sometimes more with coaxial cables. Its configuration is dipole-dipole and it can be pulled on the ground to get continuous profiles. The transmitter dipoles inject current into the ground and the potential measurements is operated by receivers that are placed horizontally on the surface of the ground. Apparent resistivity profiles are made, when Alternating Current (AC) is induced with 16.5 kHz frequency by the subsurface and the AC voltage is measured by the receiver's dipole (Hauck and Kneisel, 2006). To get two dimensional (2-D) datasets for tomographic inversion, we can use an array of multiple receivers at different distances or we can repeat the acquisition along a survey line with different transmitter-receiver spacing (Hauck and Kneisel, 2006). CCR system is also applicable on the ground where the metallic electrodes are not easily be penetrated into the ground such as hard, frozen ground surfaces, carpeted, roads with gravels or snow (Timofeev et al. 1994, Calvert et al. 2001). CCR is very feasible and suitable in permafrost study as the frozen ground enhances the propagation of the signals and delineate the different materials on the basis of different resistivity (De Pascale et al. 2008). To determine spatial distribution and to characterize the frozen ground, the CCR system is considered as more effective geophysical tool (Fortier and Savard, 2010).

The applicability of the OhmMapper on highly resistive environment of Arctic permafrost has been observed and successfully overcome the problem that was facing due to the direct contact of electrodes with resistive ground and then results were compared with other multi-electrodes resistivity system (Timofeev et al. 1994). To our understanding, the OhmMapper had not yet been employed in Svalbard.

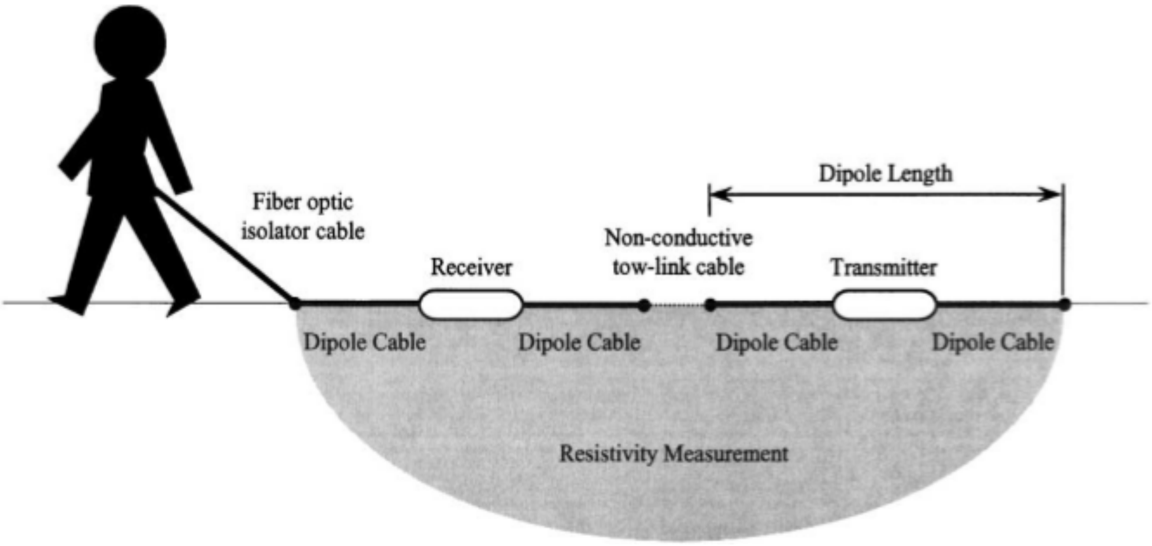

Figure 2.5: *Schematic illustration of the OhmMapper instrument. Figure from (Walker and Houser, 2002).*

Figure 2.6: *Photo of OhmMapper surveying in Svalbard. (Picture credit goes to Dr Sara Bazin).*

3. Study area

3.1. Svalbard archipelago

Svalbard is located between 74° – 81° North and 10° – 35° East in the Barents Sea (Figure 3.1). Svalbard is an archipelago located on the edge of arctic zone (Åkerman, 1992). Svalbard mainly comprises Spitsbergen, Nordaustlandet, Barentsøya, Edgøya, Kong Karls Land, Prins Karls Forland and Bjørnøya. 60% Svalbard area is covered with glaciers. Svalbard occupies 62,160 km^2 as total land area (Hagen et al. 2003). The rest of the area that is 40%, is having continuous permafrost (Humlum et al. 2003). The range of thickness of permafrost varies in different Svalbard areas, for instance, in valleys the thickness of permafrost is almost 100m and in mountain region it is 400 to 500m thick (Humlum et al. 2003, Christiansen et al. 2010). The altitude range of Svalbard is from sea level to 1700m above sea level (a.s.l) in the north eastern Spitsbergen (Ingólfsson, 2011).

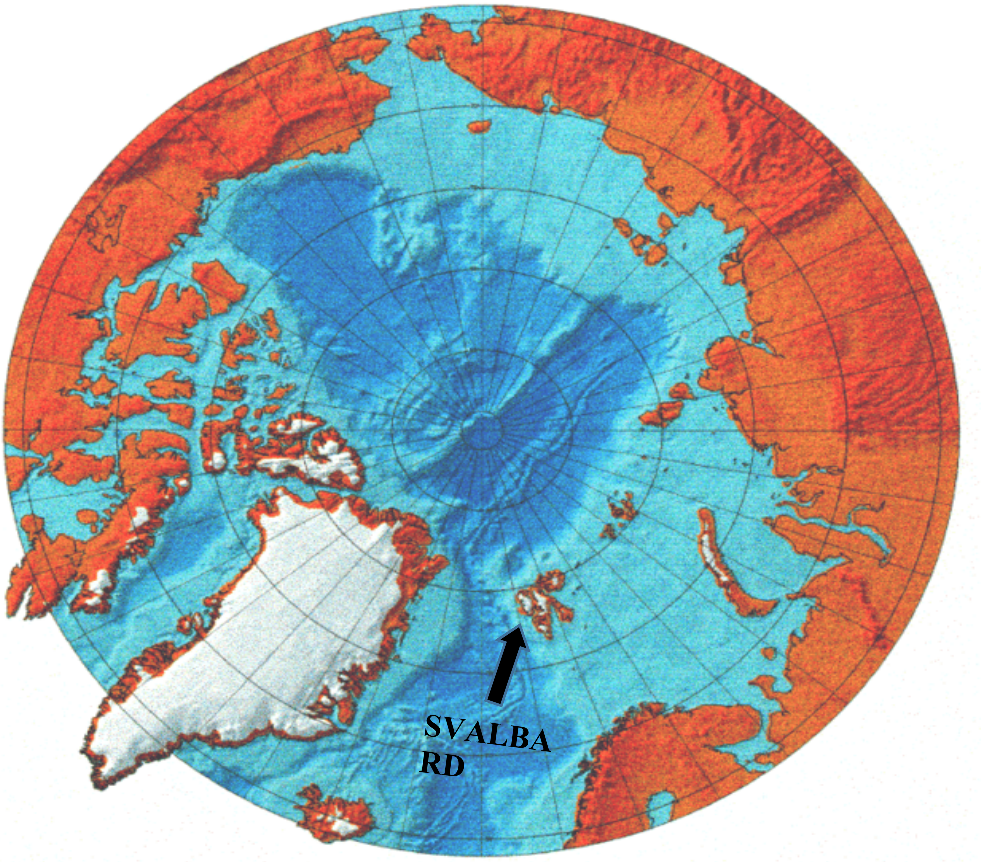

Figure 3.1: *Location of Svalbard in Barents Sea. (Figure is taken from* https://www.ngdc.noaa.gov/mgg/bathymetry/arctic/images/ibcao2.gif*)*

3.2. Climate and meteorology of Svalbard

Svalbard is having Arctic climate as it is in the Arctic Ocean. The current from west of Spitsbergen that is the part of North Atlantic current hits the west coast of Svalbard and operates as a climate moderator. This is the main reason for unfrozen sea water throughout the year (Ingólfsson, 2011). The other moderator that control temperature in Svalbard is Siberian High (Humlum et al. 2003). This cold and intense anticyclone develops in the eastern part of Siberia and causes an outbreak of cold air in eastern part of Asia during winter. The falling of air temperature in northern hemisphere is caused by the strong cooling effect produced in this region. In winters the Siberian high extends to the west part and also covers Russia and some parts of the Europe (Humlum et al. 2003). The advection of hot air enters Svalbard during the event of cold outbreaks in Svalbard, causing heavy rainfall and snow melting even in the middle of the winter season. In Svalbard and in northern Europe, thermal "sea saw" was observed when warm airflow was reported over Siberia, resulting in cold and dry periods during the winter in Svalbard (Humlum et al. 2003).

At the start of the 21st century the value for MAAT is –5° C in Svalbard at sea level and the minimum value that can be dropped is –15° C in mountainous areas (Ingólfsson, 2011). The isotherm of –10° C is present at almost 700 m above sea level (Humlum et al. 2003). Figure 3.2, shows that the MAAT at Longyearbyen airport remains steady year to year especially in summer but shows big variations in winter. The value for annual precipitation at Longyearbyen is 180 mm. The value for mean vertical precipitation gradient is 15-20% over 100 m in coastal areas and 5-10% over 100 m in central region. The value of precipitation is recorded 400-600 mm at eastern and western coastal areas of Spitsbergen which is the value for precipitation per year (Ingólfsson, 2011). It is considered that the Longyearbyen is the driest place in Svalbard (Christiansen, 2005). Increased orographic effect is the main reason in decreasing the precipitation gradient in the central region of the Svalbard (Humlum et al. 2003).

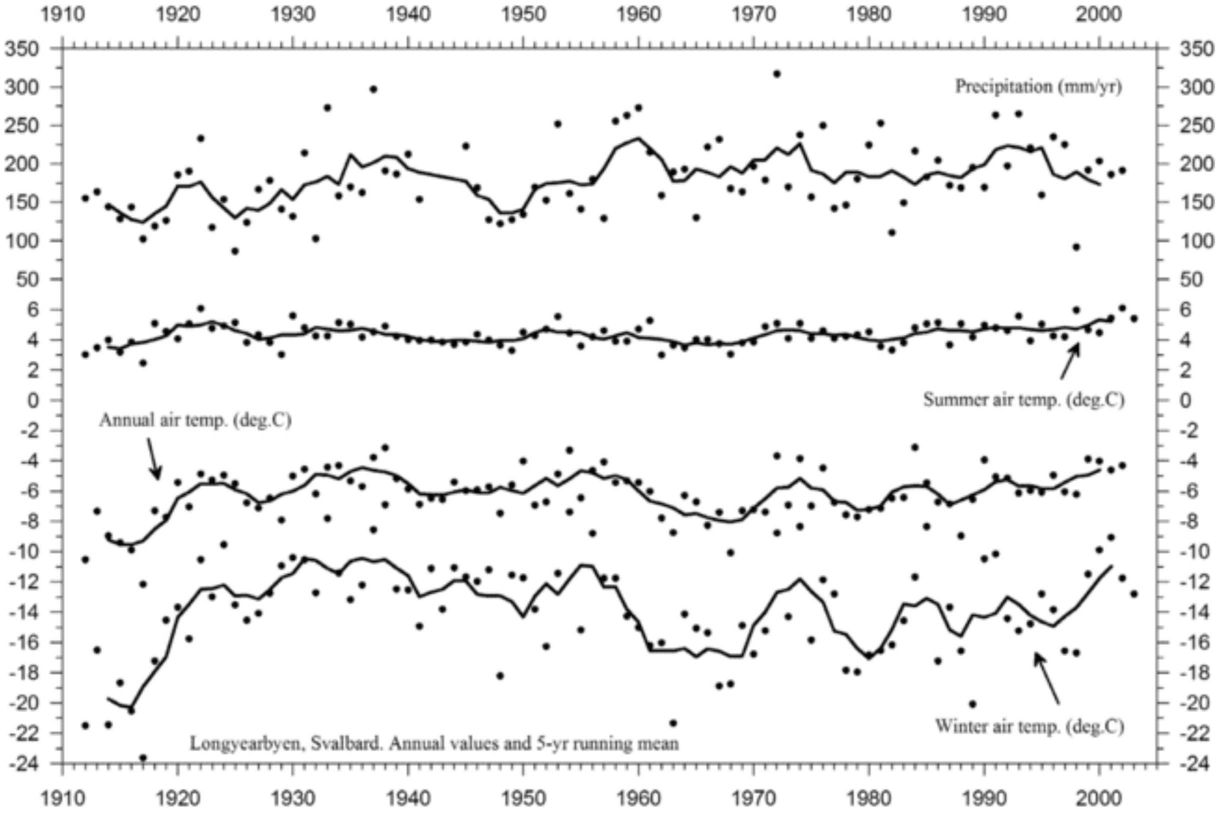

Figure 3.2: *The values of Mean Annual air temperature (MAAT) and precipitation recorded since 1911 at Longyearbyen airport. (Figure is taken from (Humlum et al. 2003)).*

Geology of Svalbard is interesting for many researchers as it has exposed rocks of different ranges from present to Archean times (figure 3.3, (Dallmann, 1999). It is useful to make analogues of exposed geology of Svalbard and what is inside the subsurface of Barents Sea (Steel and Worsley, 1984). During the Late Mesozoic era, uplift of Barents Sea shelf was started because of the movement of the crust. Now Svalbard is exposed to the North Western side of Barents Sea shelf (Dallmann, 1999). Mountainous topography in Svalbard is formed after several tectonic events that occurred in the history of Svalbard.

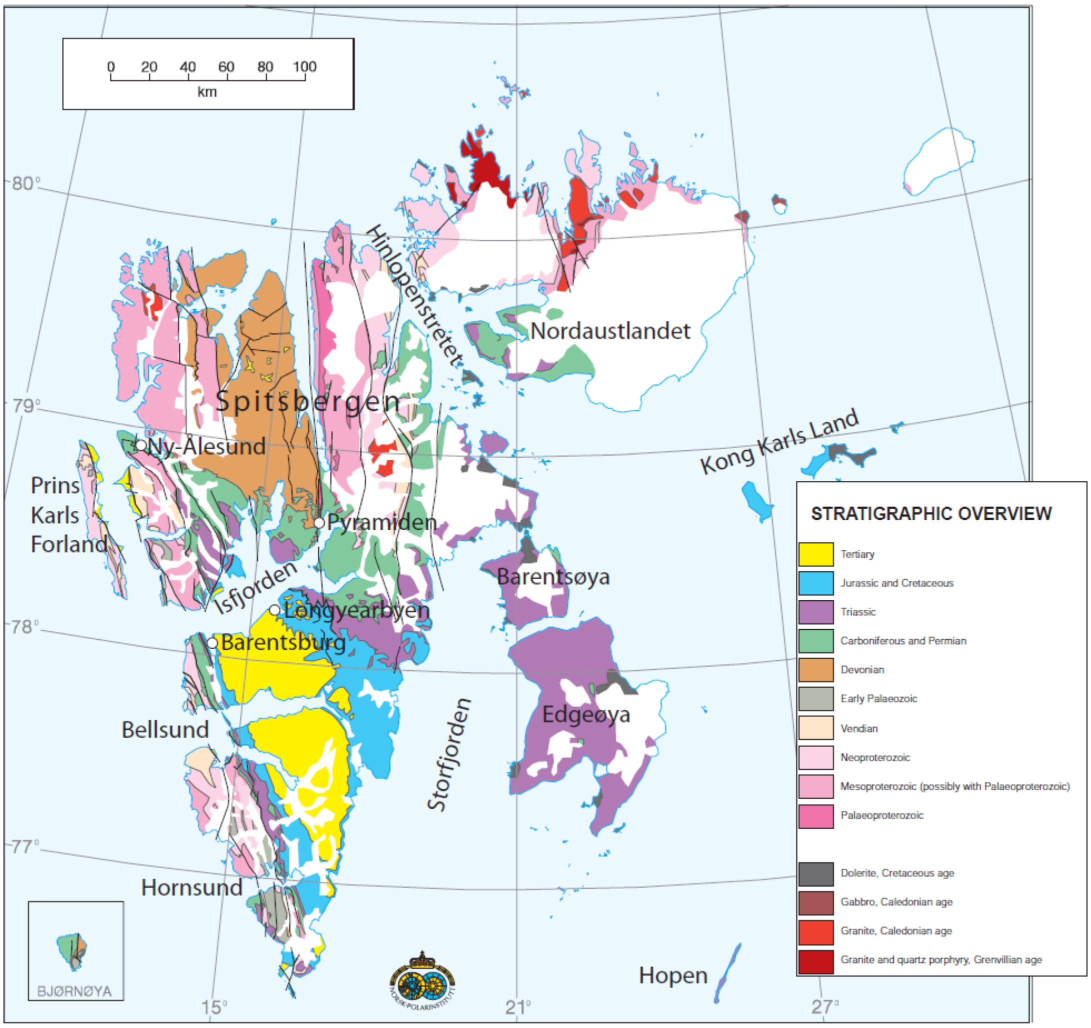

Figure 3.3*:* *Geological map of Svalbard. (Figure is taken from Norwegian Polar Institute).*

Almost 400 million year ago, in the start of mid of Devonian era, the material that contains the modern Svalbard archipelago was shifted towards current location in North 78° N from Equatorial plane (figure 3.4). The migration towards North can be described by different depositional phases and can be characterized by the different palaeo-climates due to the evolution of part of Eurasian Plate. Tectonic events and changes in sea level are the main causes that was controlling the sedimentary and depositional history of Svalbard (Worsley, 2008).

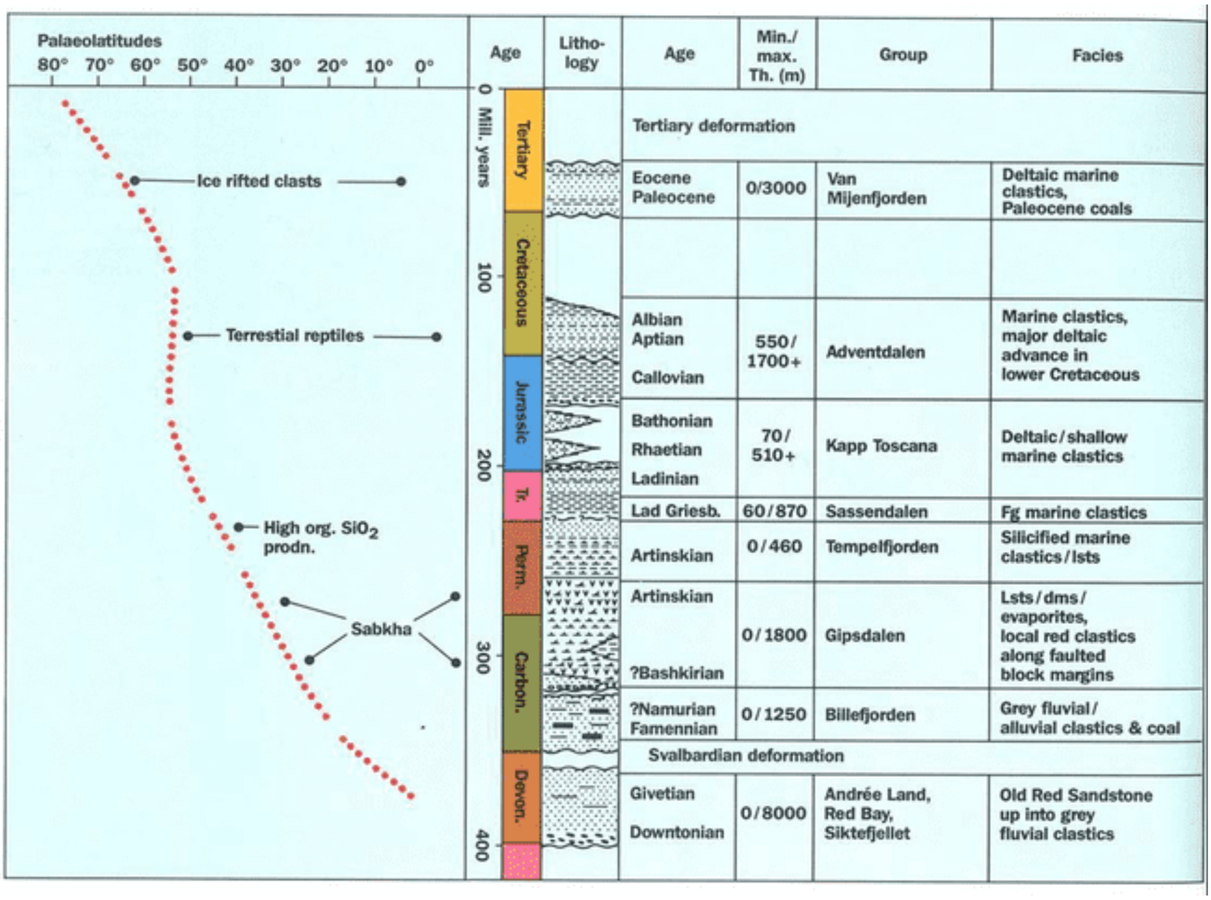

Figure 3.4: *Svalbard at palaeo-latitudes, showing characteristic lithologies and facies from each time period as Svalbard traveled from the equator to its present location. Figure is taken from (Worsley, 1986).*

The basement rock is composed of sediments, igneous rocks and meta-sediments that was formed in Precambrian to Silurian era, before the migration of Svalbard's current location from equatorial region to the arctic region (Elvevold et al. 2007). The rock type include 20 independent litho-stratigraphical groups that reflects the wide variety and complexity in exposure (Worsley, 2008). So, the bedrock experienced the folding and metamorphism during Caledonian Orogeny that occurred in Silurian era almost 400 million years ago (Elvevold et al. 2007).

The transition of sediments from red color to grey color is the main clue for change during early Devonian era and it occurred when Svalbard switched its climate from arid to equatorial tropics (Worsley, 2008). The movement towards North during the last Caledonian orogeny occurred in the era of late Devonian (Worsley, 2008). Old Red Sandstone is the dominating rock in the era of late Devonian (figure 3.4, (Elvevold et al. 2007). It is basically silt and sandstone conglomerate which changed in to shale and carbonate rocks (Elvevold et al. 2007).

Plateau shaped mountains are deposits from the Carboniferous and Permian era and are located in the central area and along northeastern side of Svalbard (Elvevold et al. 2007). The strata of Carboniferous and Permian eras have beds of limestone and dolomites with fossils also containing white layers of anhydrite and gypsum (Elvevold et al. 2007). Climate was damp and temperate during Mesozoic era (Triassic, Jurassic and in Cretaceous) (Elvevold et al. 2007). Rocks from this era are predominantly made of shale, sandstone, siltstone and limestone located in south of Spitsbergen. At the end of Cretaceous time period, volcanic processes and faulting damaged Svalbard's stable condition (Elvevold et al. 2007).

The plate movement characterized by the end of the Mesozoic era created a new belt of mountain in west of Spitsbergen. This was possibly the result of movement of continental plate of Greenland towards Svalbard as Svalbard was sliding over north of Greenland. This happened at the same time as the opening of the Northern Atlantic and the Arctic Ocean formation. Central Tertiary Basin is formed by the subsidence of the land to the adjacent of the new series of mountains. Sandstone and shales were deposited in this basin (Elvevold et al. 2007). Coal seams of tertiary age are now extracted from this basin. These coal reservoirs are the indication of the great vegetation that was present in Svalbard during this era (Ingólfsson, 2011).

Current latitude was reached by Svalbard in Quaternary era. This is the time when an ice age had started, Svalbard experienced glacial and interglacial times (figure 3.5), which caused the erosion controlling the landscape: the sediments that were deposited by the glaciation, were removed by intermittent erosions (Elvevold et al. 2007).

There are two different records that can help understanding Svalbard landscape. Marine records illustrate how the ice sheet was eroded and sediments were deposited into the Barents Sea (Ingólfsson, 2011). Terrestrial records explain how glaciers form the landscape and influence the fluvial system. These includes glacially eroded valleys and fjords (Ingólfsson, 2011).

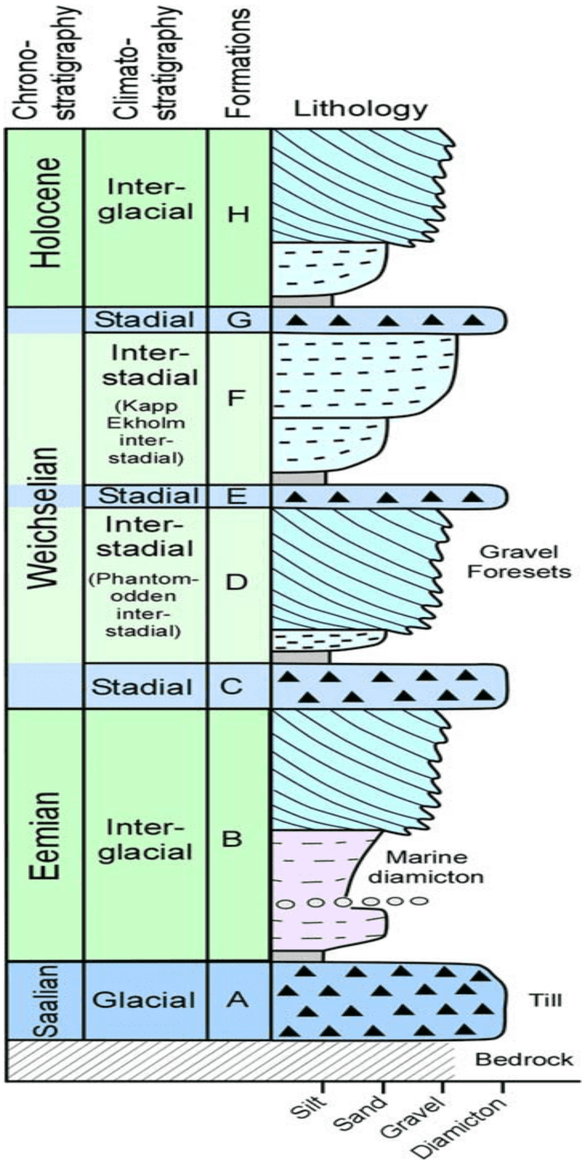

Figure 3.5: *Kapp Ekholm stratigraphy reflecting glaciation and deglaciation (marine-to-littoral sediments). Figure from (Ingólfsson, 2011), modified from (Mangerud and Svendsen, 1992).*

3.3. **Geomorphology and geography of Svalbard**

The different temperature and rainfall regimes across the archipelago, make it difficult to give the simple overview of the geomorphology and topography of region of Svalbard. But there are two main features that dominate the present landscape glaciers and permafrost. About 60% of the area in Svalbard is covered with glaciers and rest of the areas, almost 40%, have continuous permafrost (figure 3.6, (Christiansen et al. 2010))**.** Glaciers, weathering, frost processes, mass wasting and fluvial processes are the reasons of formation of the characteristic landscapes in Svalbard (Sørbel et al. 2001, Ingólfsson 2011). The glacial and periglacial environment makes the unique geomorphological phenomenon on the land of Svalbard (figure 3.7).

Figure 3.6: *Distribution of glaciers and permafrost on Svalbard. Glaciers are indicated in white, permafrost in grey. Figure is taken from (Humlum et al. 2003).*

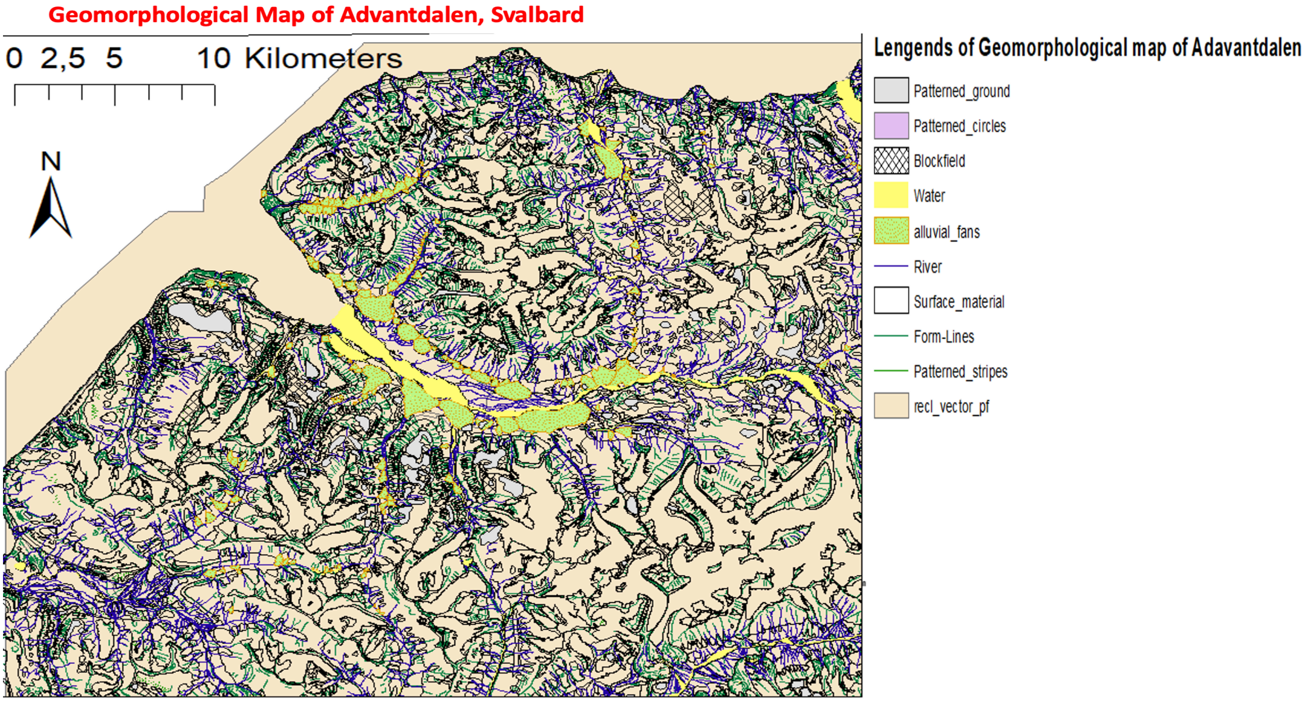

Figure 3.7: *Geomorphological map of Adventdalen site, Svalbard.*

The main mass of ice in Svalbard is on the east side and it is segregated into ice streams by ridges of mountain and nunataks (Hagen et al. 2003). On western side of Svalbard, number of small sized cirque glaciers are observed. Most of the current status of glaciers are poly-thermal. The ice thickness depends on the differences in the zone of accumulation and ablation of glaciers. Surging glaciers are also distributed all over Svalbard. Surging of glaciers usually happens when the flux of ice is less than the accumulation (Hagen et al. 2003). Surging glaciers can produce the unique form of landscape such as folded moraines (Sørbel et al. 2001).

Continuous permafrost is present all over Svalbard especially in those areas that are not covered with glaciers or are not under large water bodies (Humlum et al. 2003, Christiansen et al. 2010). It is considered that the permafrost in mountain regions in Svalbard belong to Weichselian era while those permafrost that is located in valleys and in the coastal areas are belongs to Holocene era (Humlum et al. 2003, Christiansen et al. 2010). Permafrost is considered as an influencing factor on the geomorphology of the Svalbard as it is impermeable. This is the reason for the water runoff on the surface or water melting in the active layer.

Slopes and fluvial processes play also as important contributors the development of the geomorphological landscape in Svalbard (Sørbel et al. 2001).

3.4. **Adventdalen and UNIS East sites**

The MAAT of Svalbard has increased up to 5° C during last 40 years. This increased warming trend is the serious issue. Researchers aim to monitor and observe permafrost on regular basis to secure and protect areas from slope destabilization and failure in engineering structures (Gilbert et al. 2019). For geotechnical testing and monitoring the condition of permafrost two sites have been developed under Norwegian GeoTest Sites (NGTS) project in Svalbard near Longyearbyen (Gilbert et al. 2019). These two sites are located in Adventdalen and near UNIS campus. The first is located in Adventdalen valley and it is almost 5 km away from Longyearbyen towards east. It is approximately 6 m above sea level (figure 3.9, (Gilbert et al. 2019). Its latitude and longitude are 78.2003° N and 15.8333° E. The area of this site is approximately 400m x 200m and is situated on the terrace of aggrading loess.

The cover of loess is almost 3 m thick with different types of deposits such as fluvial, deltaic, marine and glacial. Permafrost in this site is epigenetic (formed later than surrounding rocks) and it has less content of ice. The permafrost with high content of ice, syngenetic permafrost is bound to be present on the top 3 to 4 m of the soil surface (Gilbert et al. 2019). The thickness of the active layer in this site is approximately around 1 m and the temperature of the ground at depth of 10 m is -5° C (Gilbert et al. 2019). The value of elevation is almost 3 to 4 m above the river of Advent that has ice wedges.

Ice wedges are the features that mostly present in permafrost areas, observed while studying the stratigraphic sequence of present and past areas of permafrost and used as indicator of paleo-environmental condition (Shroder, 2013). Some studies have revealed that ice wedges in Svalbard like other areas that have continuous permafrost are mostly present in polygons pattern with more than 10 m diameters (Matsuoka, 1993). Polygons of ice wedges in Adventdalen are characterized by 30 to 40 cm deep, 20 to 100 cm wide, low centered (also observed in USA, figure 3.8) and mainly described by troughs of few centimeters. Ramparts are usually present where the large ice wedge troughs are present (Christiansen, 2005). Ice free areas in Svalbard are the places where ice wedges polygons are usually present from near sea level to 500 m a.s.l. The youngest polygons are located near sea level as these areas are recently emerged with sea due to isostatic rebounding. So, many of them are developed during recent climatic conditions. In Adventdalen area, MAAT is -5.5°C (Sørbel and Tolgensbakk, 2002).

Figure 3.8: *Low centered ice wedge polygons spotted in Alaskan North Slope, USA. Figure from (French, 2007)).*

The UNIS site is 1 to 8 m above sea level and it is 100 m to 300 m away from the UNIS building (Svalbard Science University) towards southeast (figure 3.9). The western area that is zone 1 is

5 and 8 m above sea level and it is regularly used by UNIS to collect different samples of soil that is fine grained. The other area that is more towards east is known as zone 2 is located 1 to 4 m above sea level. This site has almost 50 km^2 area in total.

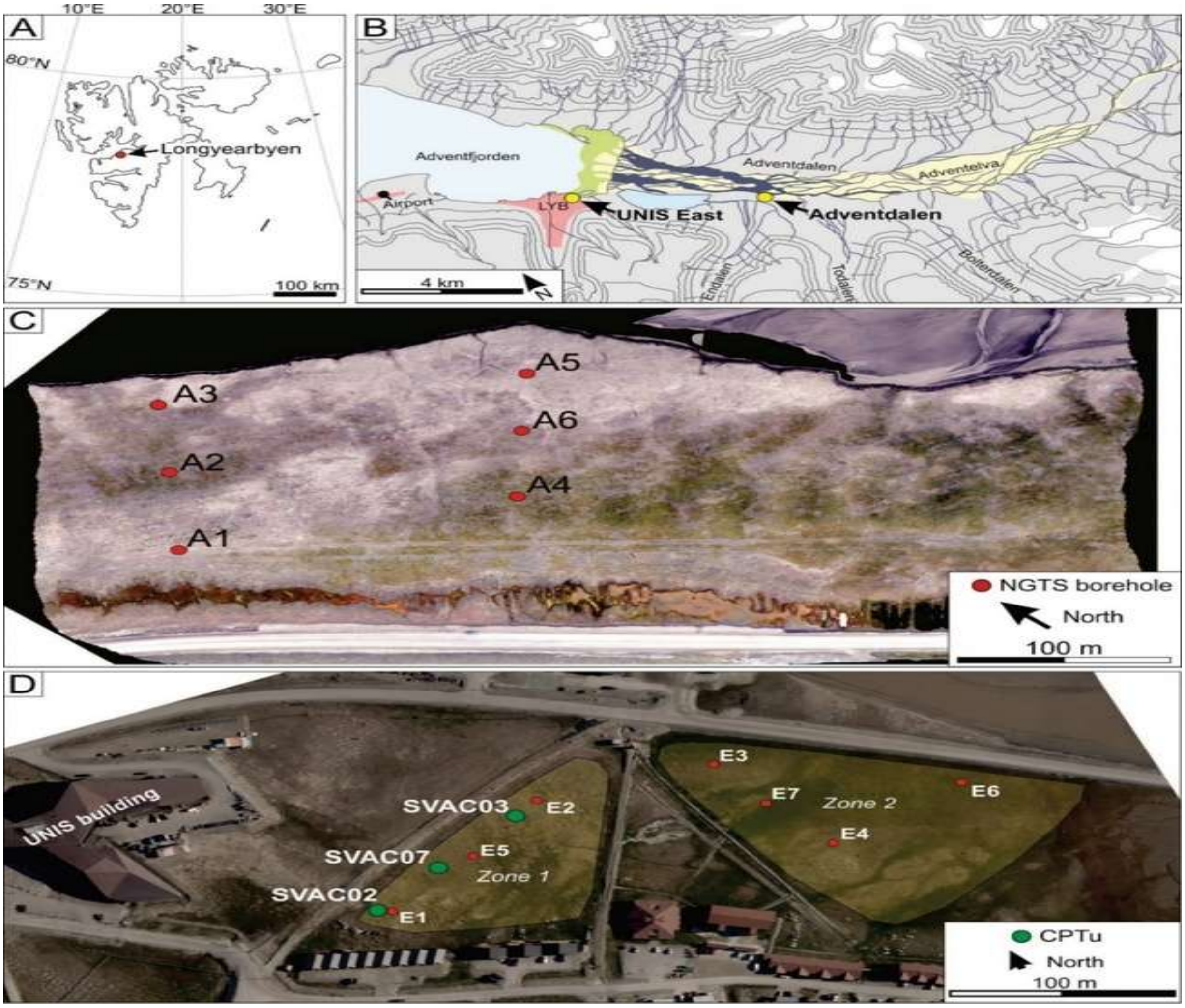

Figure 3.9: *A) Location of Longyearbyen in Svalbard. B) Location of the two survey areas near Longyearbyen. C) Details of Adventdalen site. D) Details of the UNIS site. A6 is ground temperature monitoring borehole. Figure is taken from (Gilbert et al. 2019).*

3.4.1. Climate of Adventdalen and UNIS east sites

An increase in the MAAT has been observed in the range of 3 to 5° C during last 4 to 5 decades in Svalbard. Figure 3.10 shows the measured values and means of the MAAT at Longyearbyen. In figure 3.11 and 3.12, the relevant indices of air freezing and air thawing are elaborated respectively. From these figures, it is clearly seen that the increase in mean annual air temperature for 30 year from value of -6.8° C in 1989 to the value of -3.9°C in year of 2018 (Gilbert et al. 2019). The same trend has been observed for mean air thawing index for 30 year data, the value for index has increased from 400° C.days to the value of 575° C.days. In case of air freezing index, the values has decreased from 2850° C.days in the year of 1989 to the value of 2000° C.days in year of 2018 (Gilbert et al. 2019).

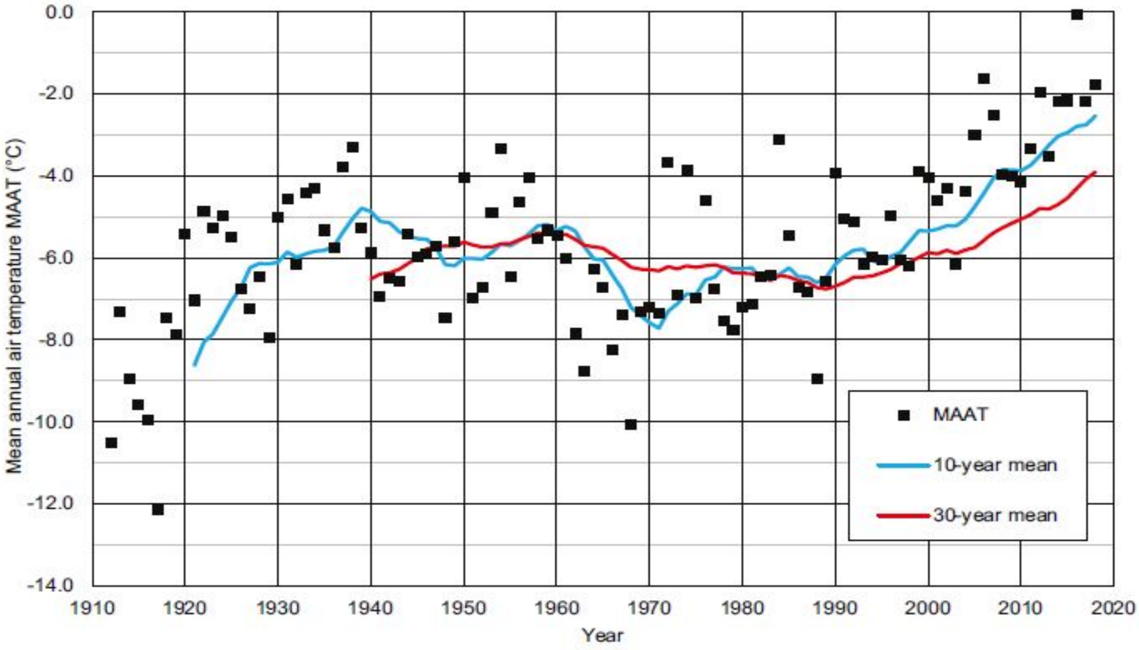

Figure 3.10: *Mean annual air temperature Longyearbyen, Svalbard. Figure modified from (Instanes, 2016) based on data from Norwegian Meteorological Institute.*

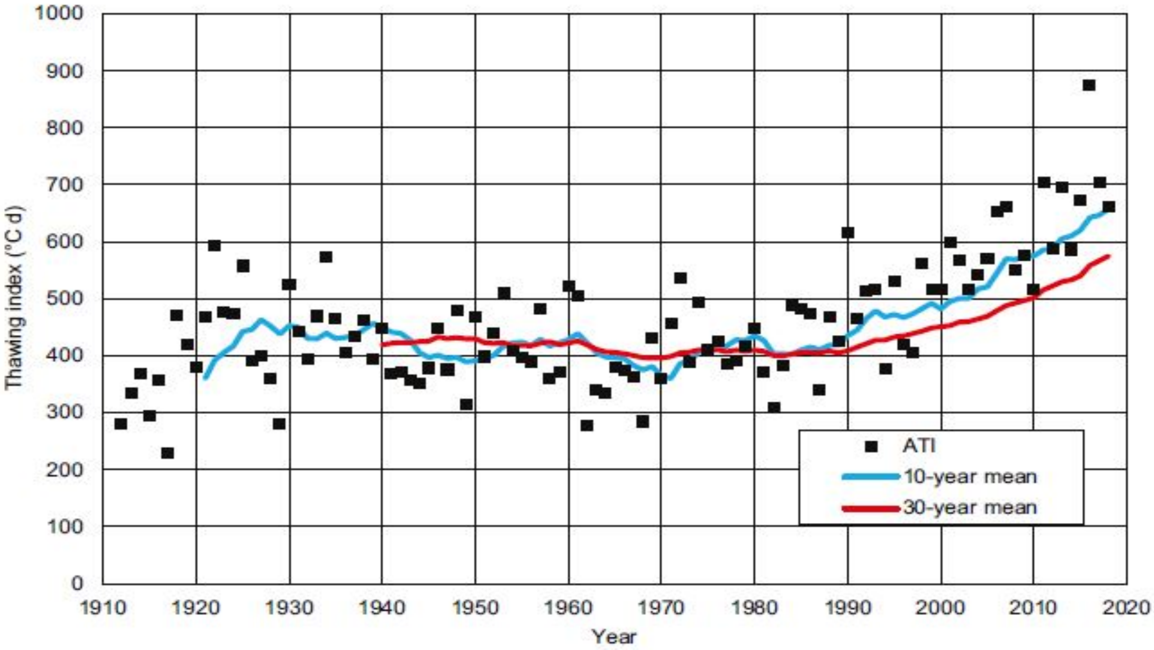

Figure 3.11: *Air Thawing Index (ATI) Longyearbyen, Svalbard. Figure modified from (Instanes, 2016) based on data from Norwegian Meteorological Institute.*

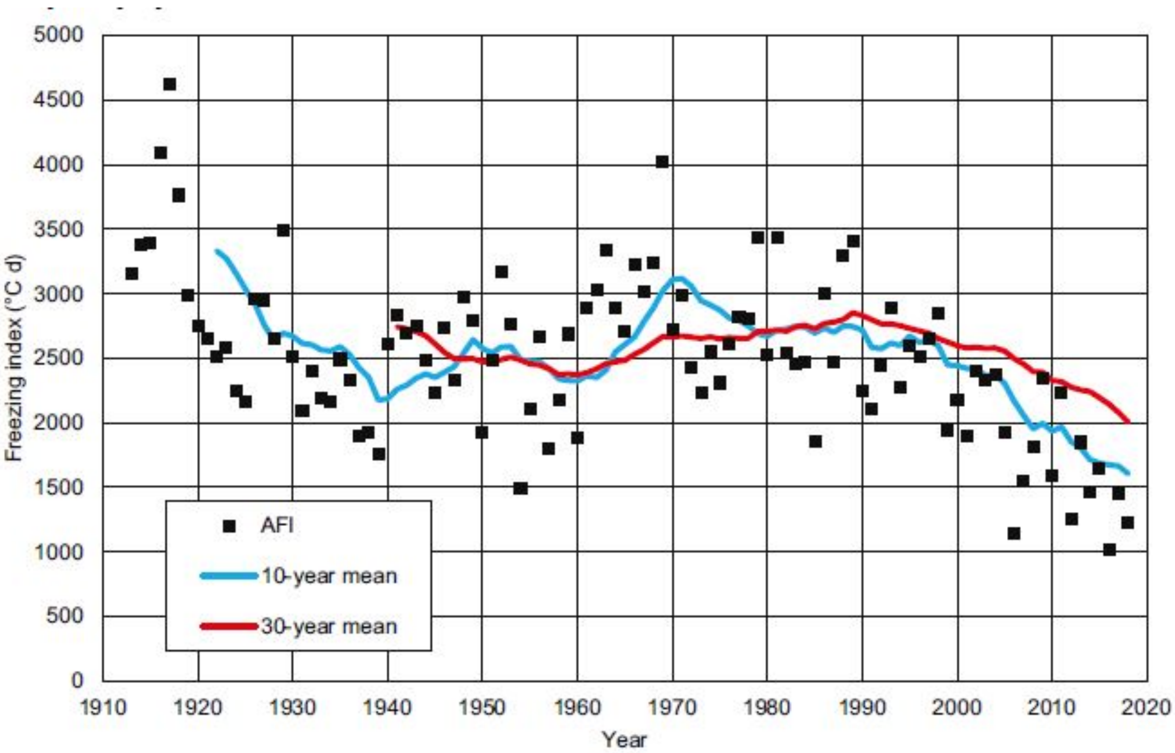

Figure 3.12: *Air Freezing Index (AFI) Longyearbyen, Svalbard. Figure modified from (Instanes, 2016) based on data from Norwegian Meteorological Institute.*

3.4.2. Geology of Adventdalen and UNIS east sites

These sites are situated where the former fjords are now filled with sediments. These fjords are considered as the valleys of incised bedrock which were produced during of glaciation and inundated with the seawater (Gilbert et al. 2019). These sites were sourced by the flow of ice and the subglacial deposits were accumulated during glacial era and during the period of deglaciation and post glacial time period, fjord delta heads were deposited (Corner 2006, Gilbert 2018). In a fjord valley, the till is overlain marine deposits. The deltaic sediments and fluvial deposits have upwards sequence of coarsening. The majority of the filling of a fjord valley with deposits, was through marine setting. (Gilbert et al. 2019).

3.4.3. Stratigraphy of Adventdalen and UNIS east

The Soil stratigraphy of the Adventdalen site is made up with the top most layer of sandy clayey silt (it is Unit D3 and its depth is approximately 3m from the surface of terrain), followed by the layer of silty sand with approximately depth of 13m (it is unit D2) over the layer of clay or silty clay with almost depth of 16m to 30m (it is unit D1) (Gilbert et al. 2019). The vertical distribution of soil stratigraphy can be seen in figure 3.13.

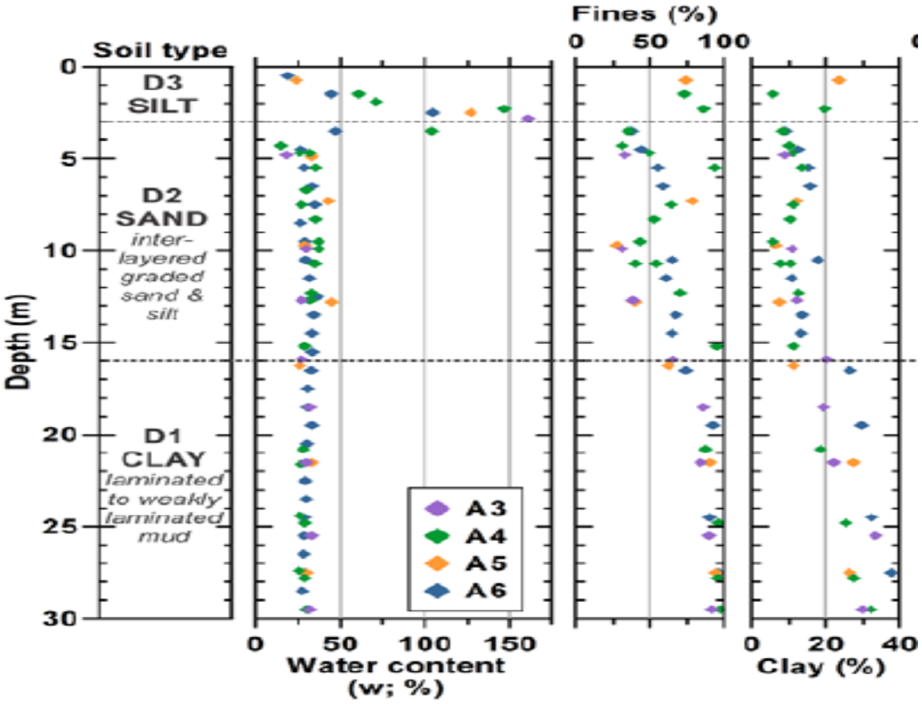

Figure 3.13: *Illustration of vertical distribution of soil type at Adventdalen site. A3 to A6 are the Borehole locations as mentioned in figure 3.9. Figure is taken from (Gilbert et al. 2019).*

The stratigraphy of soil at the site of UNIS East is composed of with the topmost layer of gravelly silty sand with the approximate depth of 3 m from the terrain surface (It is Unit 3), underlain by the layer of silty clay (Unit 2) over poorly sorted layer of sandy, silty, clay (Unit 1). The unit’s thicknesses vary in the different drill holes. The range of depth of the bed rocks at the site of UNIS East is from 21m to 30m (Gilbert et al. 2019). The vertical distribution of the soil stratigraphy can be seen in figure 3.14.

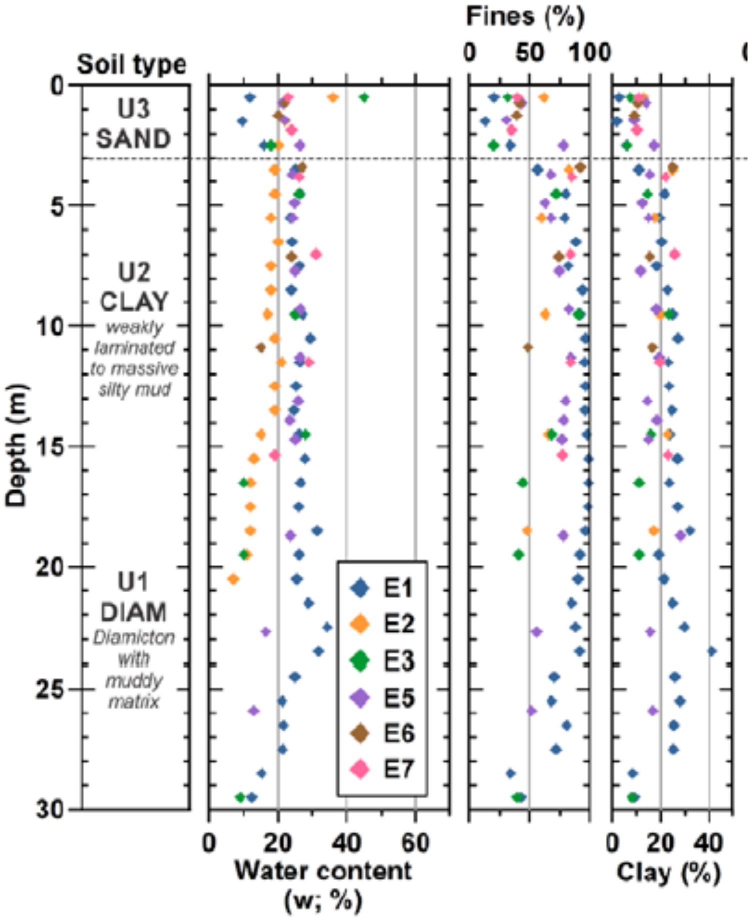

Figure 3.14: *Illustration of vertical distribution of soil stratigraphy at UNIS East site. Bore holes locations are from E1-E7. The boundary between U2 and U3 varies between borehole locations and is not indicated. Figure from (Gilbert et al. 2019).*

4. Methodology and data acquisition

As described before, ground resistivity is considered the most useful geophysical property to monitor permafrost. Electrical resistivity distribution in subsurface can be measured with the voltage observed at the surface of the ground while an electrical current is injected in the ground. After acquiring the surveys, we can compute the resistivity distribution in the ground. Two different types of electrical surveys can be used with direct current (DC): 1) Galvanic coupling and 2) Capacitive Coupled Resistivity (CCR). In first survey method, the electrodes are installed in the ground and DC is injected to the ground through these current electrodes and the electrical potential is measured through potential electrodes (Hauck, 2002). In the second type of survey, CCR uses two dipoles, one is transmitter and other is receiver. By using capacitive coupling, a direct current is applied on the ground through a transmitter antenna and the electric potential is measured at a receiver antenna. This survey is free from the direct surface contact of electrodes to the ground and data acquisition is easy and rapid. A streamer with two dipoles can be towed over a large area (De Pascale et al. 2008).

The OhmMapper is commercially developed by Geometrics Limited company and its use is optimal in permafrost environments (Angelopoulos et al. 2013).

Filed work was conducted on 1st of July 2019 in Svalbard for 5 continuous days and there were two main survey sites in Longyearbyen and these are: 1) UNIS East site, and 2) Adventdalen site. These two sites are also the benchmarks sites in NGTS project. OhmMapper is the device that was used as a primary source for geophysical investigations on these sites to acquire data in order to map the electrical resistivity of the subsurface permafrost in these areas. The OhmMapper streamer was towed along several profile lines. It was difficult to pull it on the rough surface covered with water pounds and uneven grass.

We collected 3 different datasets at UNIS east site: dataset 1, dataset 4, and dataset 5. The mode of survey was “simple survey” and the profile was 160 m long. These datasets were acquired by pulling the streamer along the same profile line with different rope lengths and dipole cable lengths in order to sample different depths of the subsurface.

In dataset 5, the survey was conducted with the 10 m dipole cable and the rope length was increased from 2.5 m to 15 m. The survey was conducted 6 times along the same profile line and every time the rope length was increased by 2.5 m to collect the deeper data points. In dataset 1, the survey was conducted with the same 10 m dipole cable with 17.5 m rope length, the largest possible length in this environment. A longer streamer could not measure a sufficient signal to noise ratio. A mark spacing of 10 m was used during the acquisition for a geometric reference.

In dataset 4, the survey was conducted with the dipole cable of 5 m length and the maximum rope length was up to 10 m. So, after every survey along same profile line, the rope length was increased by 2.5 m and therefore survey was conducted 5 times.

We used the same dipole cable length of 10 m for dataset 1 and dataset 5 but with different range of rope lengths. In order to obtain the best image of the subsurface, these two datasets are merged together into a single dataset. By increasing the distance between transmitter and receivers when changing the rope length, a deeper image of the subsurface can be obtained.

At Adventdalen site, there were three datasets that were acquired during the survey and those datasets were named as: dataset 1, dataset 2 and dataset 5. The mode of survey for dataset 2 and dataset 5 was selected as a “map survey” and this survey was conducted in a 100 m x 100 m square area. Dataset 2 was collected after using 5 m dipole cable length with fix rope length of 5 m between transmitter and receiver and the survey was started from the NW corner and ended at the SW corner of the area. The survey grid is composed of 21 profile lines and each line is 100 m long. The distance between each profile is 5 m. This survey was bidirectional and the streamer was pulled along the Y axis. Again, a mark spacing of 10 m was used during the acquisition for a geometric reference.

In dataset 5, the data was acquired while using 5 m dipole cable length and 2.5 m rope length between transmitter and receiver and this survey was collected along the X axis. We started the survey in the SE corner and ended it at the SW corner of the area. Again, the survey grid is composed of 21 profile lines and each line is 100 m long, but the streamer was pulled in a direction perpendicular to the one of dataset 2.

The mode of survey for dataset 1 was selected as a “simple survey” and the survey was along 50 m long profile with 5 m dipole cable and rope length goes up to 20 m. The survey was started from the NW corner and ended at the SW corner.

4.1. Data processing

Several softwares were used to process the data: Magmap2000 and Res2DInv or Res3DInv. Magmap2000 is a software from Geometrics necessary to pre-process field data in the format of the OhmMapper. It can apply basic filters to the raw data. This software was used to remove the noisy data points (seen as spikes in the voltage data) using despiking option or the dropouts due to loss of signal acquisition.

Then pseudo-sections were plotted with respect the pseudo-depth, which is considered as a function of the distance between the dipoles. A pseudo-section is considered to be a geometrical view of the apparent resistivity measured along a profile (De Pascale et al. 2008). This pseudo-section was exported in a supported file format for Res2DInv software. After reading this data file into Res2DInv software, noisy points were manually removed. Then, an inversion is applied in order to obtain a model that contains resistivity values for every model block. The Res2DInv software was used to get two-dimensional (2-D) inversion of the data as resistivity profile. The inversion of data of resistivity is helpful to understand subsurface model and to identify the features such as ground ice and ice wedges (De Pascale et al. 2008). To get three-dimensional inversion and to find out the true resistivity of the subsurface, Res3DInv software was used.

5. Results

5.1. UNIS site results (Simple OhmMapper Survey)

Data is processed by using two softwares. Pre-processing of field data is done by using Magmap2000 software. The first part of this section contains the results from Magmap2000 and the next section deals with the result that obtained from Res2DInv software.

5.1.1. Results from Magmap2000

Three datasets are processed while using Magmap2000 software and these datasets are: dataset 1, dataset 2, dataset 5. The profile length is 160 m for each dataset.

5.1.1.1. Dataset 1

The description of dataset 1 is in the table 5.1. Geometry of dataset 1 is elaborated in figure 5.1. Pseudo-section of dataset 1 with pseudo-depth is shown in figure 5.2.

Cable Length	5 m
Dipole Cable Length	10 m
Rope Length	17.5 m
N- Factor	1.75 m
Mark Spacing	10 m
Number of survey (Profile) line	1

Table 5.1: *Characteristics of dataset 1.*

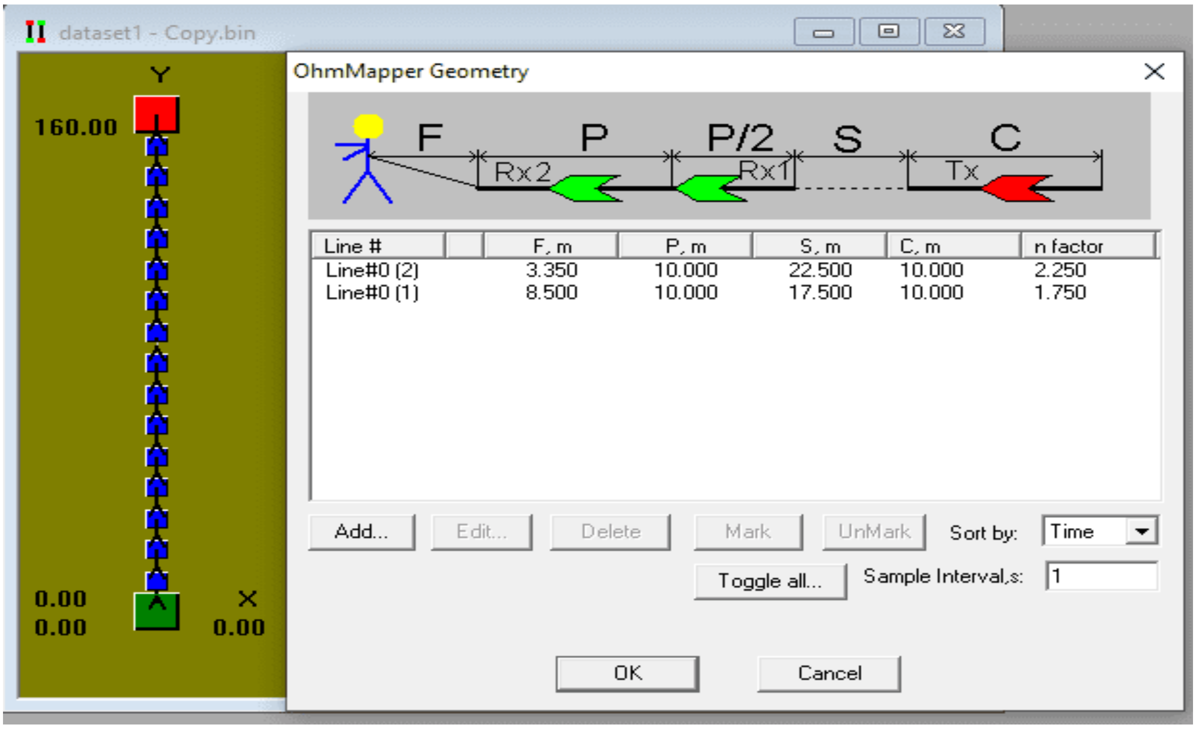

Line #	F, m	P, m	S, m	C, m	n factor
Line#0 (2)	3.350	10.000	22.500	10.000	2.250
Line#0 (1)	8.500	10.000	17.500	10.000	1.750

Sort by: Time

Sample Interval,s: 1

Figure 5.1: *Geometry of dataset 1 in Magmap2000.*

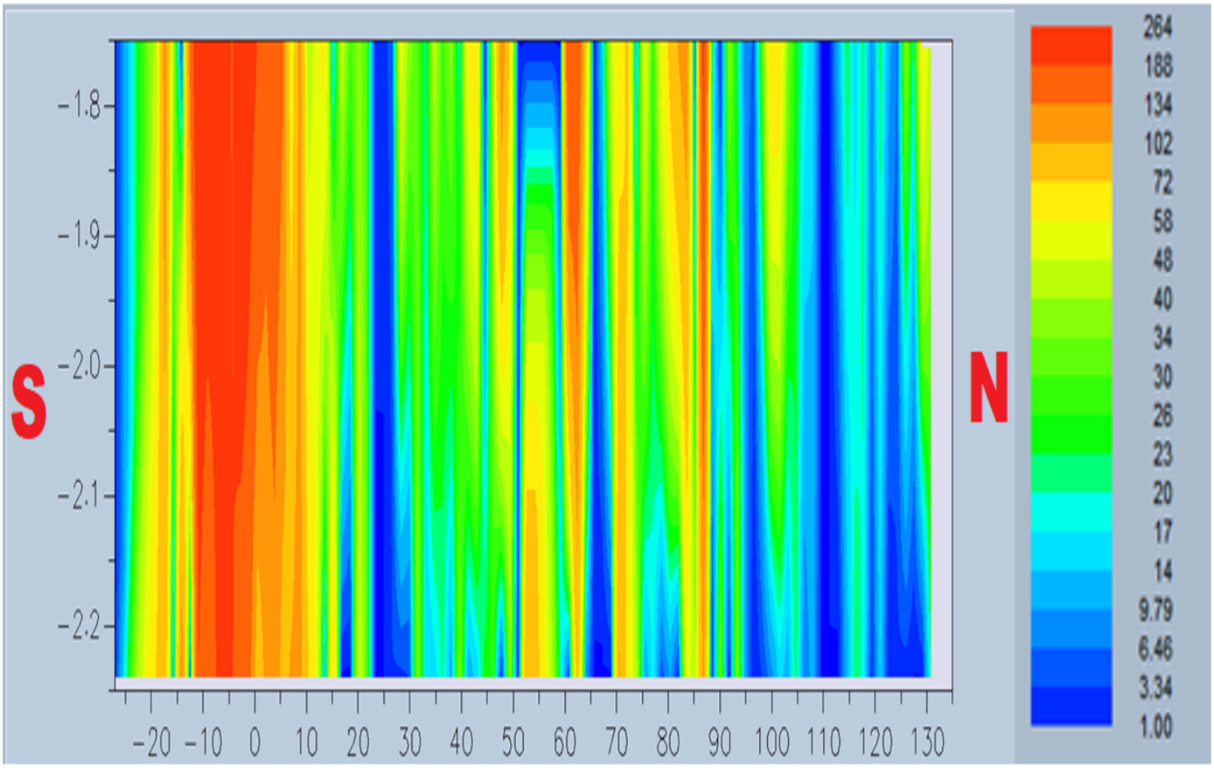

Figure 5.2: *Pseudo-section of dataset 1 with pseudo-depth on Y-axis and distance along the profile is along x-axis. North and South direction is mentioned.*

5.1.1.2. Dataset 4

Dataset 4 has following characteristics (table 5.2).

Cable length	2.5 m
Dipole Cable length	5 m
Rope length	2.5, 5, 7.5, 10 m
Mark spacing	10 m
N- factor	0.5, 1, 1.5, 2
Number of survey (profile) lines	5

Table 5.2: *Characteristics of dataset 4.*

There is some signal loss during acquisition of data while using OhmMapper (figure 5.3). It was 5 survey lines but during data acquisition, receivers were not getting signals from transmitter. So, the last profile line has just 2-mark points ("A" side of figure 5.3). This survey line is removed due to incomplete marked points and then geometry is adjusted and modified accordingly while using Magmap2000. Now, it has 4 profile lines ("B" side of figure 5.3). In figure 5.4, noisy data points are removed while using filters such as despiking and dropouts and OhmMapper reading with two sensors (receivers) can be seen in red and blue curves. Pseudo-section with pseudo-depth is clearly seen in figure 5.5.

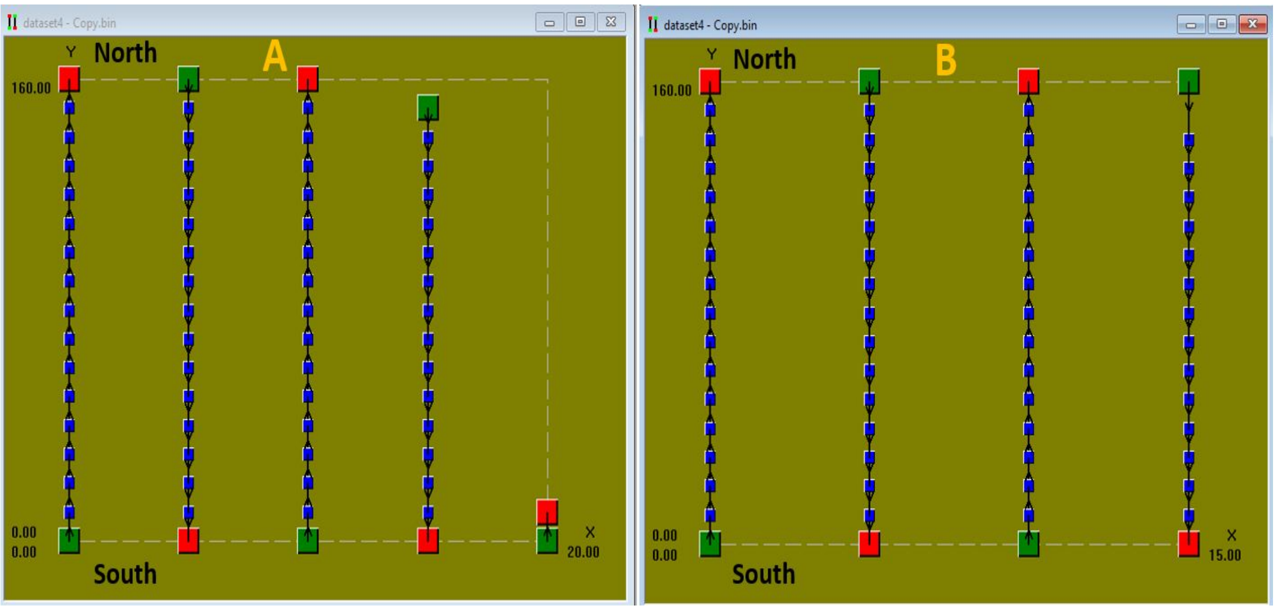

Figure 5.3: *Changes in geometry of dataset 4. On left side, "A" is the geometry before changes and on right side, "B" is the geometry after changes.*

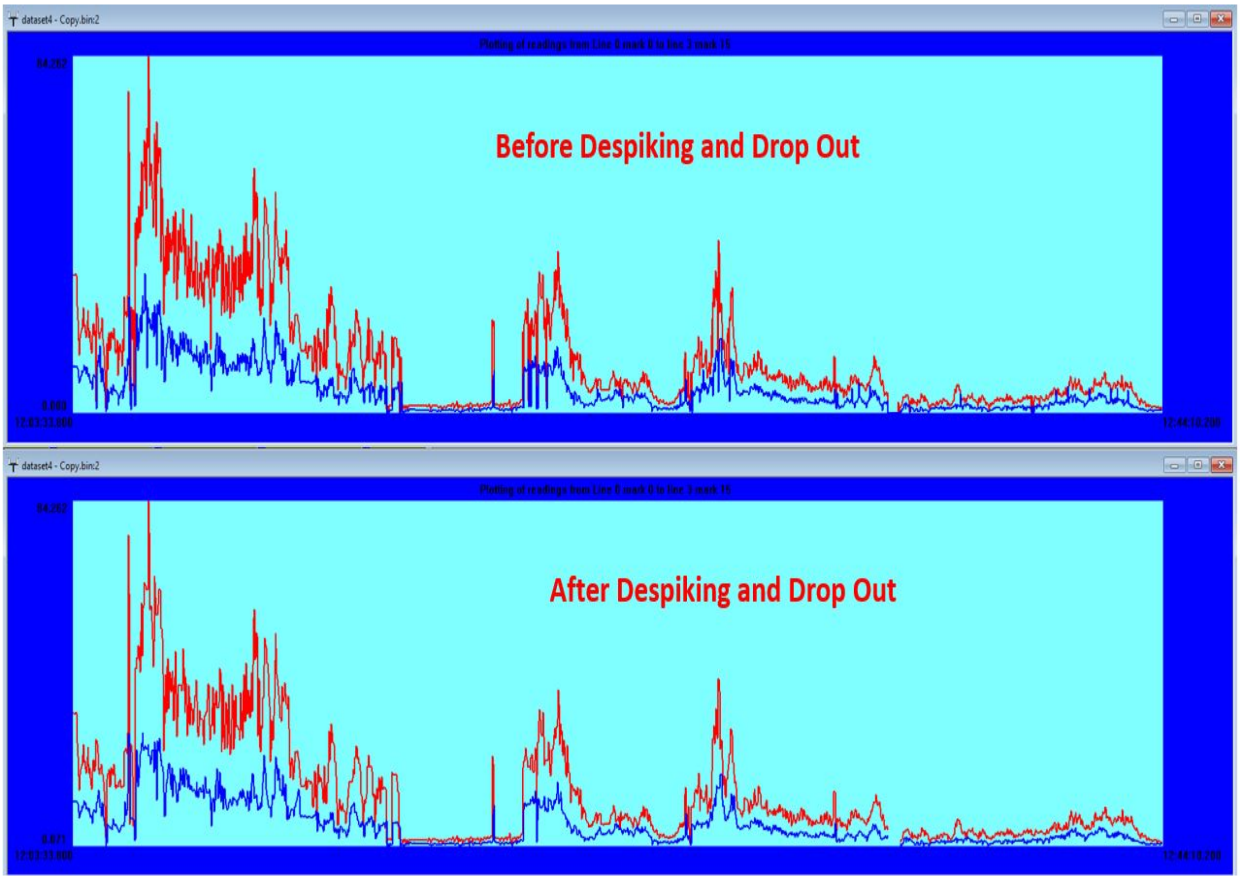

Figure 5.4: *Difference between OhmMapper reading before and after applying the filters (Despiking and dropout options). Blue color is receiver 1 and red curve is showing receiver 2.*

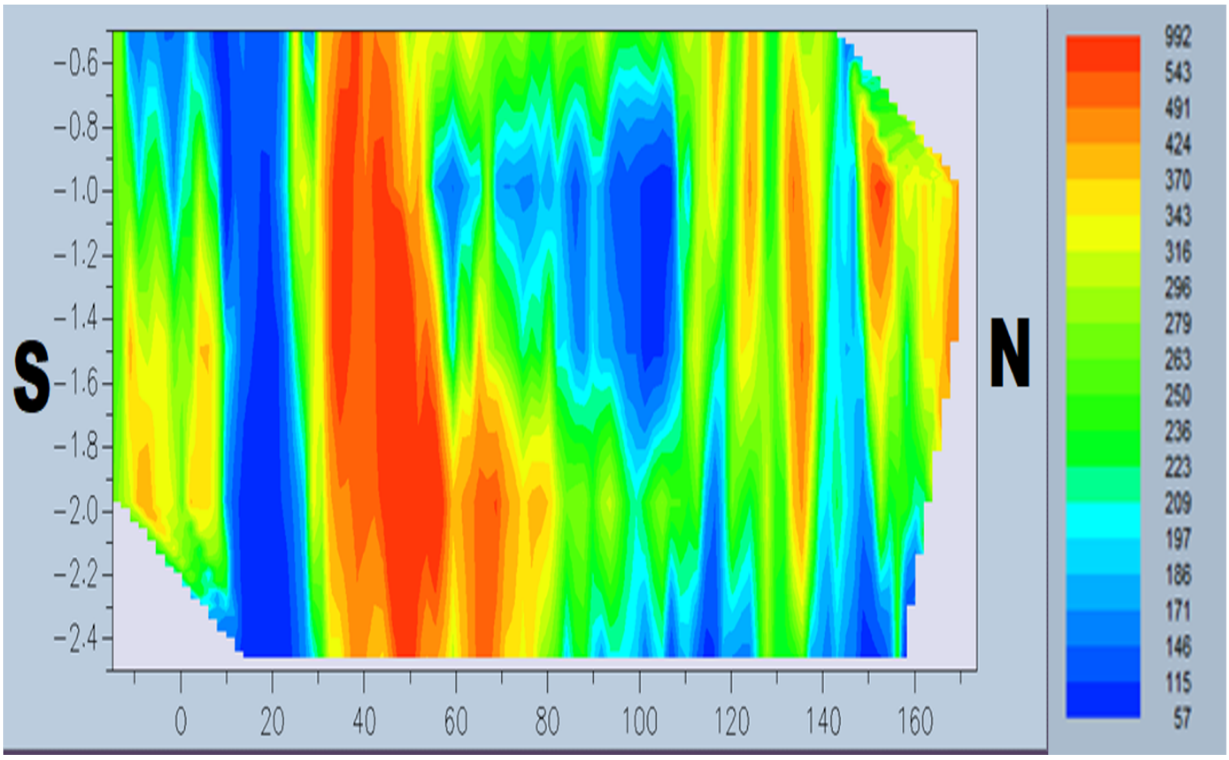

Figure 5.5: *Pseudo-section of dataset 4 with pseudo-depth on Y-axis and distance along the profile on x-axis. North and South direction is mentioned.*

5.1.1.3. Dataset 5

Description of dataset 5 is in table 5.3. Profile length is 160 m for this dataset.

Cable length	5 m
Dipole Length	10 m
Rope length	2.5, 5, 7.5, 10, 12.5, 15 m
Mark spacing	10 m
n- factor	0.25, 0.5, 0.75, 1, 1.25, 1.5
Number of survey (profile) lines	6

Table 5.3: *Characteristics for dataset 5.*

Geometry of the survey is disturbed due to the signal loss between the transmitter and receivers. So total number of acquisition survey lines are 6 but the many mark points are missing during the survey in the field site. So, in figure 5.6, geometry is adjusted and mark points are moved to the proper locations while using Magmap2000 software. OhmMapper reading is obtained to monitor the noisy points and then removed by using filters (figure 5.7). Pseudo-section is made by using filtered and modified geometry data through Magmap2000 (figure 5.8).

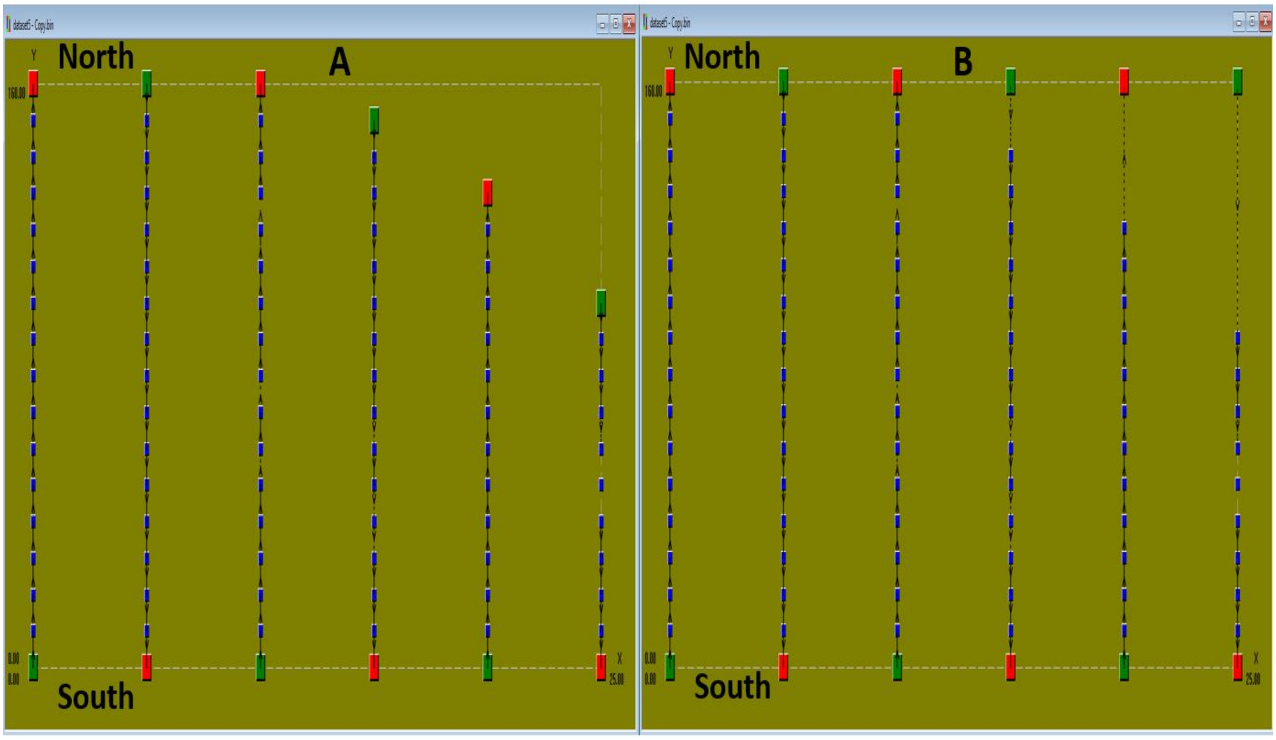

Figure 5.6: *Changes in geometry of dataset 5. On left side, "A" is the geometry before changes and on right side, "B" is the geometry after changes.*

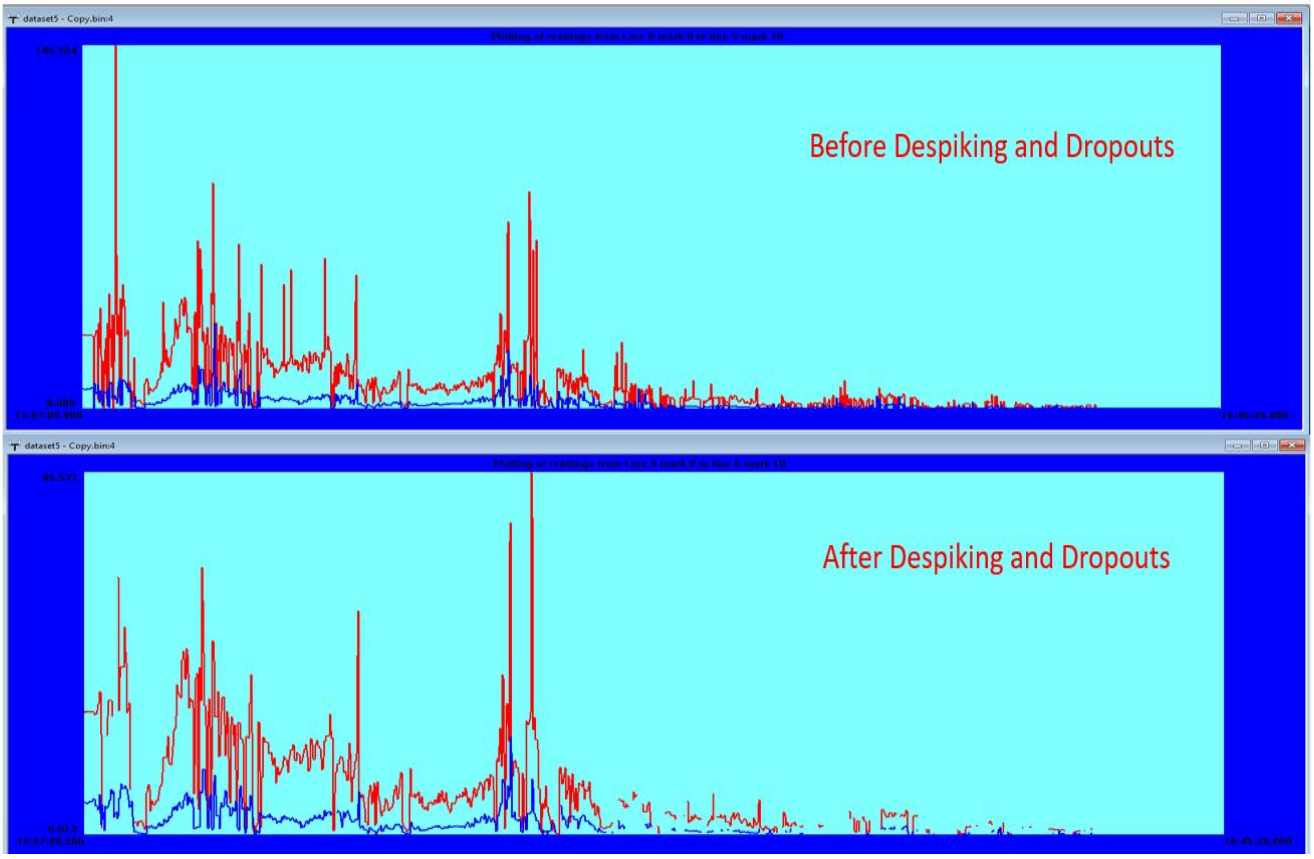

Figure 5.7: *Difference between OhmMapper reading before and after applying the filters (Despiking and dropout options). Blue color is receiver 1 and red curve is showing receiver 2.*

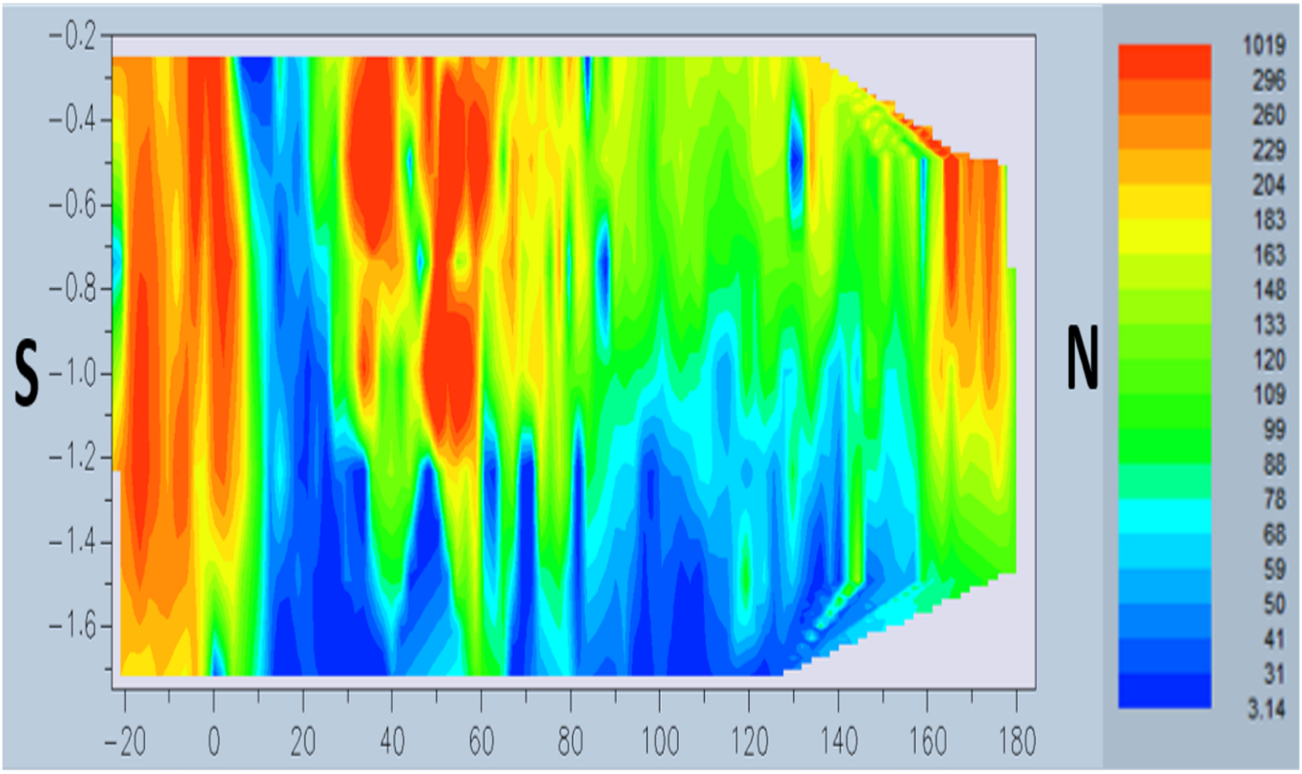

Figure 5.8: *Pseudo-section of dataset 5 with pseudo-depth on Y-axis and distance along the profile is along X-axis. North and South direction is mentioned.*

5.1.2. Res2DInv results

After making pseudo-section with Magmap2000, a data file can be exported for inversion process. One needs to choose the electrode spacing that is used for the geometry of the output file. Here, an electrode spacing of 0.625 m was chosen for the averaging of the raw data. Several data files can be merged together. Then, Res2DInv software has been used. The different processing steps are illustrated in the following paragraphs.

5.1.2.1. Dataset 4 alone

Dataset 4 was acquired with 5 m dipole cable length. So, it is processed for inversion separately and the total number of data points are 1364.

Figure 5.9, the pre-processed data points are plotted along the Y-axis (on right side) versus pseudo-depths. Noisy data points are manually removed by clicking on them.

Inversion result is obtained after a few iterations. The investigation depth is 4.61 m and the resistivity range is from 1 to 6000 Ωm. After 14 iterations, the RMS value is 10% (figure 5.10).

For removal of some outliers and to improve the resistivity model, a RMS correction can be applied by looking at the histogram of residuals and scatter plot of data points. This option allows to invert the data without outliers (figure 5.11).

Inversion result without the outliers can be obtained with a lowers RMS value of 9% (figure 5.12).

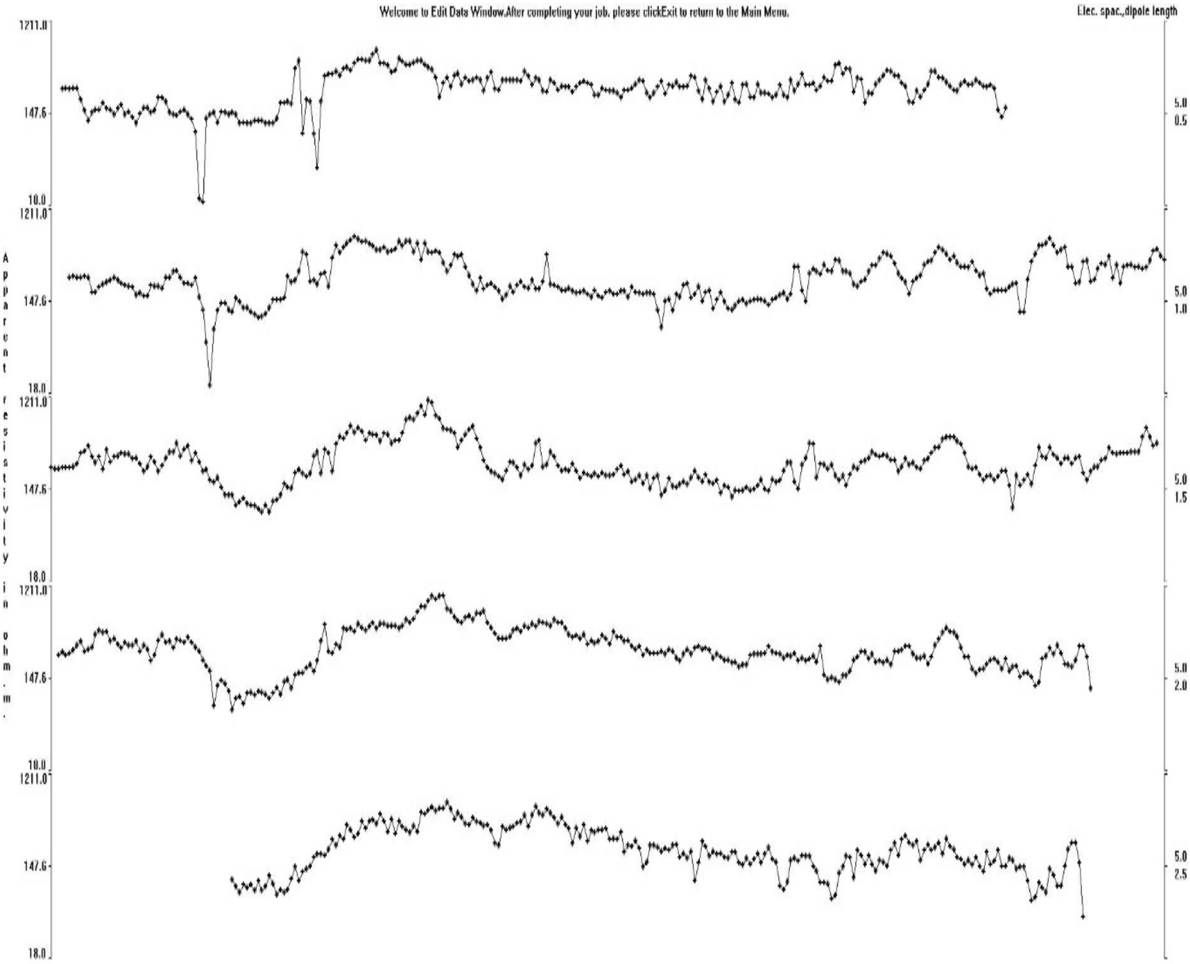
Welcome to Edit Data Window.After completing your job, please clickExit to return to the Main Menu.

Figure 5.9: *Layout of data points for dataset 4. On right side (on Y-axis), apparent resistivity is written and on left side (on Y-axis), electrode spacing and dipole length is written.*

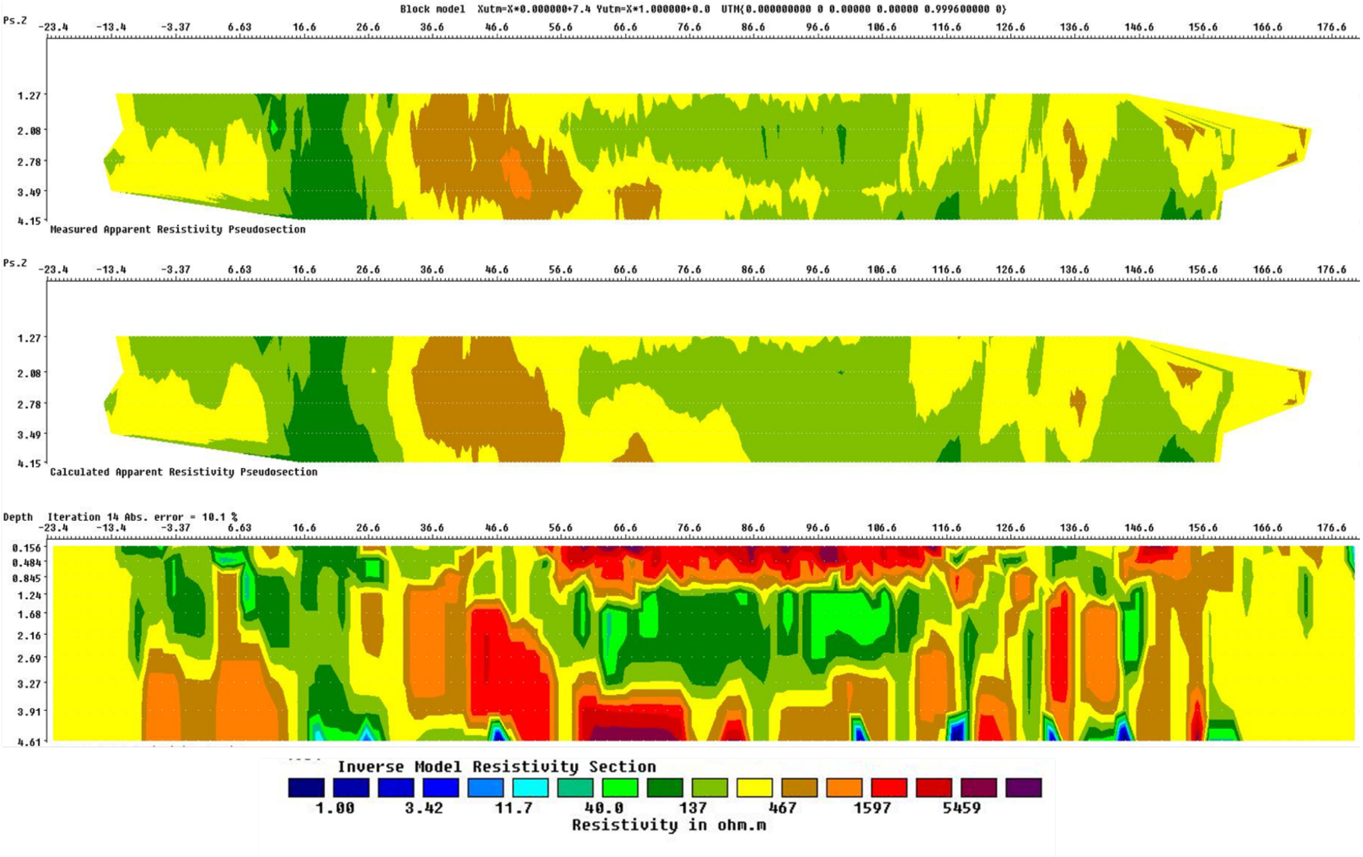

Figure 5.10: *Inversion result of dataset 4 after manual removal of noisy data points. The investigation depth is 4.61m. Range of resisitivity is between 1 to 6000 Ωm. The RMS value is 10.1%.*

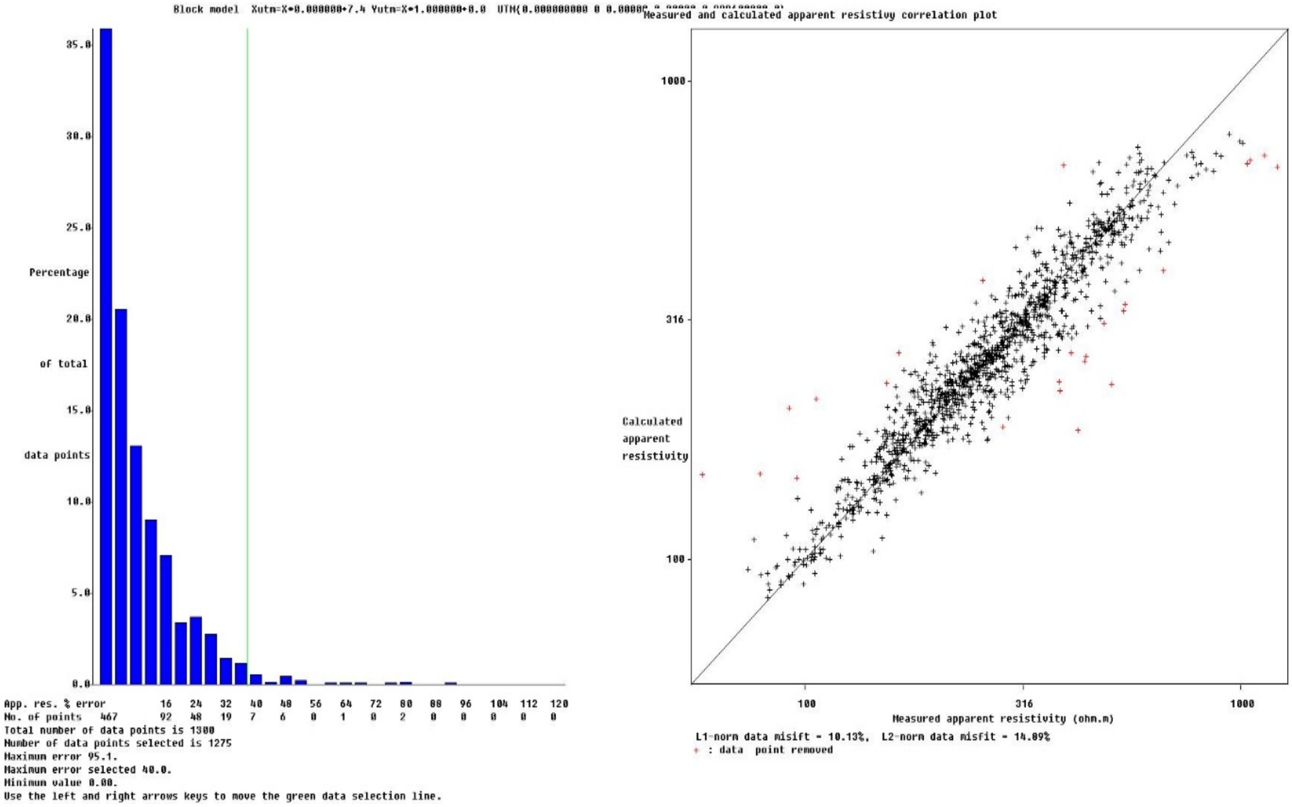

```
App. res. % error        16   24   32   40   48   56   64   72   80   88   96   104  112  120
No. of points   467      92   48   19   7    6    0    1    0    2    0    0    0    0    0
Total number of data points is 1300
Number of data points selected is 1275
Maximum error 95.1.
Maximum error selected 40.0.
Minimum value 0.00.
Use the left and right arrows keys to move the green data selection line.
```

```
L1-norm data misift = 10.13%,  L2-norm data misfit = 14.89%
+ : data  point removed
```

Figure 5.11: *Removal of outliers. Percentage of total number of data points (on left side) and (on right side) scatter plot between resistivity values (calculated vs measured).*

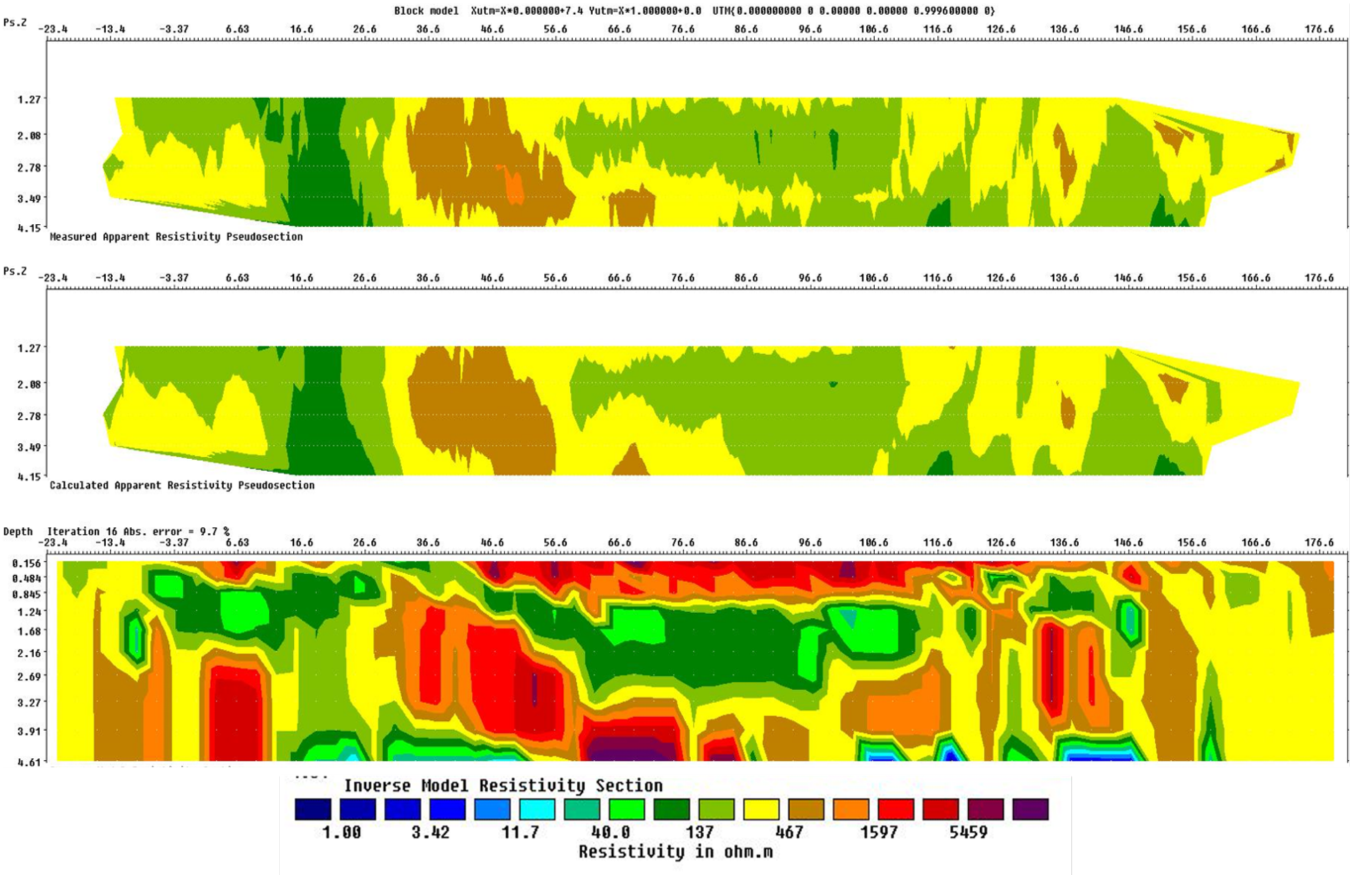

Figure 5.12: *Inversion result of dataset 4 after removal of outliers. The investigation depth is 4.61m. Range of resisitivity is between 1 to 6000 Ωm. The RMS value is now 9.7%.*

5.1.2.2. Dataset 5 alone

In dataset 5, total number of data points are 1295. Figure 5.13, total number of data points are shown with apparent resistivity range in Ωm. Some data points are removed to improve the data and to process the inversion.

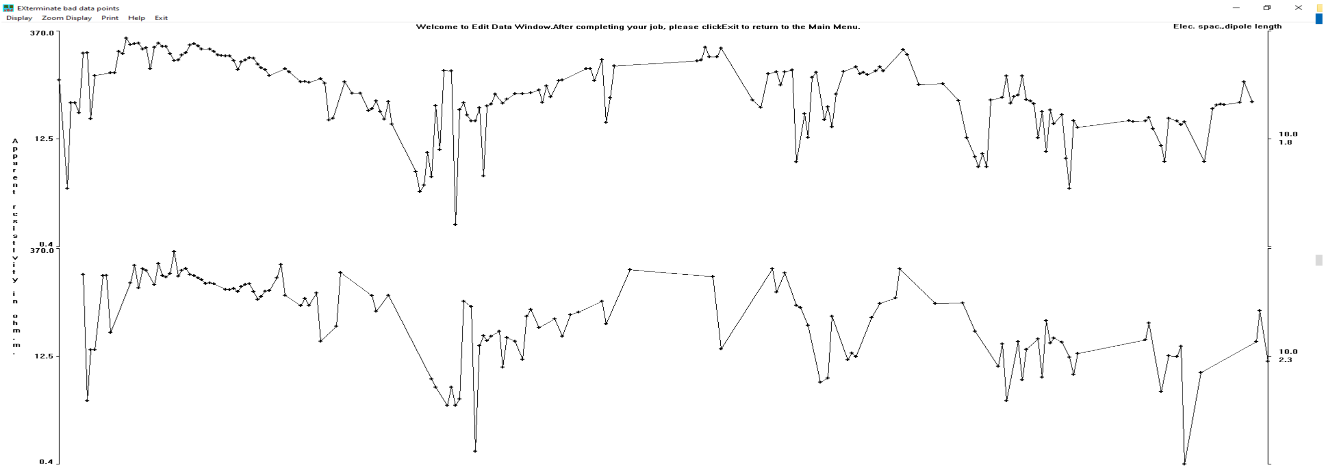

Welcome to Edit Data Window.After completing your job, please clickExit to return to the Main Menu.

Figure 5.13: *Layout of data points for dataset 5. On right side (on Y-axis), apparent resistivity is written and on left side (on Y-axis), electrode spacing and dipole length is written.*

Inversion is being done after manually removing bad points from dataset 5 while using Res2DInv software. The investigation depth is recorded as 7.17 m after 10 iteration and the RMS value is 19% (figure 5.14).

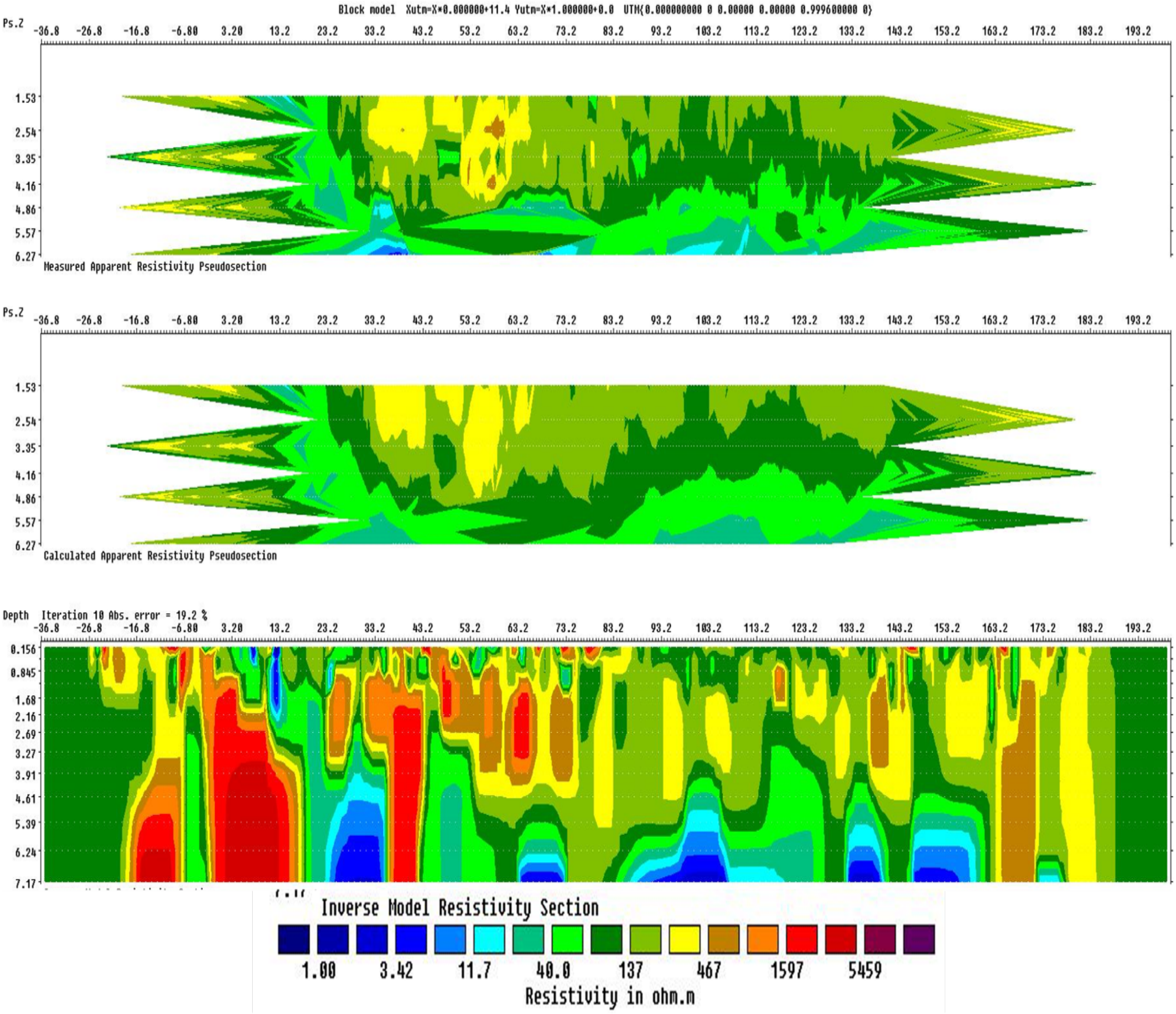

Figure 5.14: *Inversion result of dataset 5 after manual removal of bad points. The investigation depth is 7.17m. Range of resisitivity is between 1 to 6000 Ωm.*

Some outliers are also automatically removed to improve the resolution of the inversion result. So, in figure 5.15, RMS value is decreased up to 13% after 10 iterations.

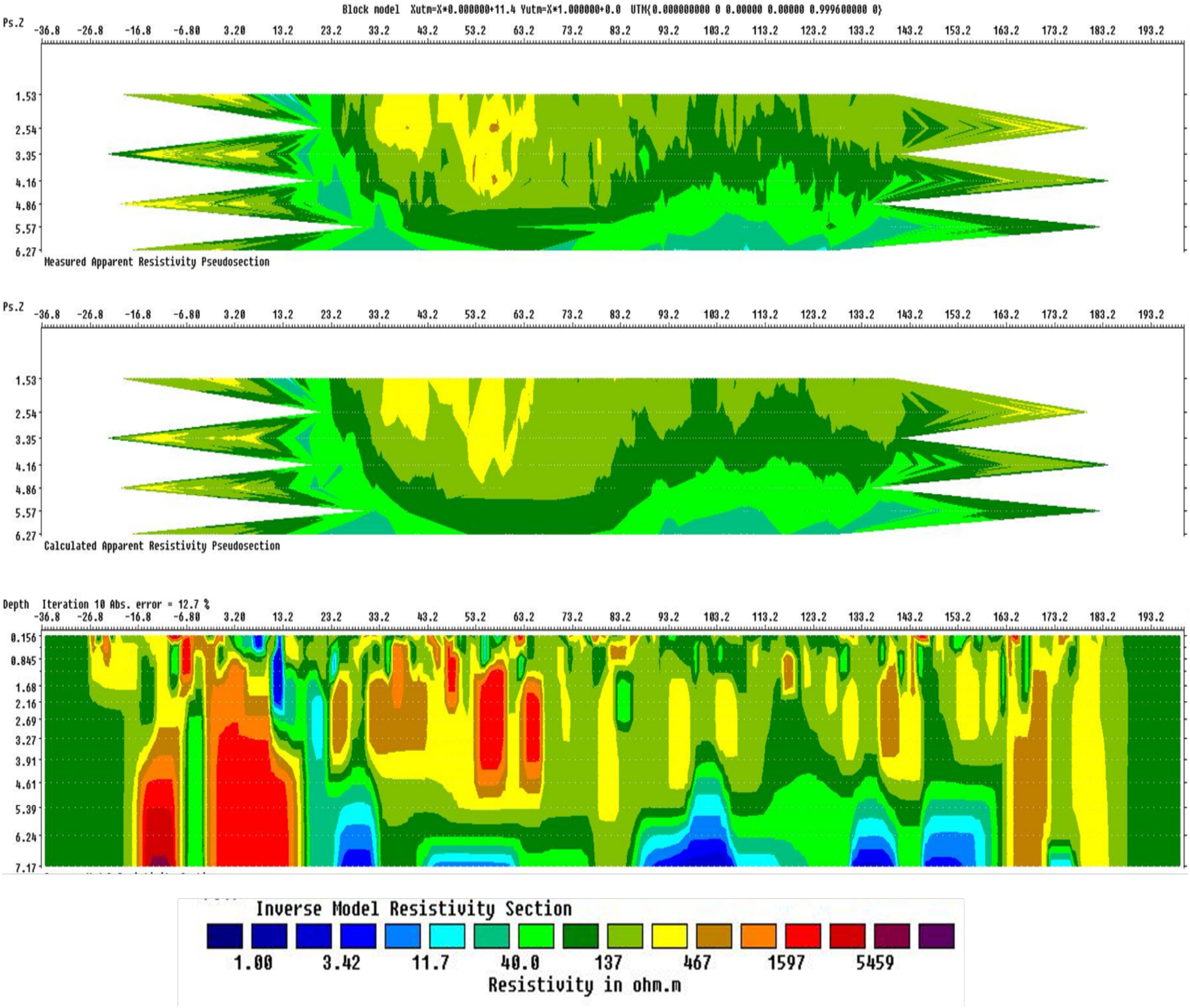

Figure 5.15: *Inversion result of dataset 5 after automatic removal of outliers. The investigation depth is 7.17m. Range of resisitivity is between 1 to 6000 Ωm.*

5.1.2.3. Merging of datasets 5 and 1

The reason behind merging these two datasets are; both have the same dipole cable length (10 m) and the survey or profile line length (160 m) is also same. Rope length for dataset 1 is just 17.5 m but the rope length for dataset 5 is from 2.5 m to 15 m. So, merging these two datasets can provide deeper information of the of subsurface.

Data points for dataset 1 is 281 and data points for dataset 5 is 1295. After merging these datasets, the total number of data points are 1576.

Figure 5.16, inversion result is obtained after removal of bad points with 27 % RMS value and after 10 iterations with 8.20 m (deeper) investigation depth.

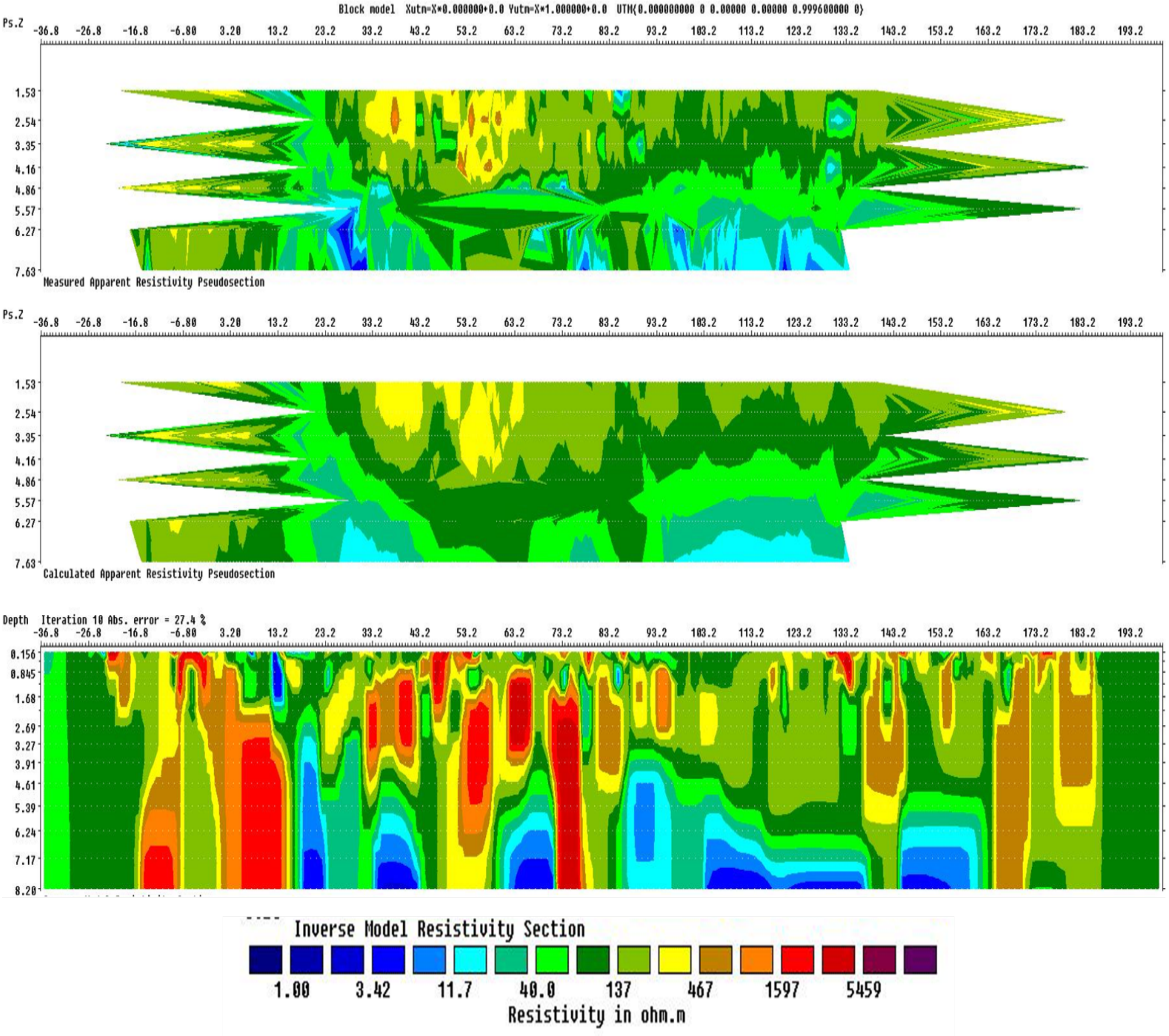

Figure 5.16: *Inversion result of dataset 5+1 manual removal of bad points. The investigation depth is 8.20m. Range of resisitivity is between 1 to 6000 Ωm.*

After automatic removal of outliers, the inversion result gets less RMS value of 23% after 10 iterations (figure 5.17).

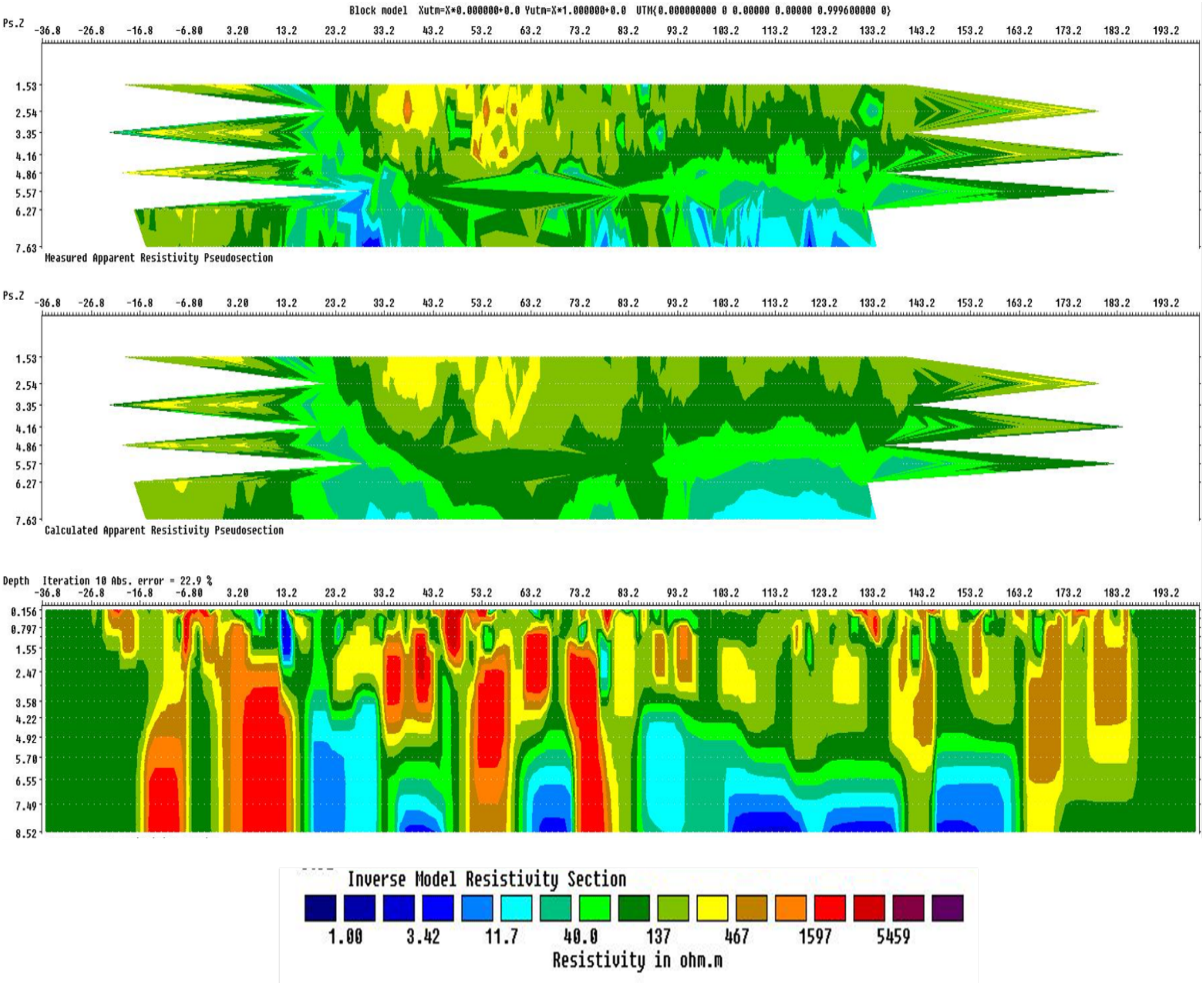

Figure 5.17: *Inversion result of dataset 5+1 after automatic removal of outliers. The investigation depth is 8.52m. Range of resisitivity is between 1 to 6000 Ωm.*

5.1.2.4. Merging of Dataset 1, 4, and 5

To get deeper information on the subsurface, all three datasets have been merged and then processed through Res2DInv. In dataset 1+4+5, the total data points are 2940. After manually removing bad points, the inversion is processed. All of three datasets have same electrode spacing of 0.625 m. In figure 5.18, the inversion result shows the investigation depth up to 8.20 m after 10 iteration and the RMS error value is 34%.

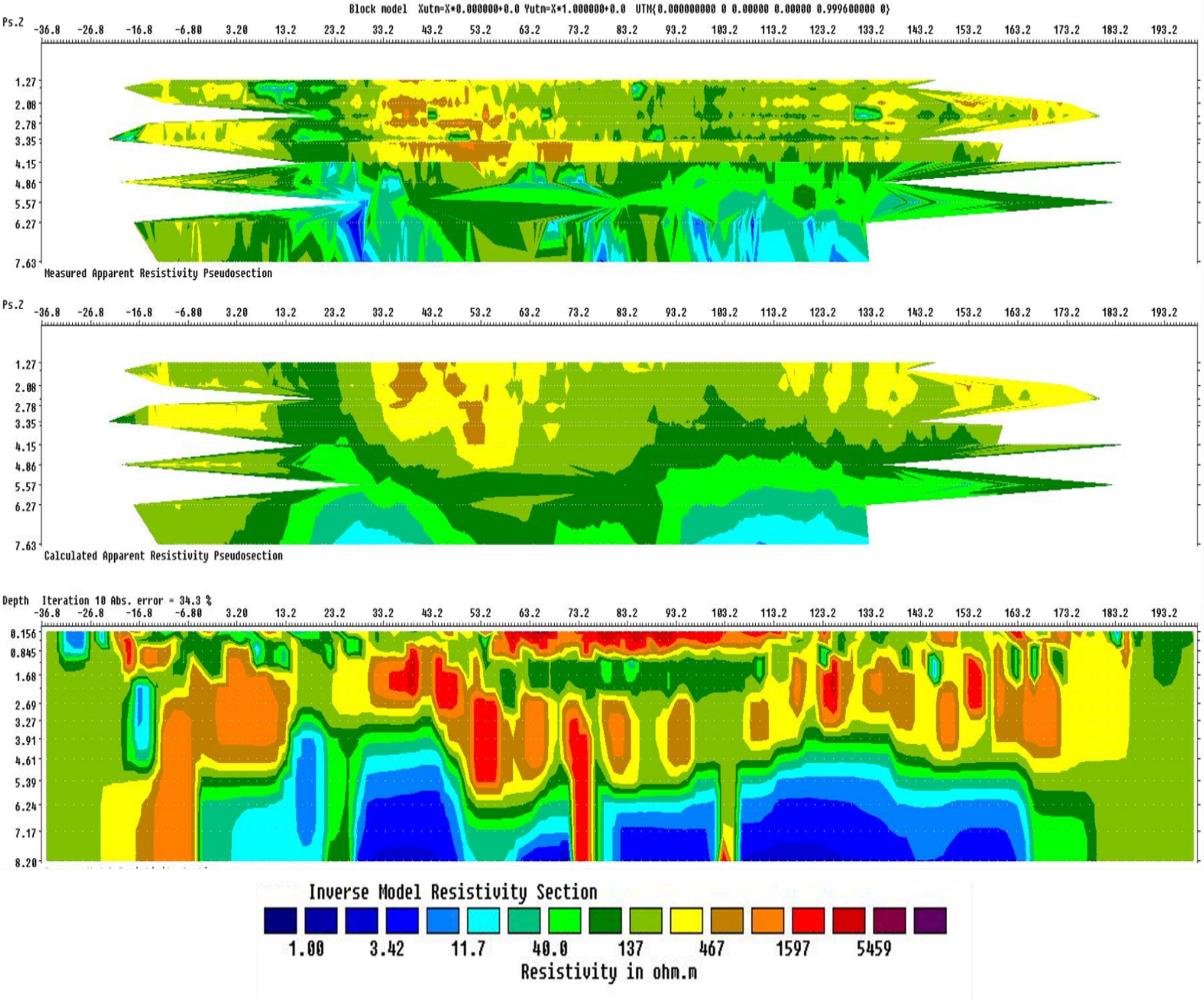

Figure 5.18: *Inversion result of dataset 1+4+5 after manual removal of bad points. The investigation depth is 8.20m. Range of resisitivity is between 1 to 6000 Ωm.*

Inversion result after automatic removal of outliers, the RMS error values goes to 27 % after 10 iterations with same investigation depth that is 8.20 m (Figure 5.19). We believe that the RMS is higher for the merged dataset than for the individual datasets because of the misalignment of the streamer during the successive paths. The resulting image in figure 5.19 brings more information than the previous models and it eases the geological interpretation.

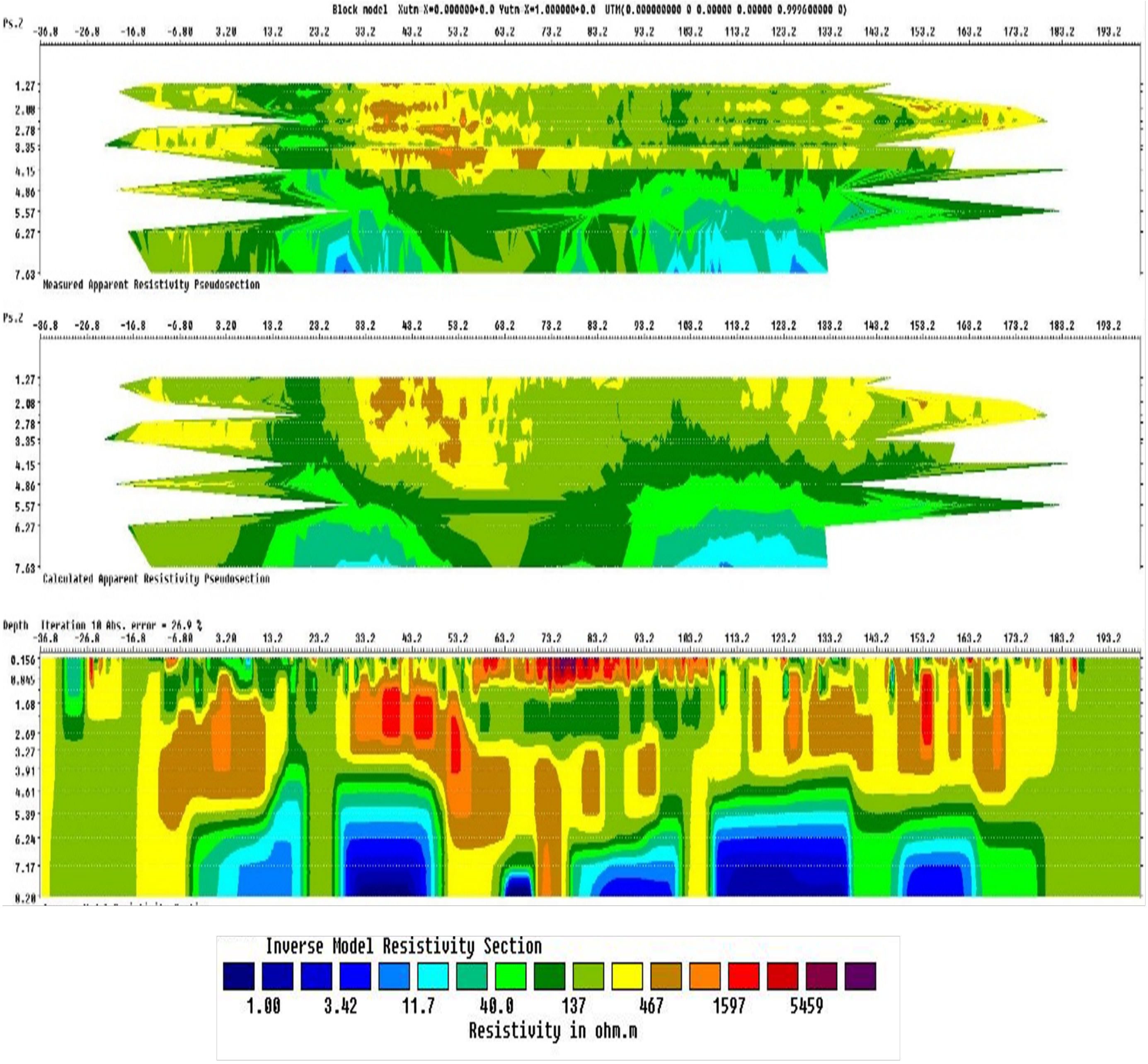

Figure 5.19: *Inversion result of dataset 1+4+5 after automatic removal of outliers. The investigation depth is 8.20m. Range of resisitivity is between 1 to 6000 Ωm.*

The depth of active layer was measured manually during survey by using a graduated metallic rod. The maximum depth was recorded as 60 cm along the profile (figure 5.20).

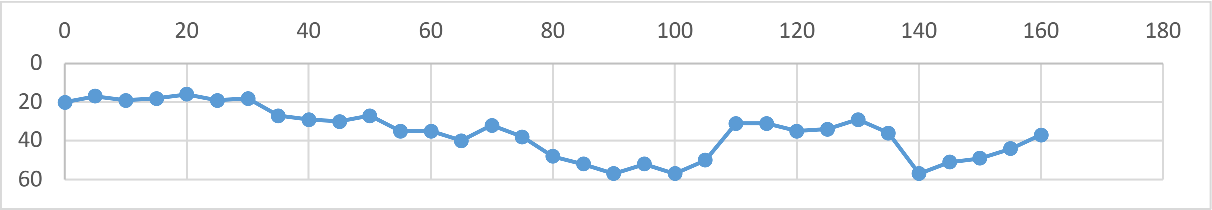

Figure 5.20: *Depth of active layer in cm, measured manually while measuring OhmMapper profile in UNIS site on 5th July, 2019.*

5.1.2.5. Terrameter results from UNIS site

NGI and NGTS had previously investigated the resistivity structure at the UNIS East site with a Terrameter device in September 2017 (Gilbert, 2020). Figure 5.21, shows the resulting resistivity model processed with Res2DInv software. The Investigation depth is 30 m. The number of iterations are 5. The color scale for this Resistivity profile is different from the OhmMapper's profile. The depth of active layer was measured manually with a graduated metallic stick in September, 2017. The average depth of active layer was 79 cm during Terrameter survey (figure 5.22).

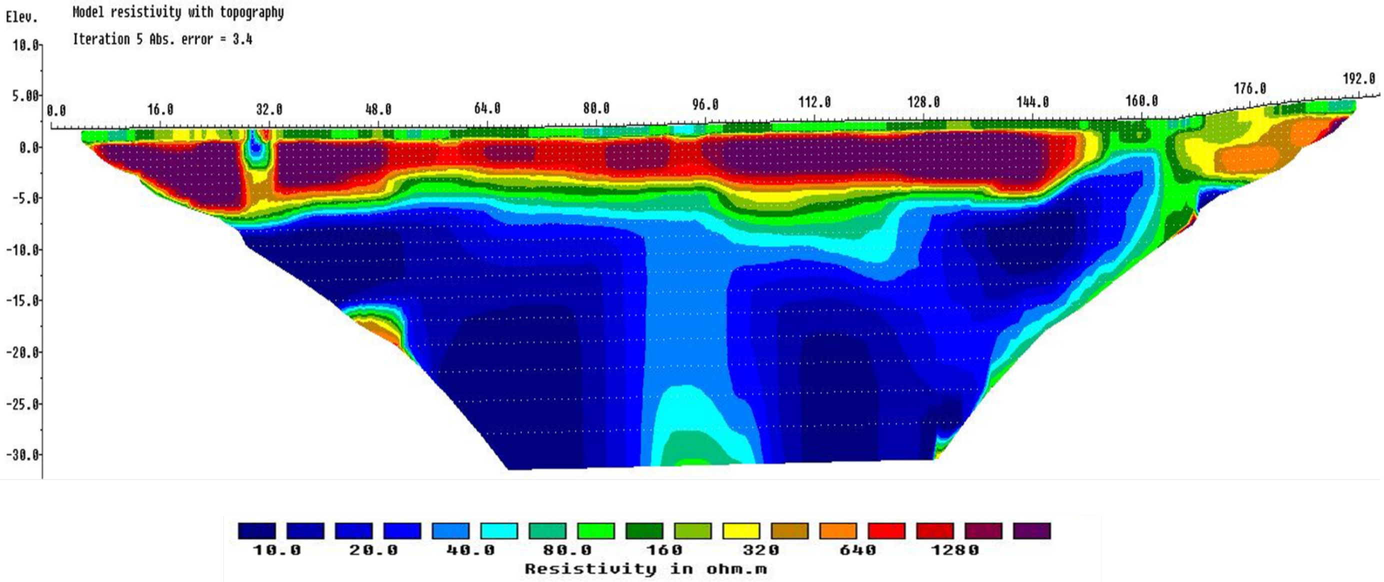

Figure 5.21: *Resistivity profile of UNIS site measured in September 2017 with a Terrameter and processed by Res2DInv software. The investigation depth is 30 m. Figure from (Gilbert, 2020).*

Figure 5.22: *Depth of the active layer (in cm) measured in September 2017 while conducting Terrameter Survey. The average depth value is 79 cm (Bazin et al., 2021).*

5.2. Adventdalen site

Two surveys in "map mode" (datasets 2 and 5) and one survey in "single profile" (dataset 1) were acquired at the Adventdalen site.

5.2.1. Results from Magmap2000

5.2.1.1. Dataset 2

Dataset 2 is acquired along Y-axis and this data is a part of map survey and has 21 profile lines and each profile line is 100 m long. Some important properties of dataset 2 is given in table 5.4.

Number of profile lines	21
Start point	NW
End point	SW
Rope length	5 m
Cable length	2.5 m
Dipole cable length	5 m
Mark points	10 m
Line spacing	5 m

Table 5.4: *Parameters of dataset 2 acquired along the Y- axis while performing a survey in "map mode".*

Some changes have been done in geometry of dataset 2 (figure 5.23). Two profile lines (line number 6 and 7) are removed as these are producing some artefacts in resistivity map (figure 5.25). Further, to remove noisy data points, filters such as despiking and dropouts are used to improve the OhmMapper readings (figure 5.24).

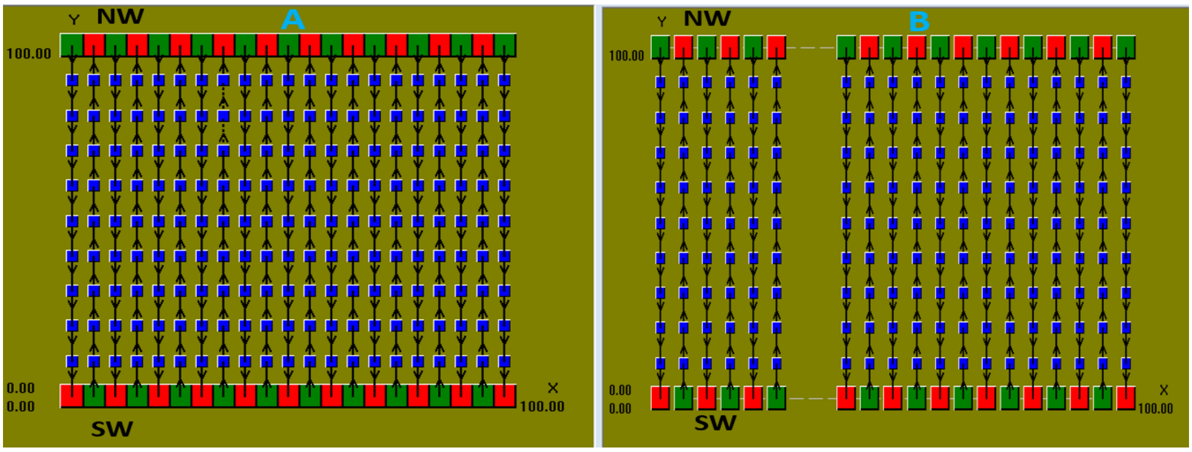

Figure 5.23: *Geometry changes in dataset 2. On left, "A" is original geometry and on right side, "B" is the modified geometry after removing line number 6 and 7. Mark spacing after 10 m and line spacing is 5 m.*

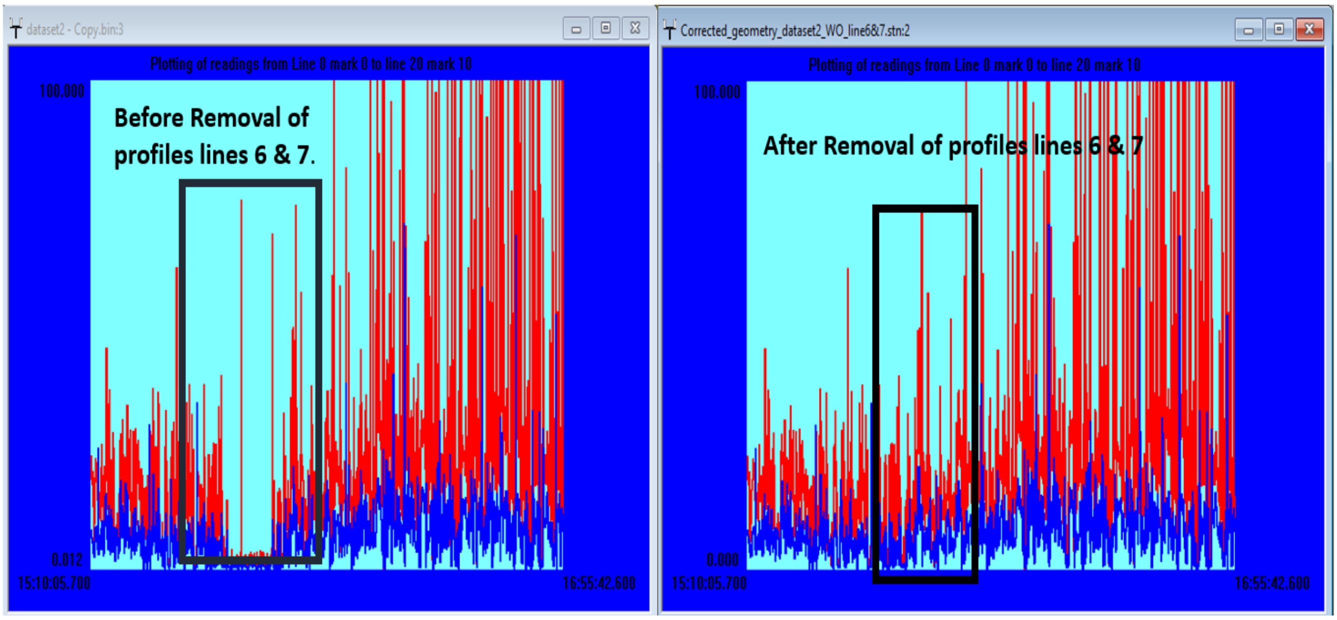

Figure 5.24: *Changes in OhmMapper Reading after removal of profile line 6 and 7. Red Color curve represents one receiver and the blue curve is showing data received from second receiver.*

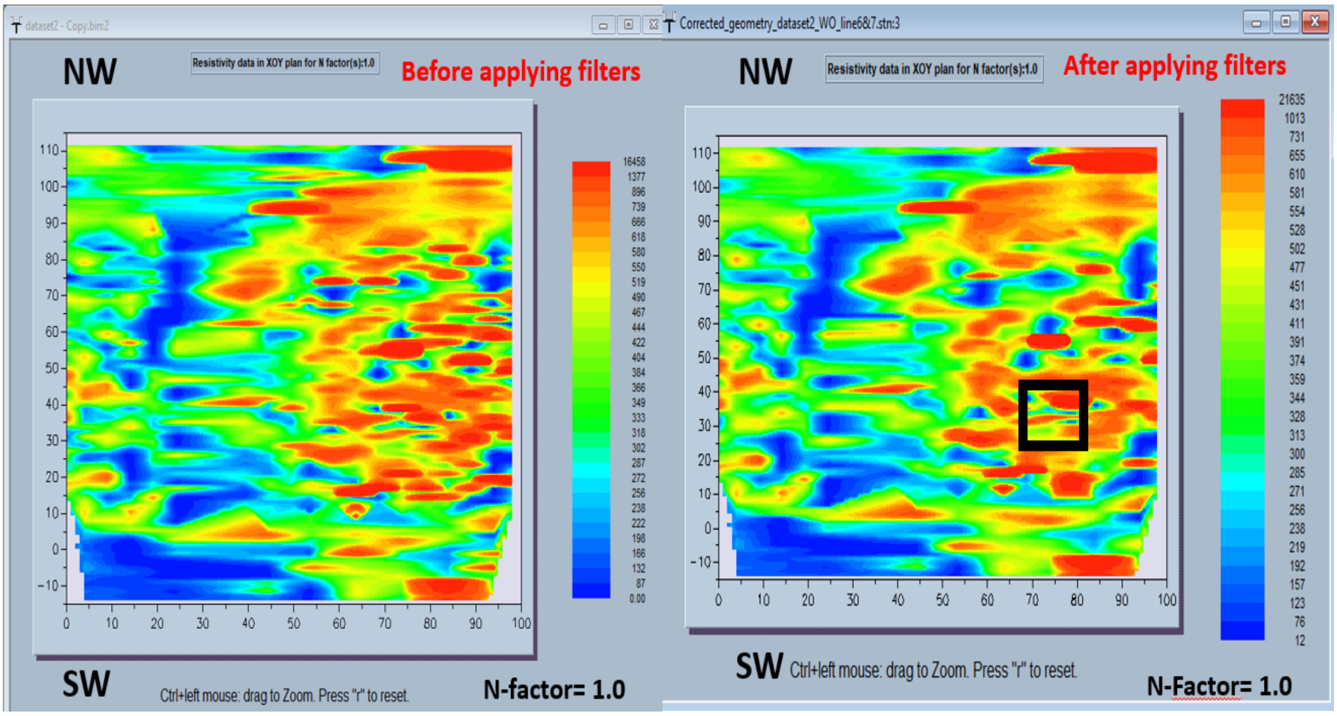

Figure 5.25: *Comparison of apparent resistivity map before and after applying filters (despiking and dropout) and removal of line 6 and 7 (on left).*

5.2.1.2. Dataset 5

Dataset 5 is gathered along X-axis and this data is also a part of map survey and has 21 profile lines and each profile line is 100 m long. Some important properties of dataset 5 is given below in table 5.5.

Number of profile lines	21
Start point	SE
End point	SW
Rope length	2.5 m
Cable length	2.5 m
Dipole cable length	5 m
Mark points	10 m
Line spacing	5 m

Table 5.5: *Parameters of dataset 5 acquired along the X-axis while performing map survey.*

After a few adjustments in the geometry (figure 5.26) and applying filters such as despiking and dropouts (figure 5.27) to remove some bad points causing artefacts in the resistivity map (figure 5.28), the dataset can be exported into Res3DInv format.

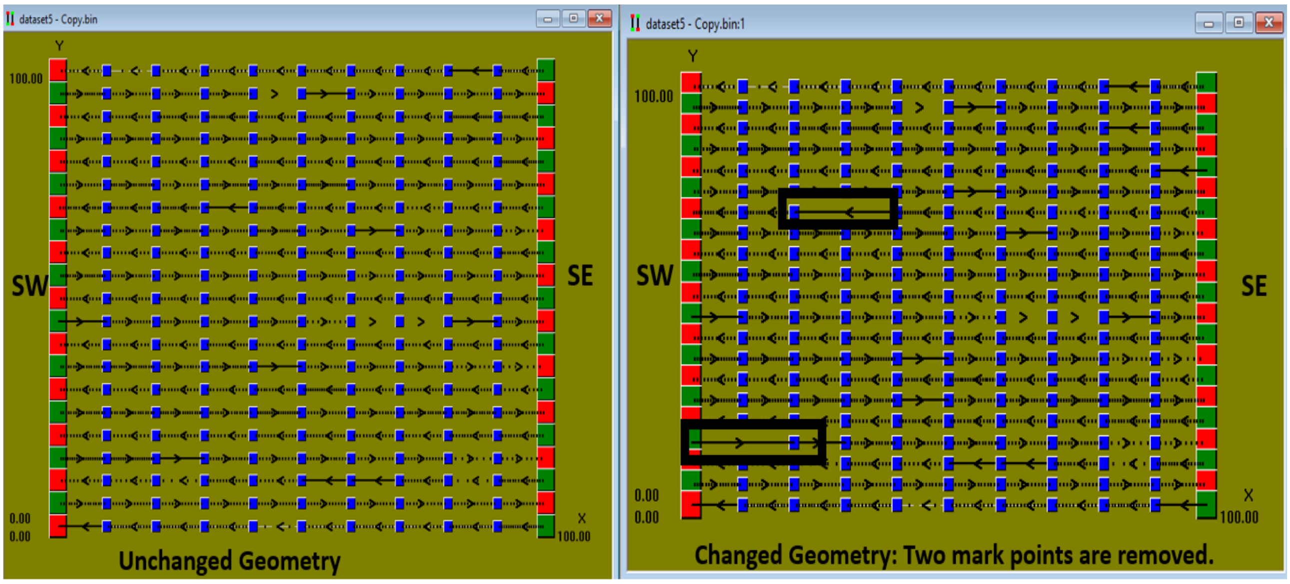

Figure 5.26: *Geometry changes in dataset 5. On left, "A" is original geometry and on right side, "B" is the modified geometry after removing two points from line number 3 and 14.*

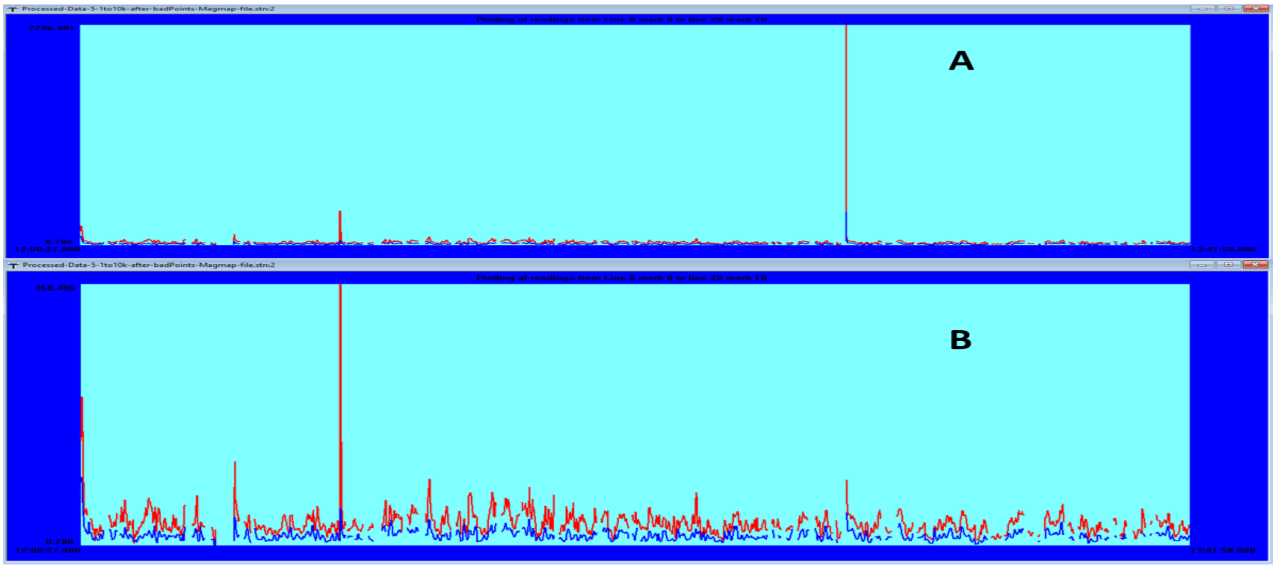

Figure 5.27: *Changes in OhmMapper Reading after removal of two points from profile line number 3 and 14. Red Color curve represents one receiver and the blue curve is showing data received from second receiver.*

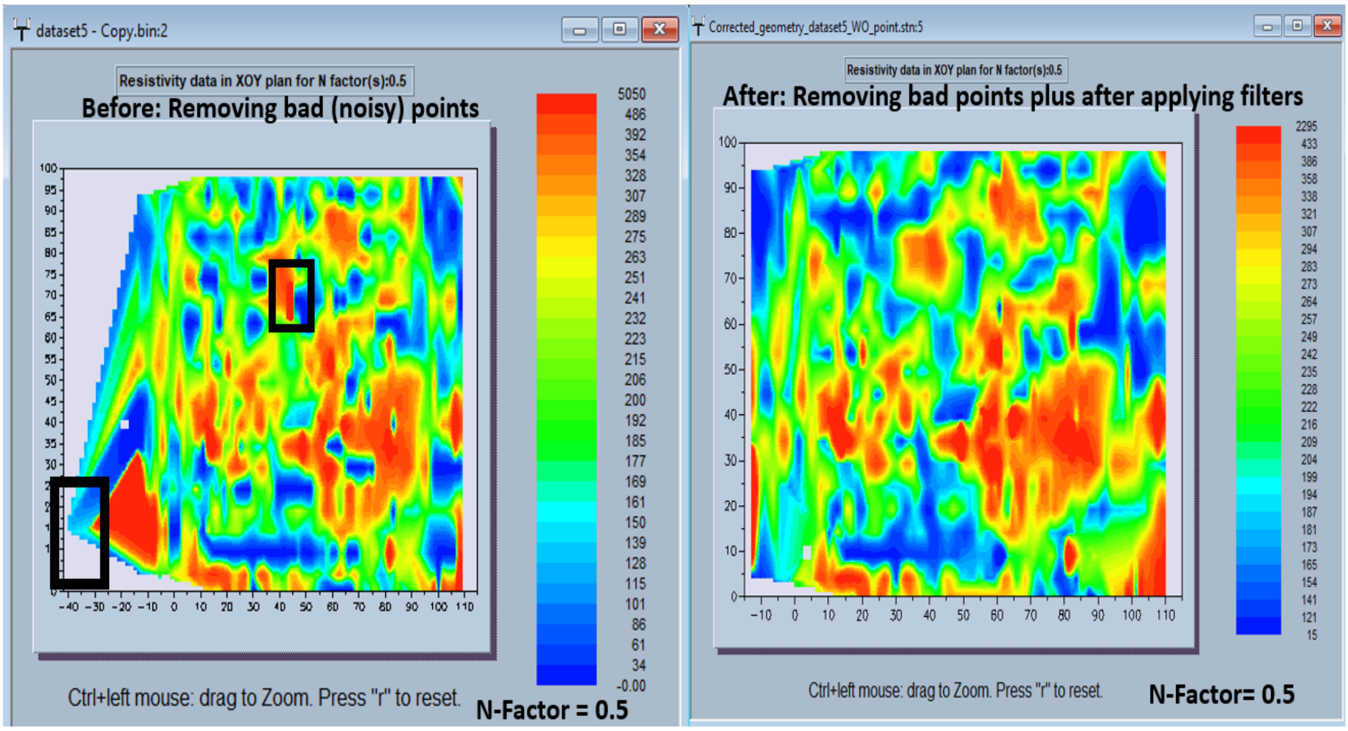

Figure 5.28: *Apparent Resistivity map: before removal noisy points (from line number 3 and 14) on left side, and after removing noisy point on right side. The black boxes are the points that are showing some artefacts or noisy part in apparent resistivity map.*

5.2.1.3. Dataset 1 (50 m long profile)

Dataset 1 is gathered along the Y-axis and it is part of simple survey and has 11 profile lines and each profile line is 50 m long. Some important characteristics of dataset 1 is given in table 5.6.

Number of profile lines	11
Start Point	NW
End point	SW
Rope length	2.5, 5, 7.5, 10, 12.5, 15, 17.5, 20 m
Cable length	2.5 m
Dipole cable length	5 m
Mark points	10 m
Line spacing	5 m
n- factor	0.5 to 2.0

Table 5.6: *Characteristics of dataset 1 while performing simple survey.*

Geometry of dataset 1 is with 11 survey lines can be seen in figure 5.29. OhmMapper reading is clearly showing the difference after applying the filters such as despiking and dropouts (figure 5.30). The black box in pseudo-section shows an artefact that could be due to the river bank (figure 5.31).

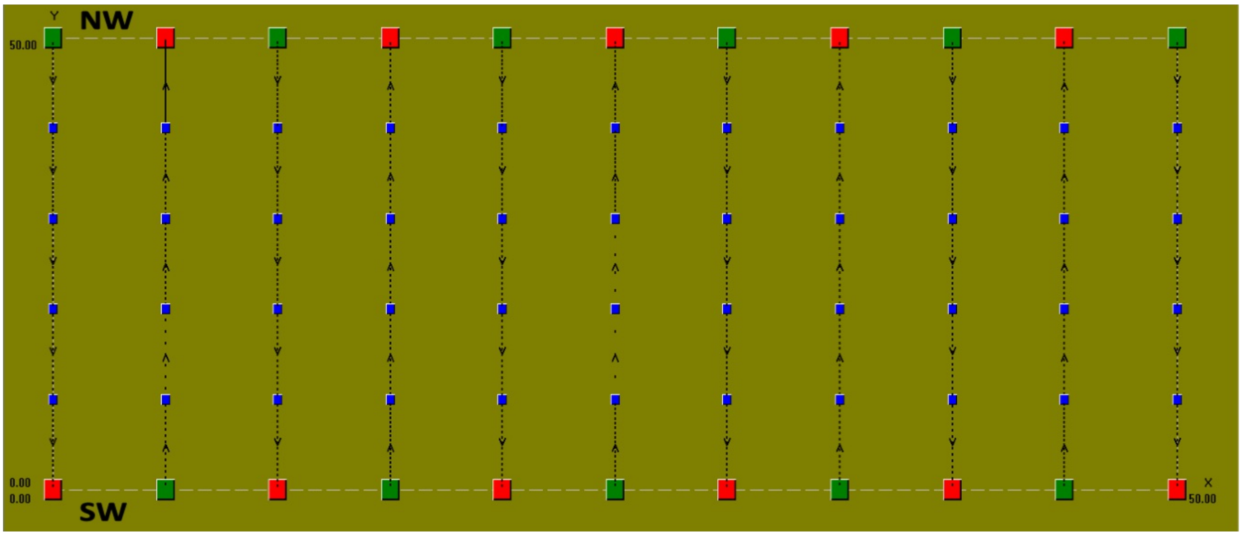

Figure 5.29: *Geometry of dataset. A 50 m long profile was acquired by 11 passes.*

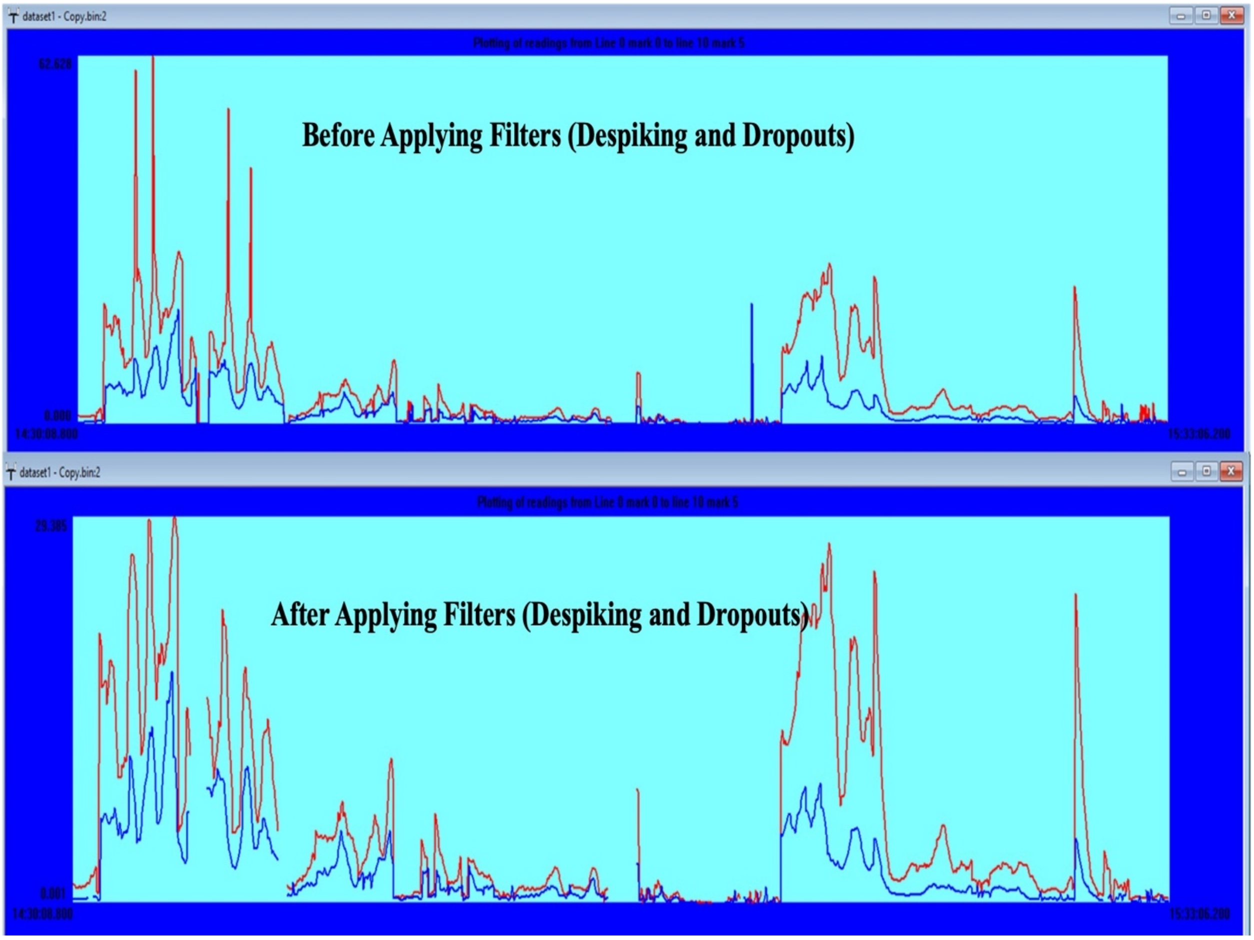

Figure 5.30: *Changes in OhmMapper reading after applying filters in dataset 1. Red color curve represents one receiver and the blue curve is showing data received from second receiver.*

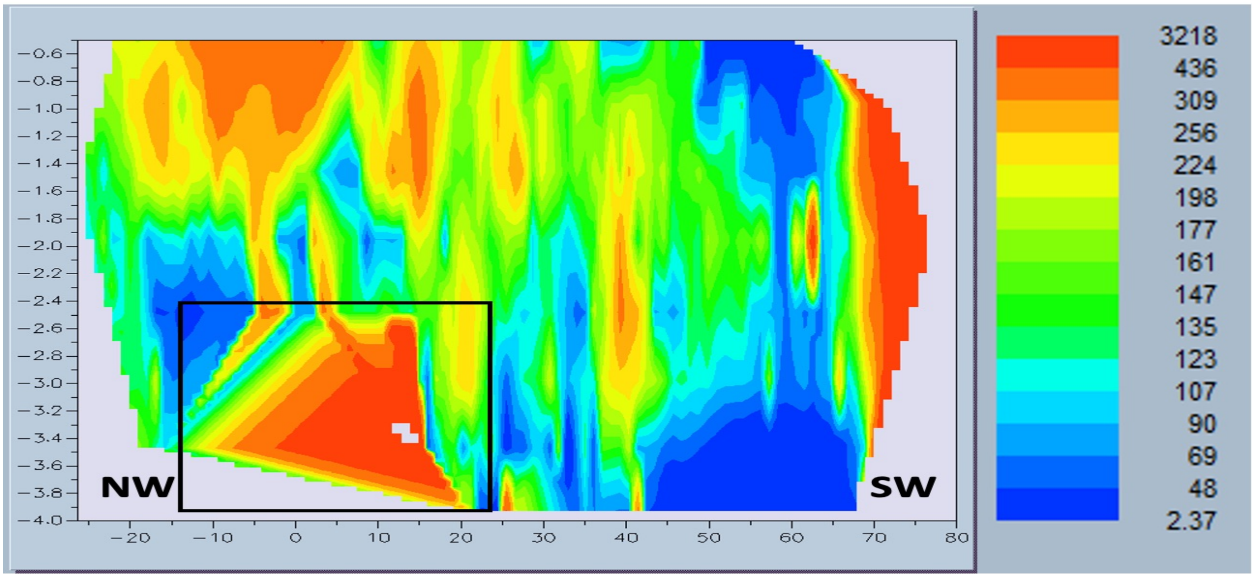

Figure 5.31: *Pseudo-section of dataset 1 with pseudo-depth on Y-axis and distance along the profile on x-axis. The black box shows an artefact that could be due to the river bank.*

5.2.2. Res3DInv results

3-D inversions are obtained with Res3DInv software using the datasets exported from the Magmap2000 software, using an averaging over 0.5m spacing. The resistivity grids are viewed using the “professional 3-D Viewer” option.

5.2.2.1. Dataset 2

In figure 5.32, after 9 iterations the inversion result with 16 % RMS error has been observed and this data set is along Y-axis started from NW to SW. The resistivity range is from 1 to 8000 Ωm. While comparing the resistivity model with the digital elevation model (DEM) of the study area, it is difficult to find feature that could be interpreted geologically (figure 5.33). Table 5.7, summarizes the RMS value after each iteration. The depth of investigation is measured while using simple inversion model and it is 2.94 m (figure 5.34).

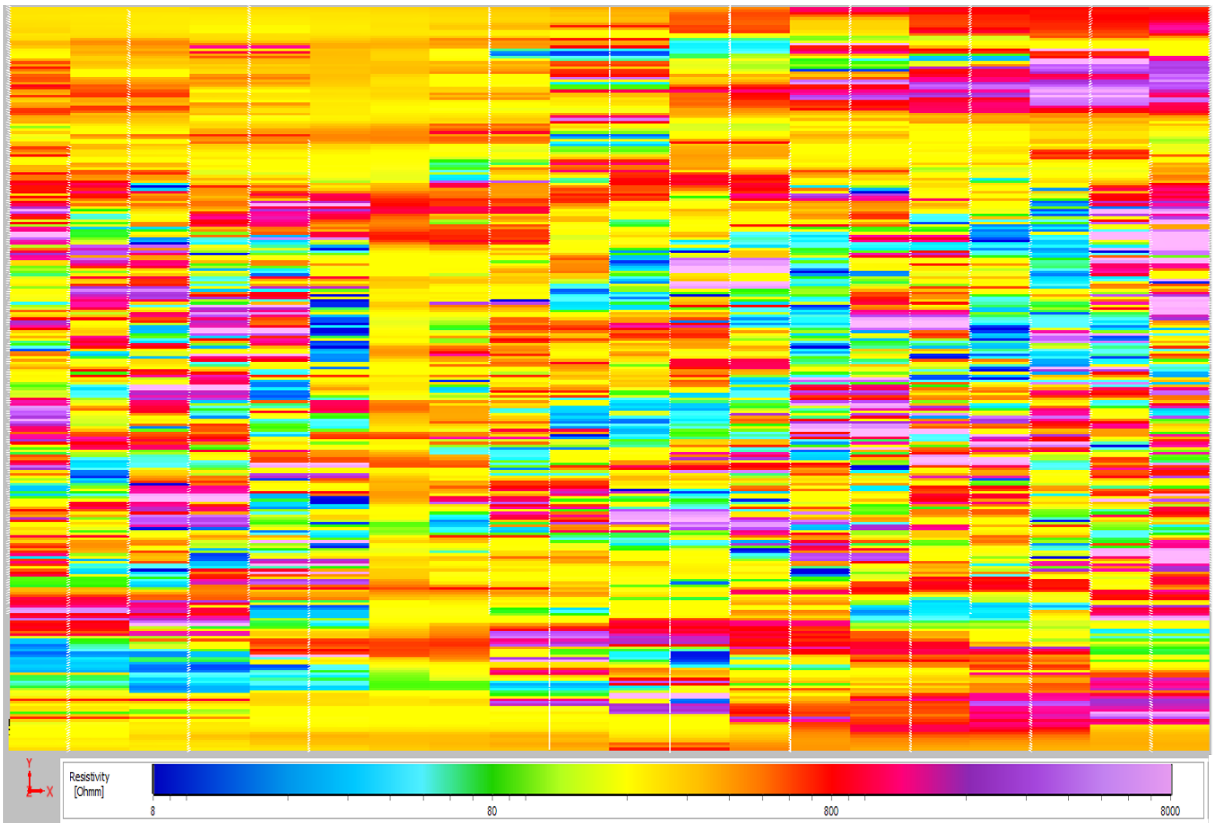

Figure 5.32: *Inversion result of dataset 2 from Res3DInv software. Range of resistivity is from 8 to 8000 Ωm. Number of iterations are 9 and the RMS value is 16% with depth of investigation is 2.94 m.*

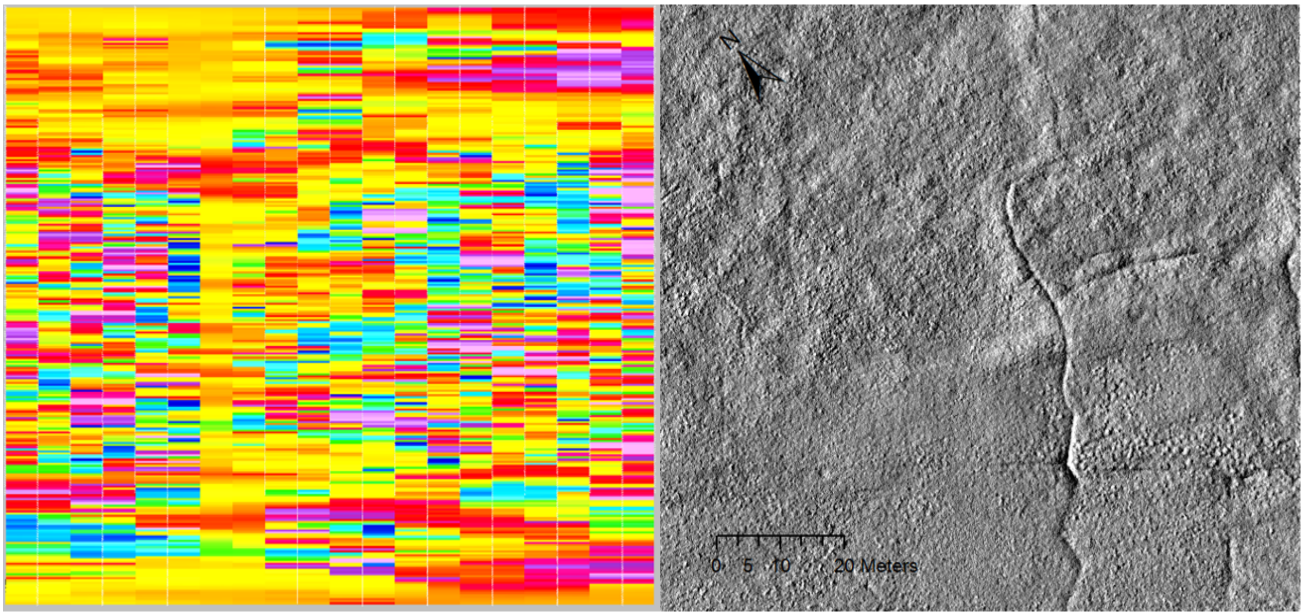

Figure 5.33: *Comparing inversion result of dataset 2 with the DEM of the study area (Adventdalen site).*

Number of iterations	RMS value (%)
1	61
2	35
3	29
4	24
5	21
6	19
7	18
8	17
9	16

Table 5.7: *RMS value for each iteration.*

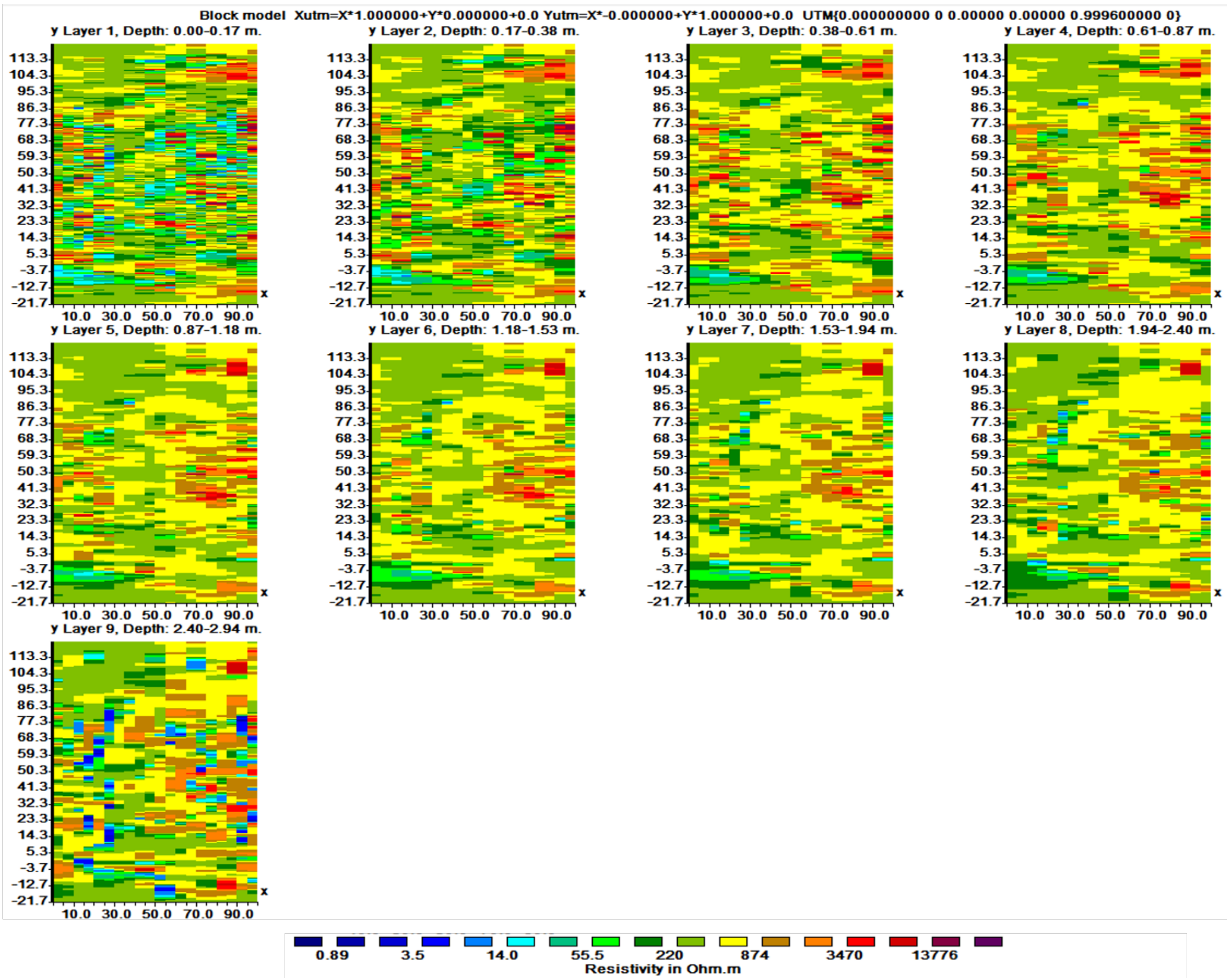

Figure 5.34: *Inversion result of dataset 2 presented at each layer of the 3-D grid. The depth of investigation is from 0 to 2.94m.*

In figure 5.35, the inverted 3D cube can easily be seen with transparency effect.

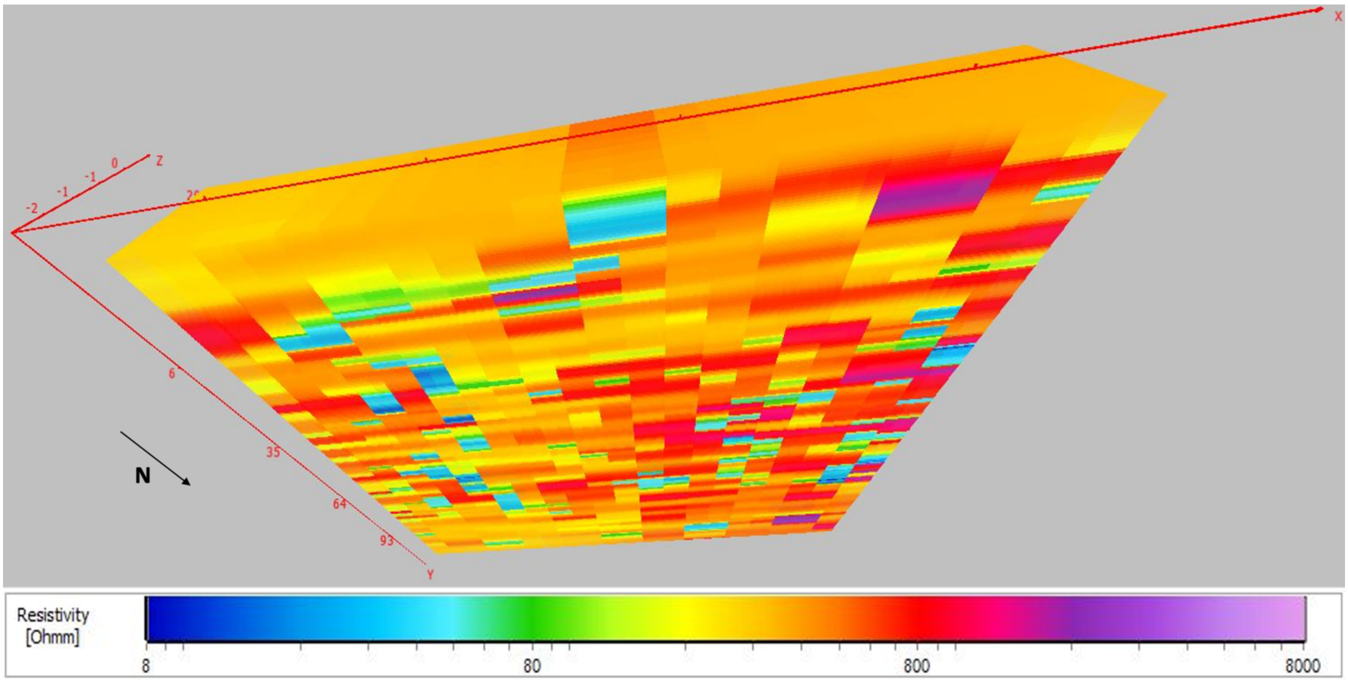

Figure 5.35: *Inversion result of dataset 2 (100m x 100m grid) illustrated with 3-D Viewer option.*

5.2.2.2. Dataset 5

After 5 iterations the inversion reaches 9 % RMS error (figure 5.36). Depth of investigation is 2.40 m. Table 5.8, summarizes the RMS value after every iteration. While comparing the resistivity model with DEM of the study area, some elongated resistive anomalies along linear features are observed in the topography (figure 5.37). These are interpreted as ice wedges. The main reason why these anomalies are visible in the inversion result of dataset 5 and not in dataset 2 might be due to the acquisition geometry. Indeed, dataset 5 profiles are run across the anomaly and there are more likely to detect anomalies across the linear features. The depth of investigation is measured while using simple inversion model and it is 2.40 m (figure 5.38).
In figure 5.39, a 3-D view of the model cube shows that the resistive structures go inside the ground and they are ice wedges.

Number of Iteration	RMS value (%)
1	22
2	18
3	13
4	10
5	9

Table 5.8: *RMS values in percentage after every iteration.*

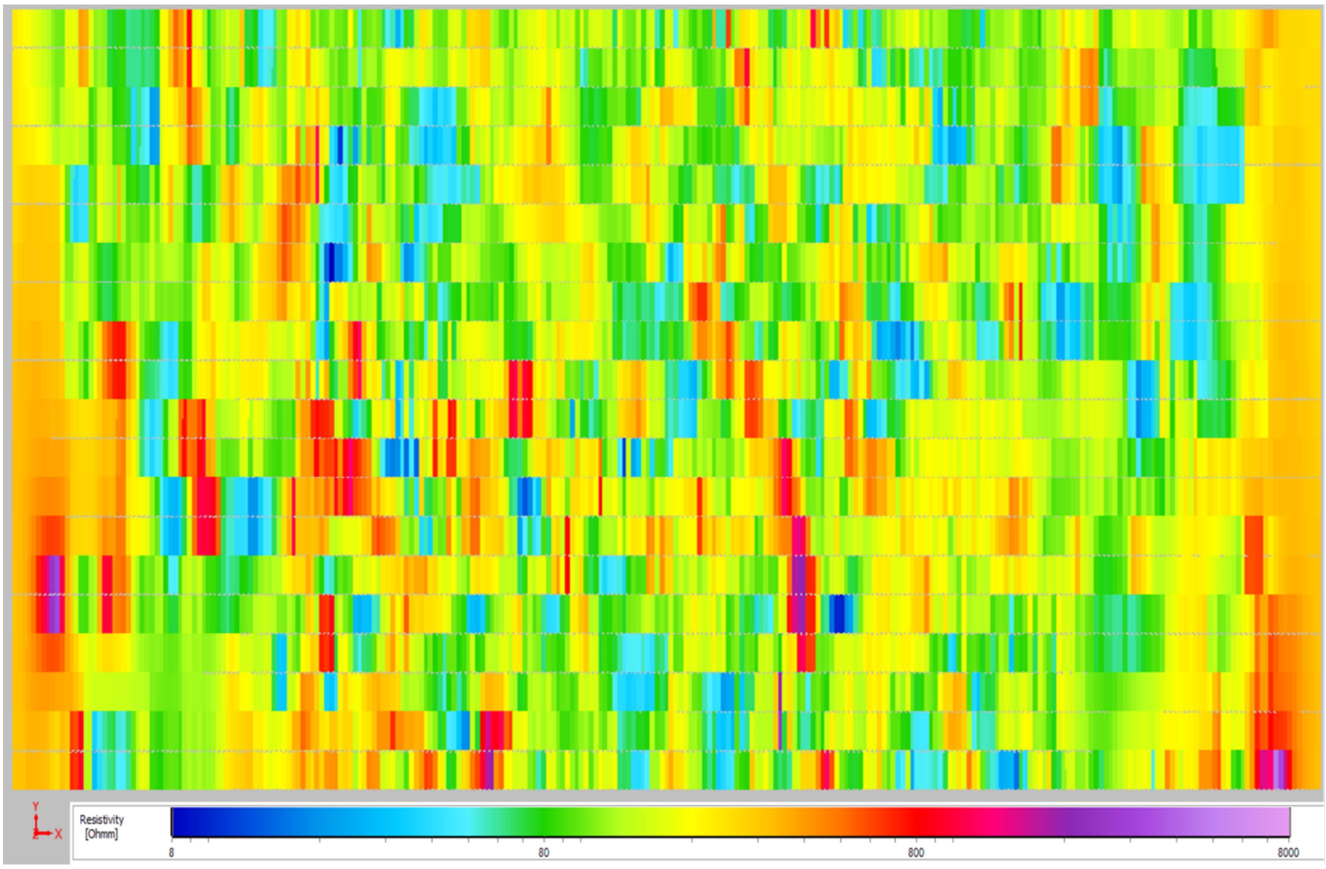

Figure 5.36: *Inversion result of dataset 5 obtained from 3-D Viewer in Res3DInv software. Range of resistivity is from 8 to 8000 Ωm. Number of iterations are 5 and the RMS value is 9% and depth of investigation is 2.40 m.*

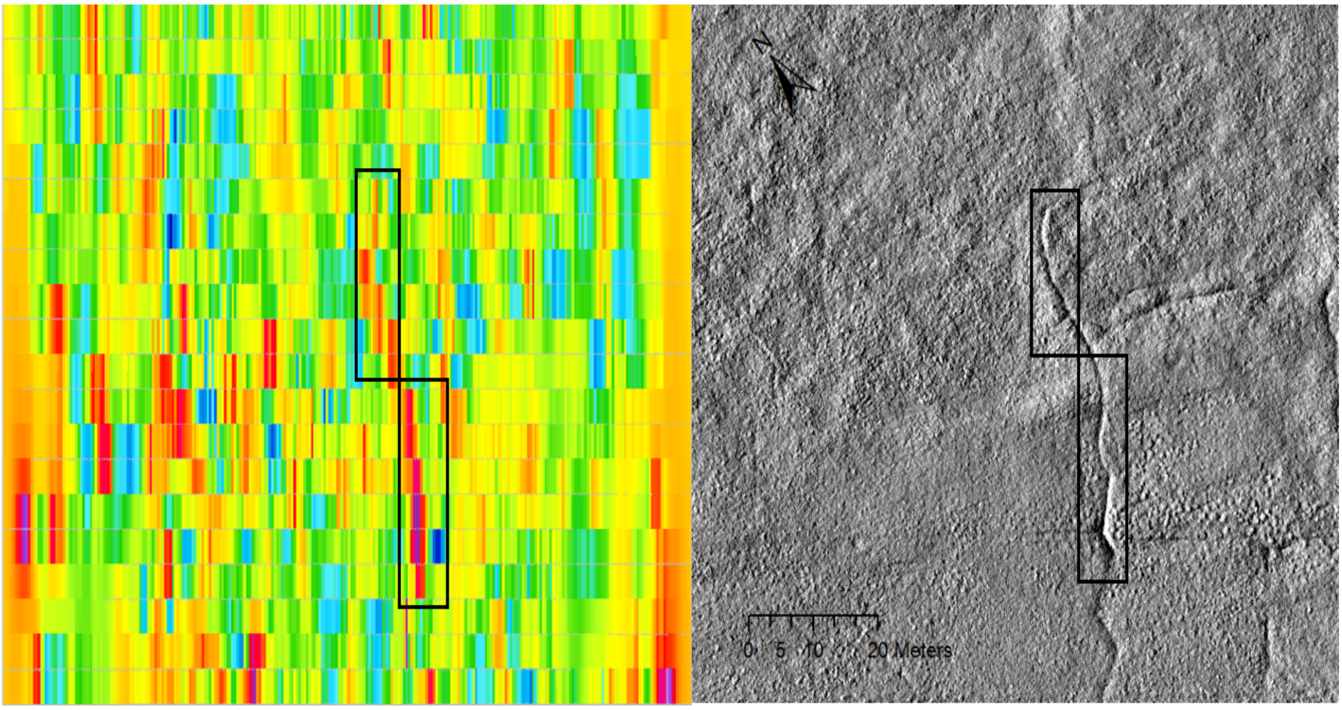

Figure 5.37: *Comparing inversion result of dataset 5 with DEM of the study area. The black box on inversion result (left side) and on DEM (right side) is the presence of resistive feature (ice wedge).*

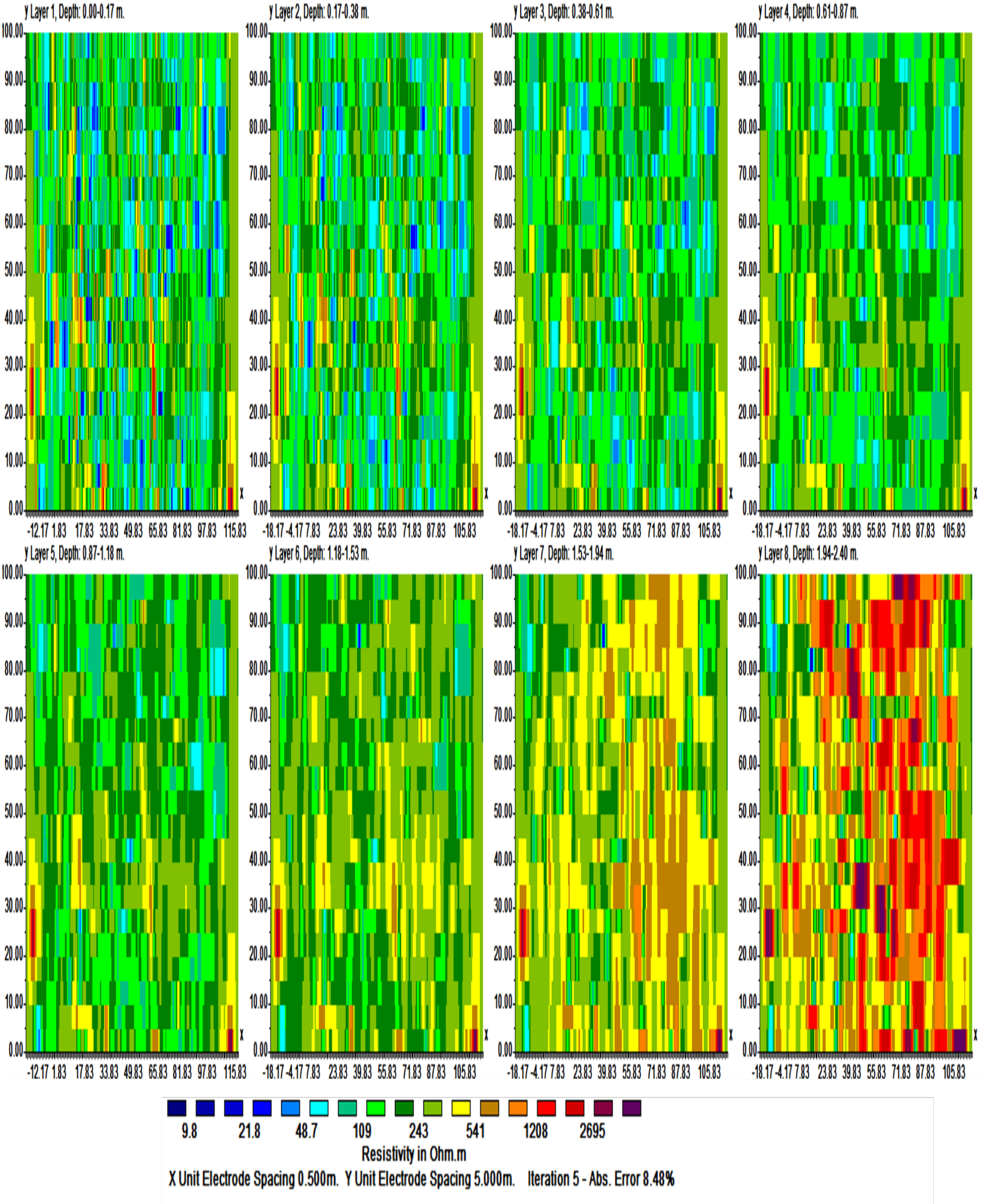

Figure 5.38: *Inversion result of dataset 5 presented at each layer of the 3-D grid. The depth of investigation is from 0 to 2.40m.*

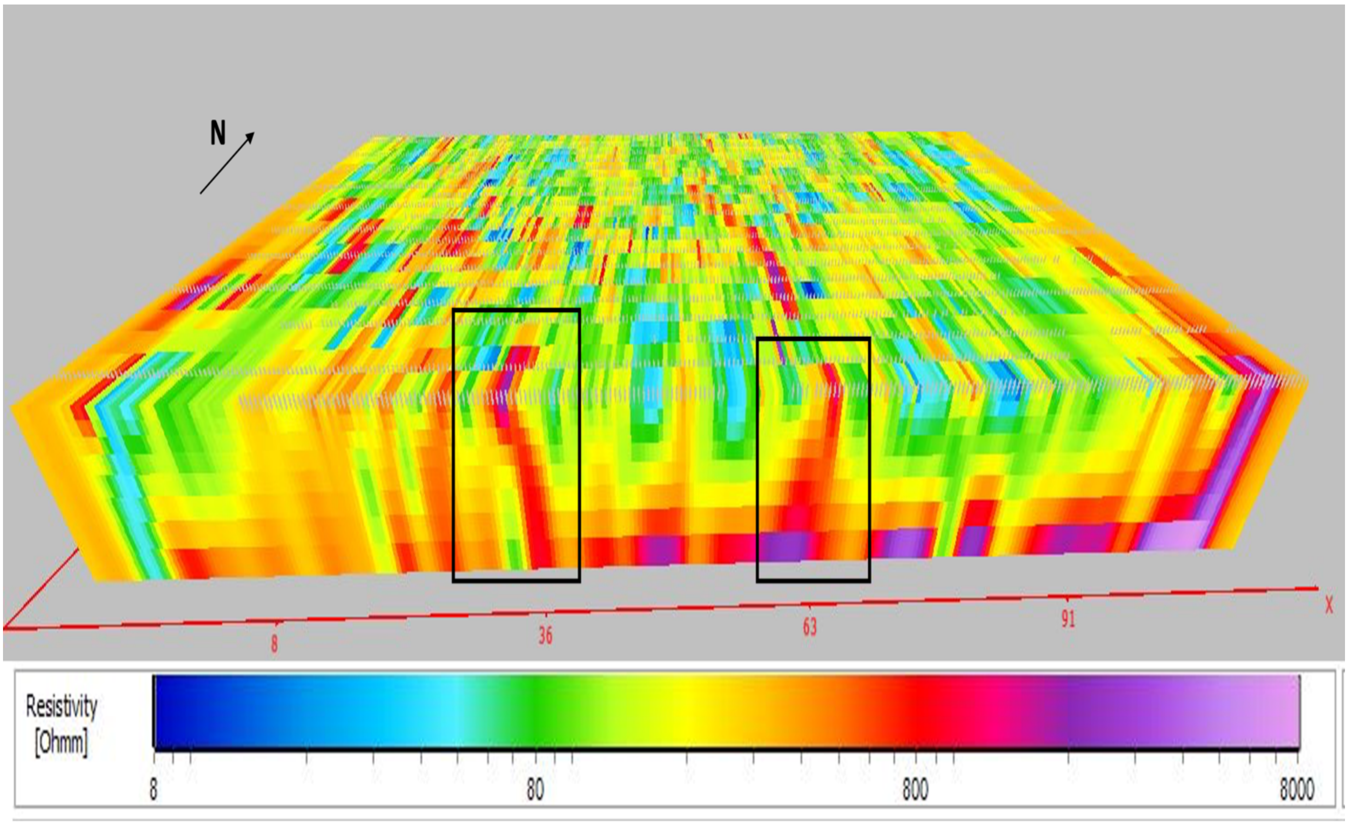

Figure 5.39: *Inversion result of dataset 5 (100m x 100m grid) illustrated with 3-D Viewer option. The black boxes are showing the presence of the ice wedge (resistive anomaly).*

5.2.2.3. Dataset 1 (50 m long OhmMapper Profile)

Figure 5.40, present the data measured along the 50 m profile in Adventdalen. Some noisy data points are manually removed before the inversion process while using Res2DInv software. The investigation depth is recorded as 9.56 m and the RMS value is 32% after 10 iterations (figure 5.41). Some outliers are also automatically removed to improve the resolution of the inversion result (figure 5.42). So, in figure 5.43, RMS value is decreased up to 12% after 10 iterations. The depth of active layer was measured manually along the profile, every 2 meters in July 2019 using a metallic rod. The average measure depth that is 59 cm (figure 5.44).

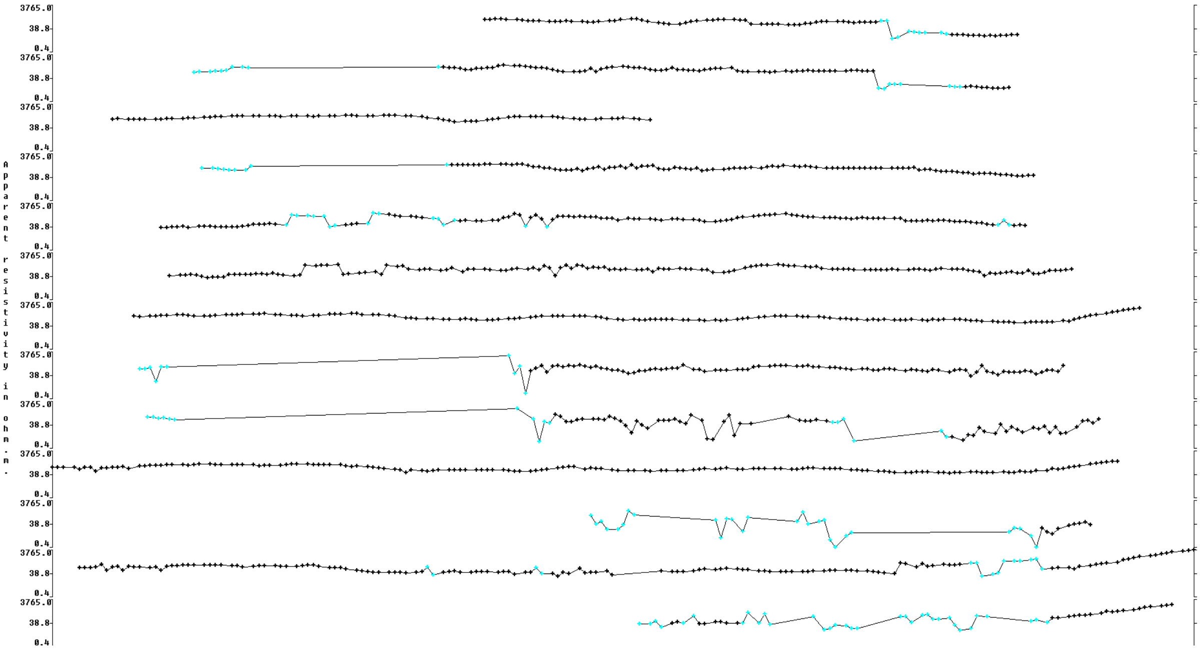

Figure 5.40: *Layout of data points for dataset 1. On right side (along Y-axis), apparent resistivity is written and on left side (on Y-axis), electrode spacing and dipole length is written.*

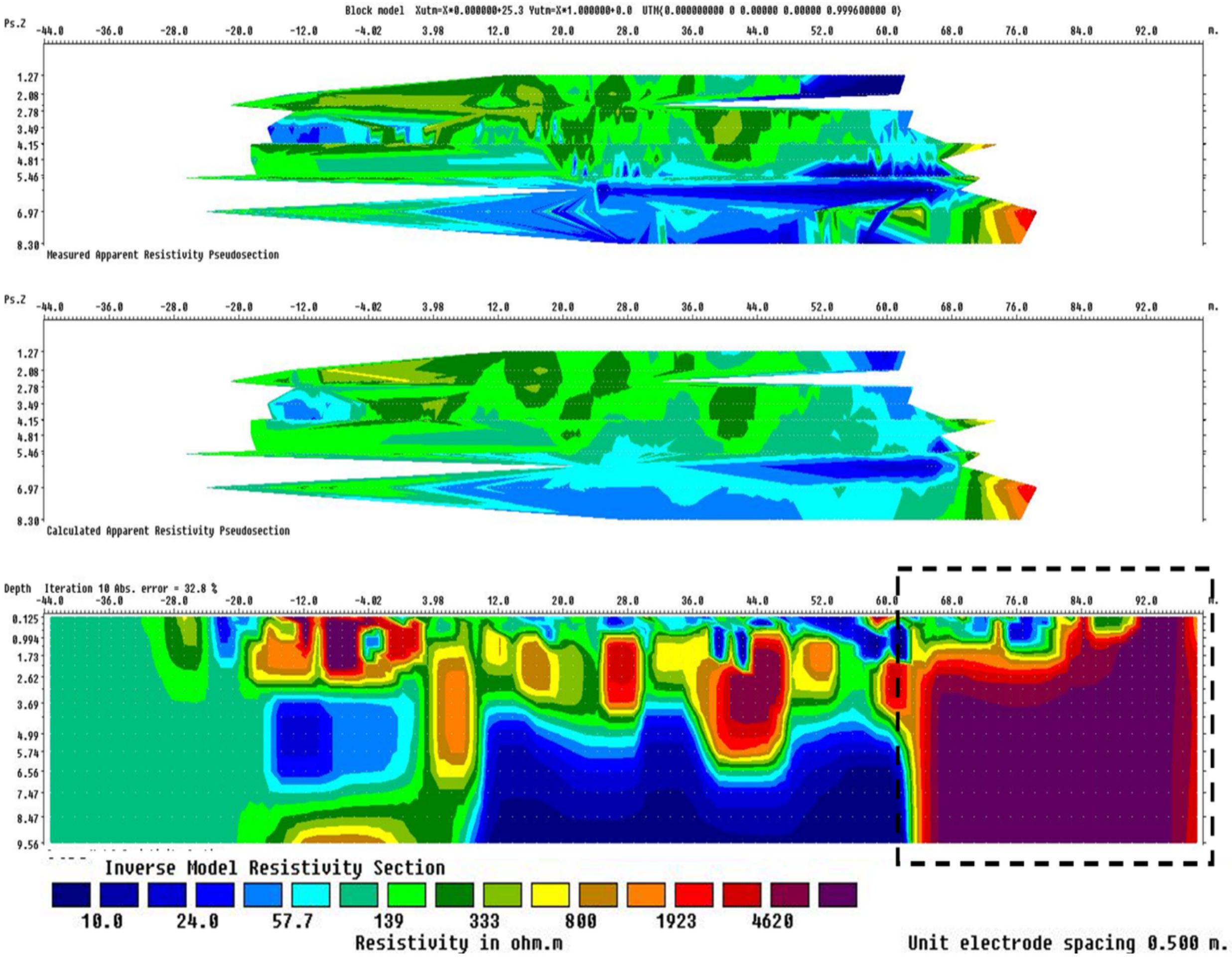

Figure 5.41: *Inversion result of dataset 1 after manual removal of bad points. The investigation depth is 9.56. m. Range of resisitivity is between 1 to 6000 Ωm. Black box represents resistive part as the streamer was not completely spread due to the river.*

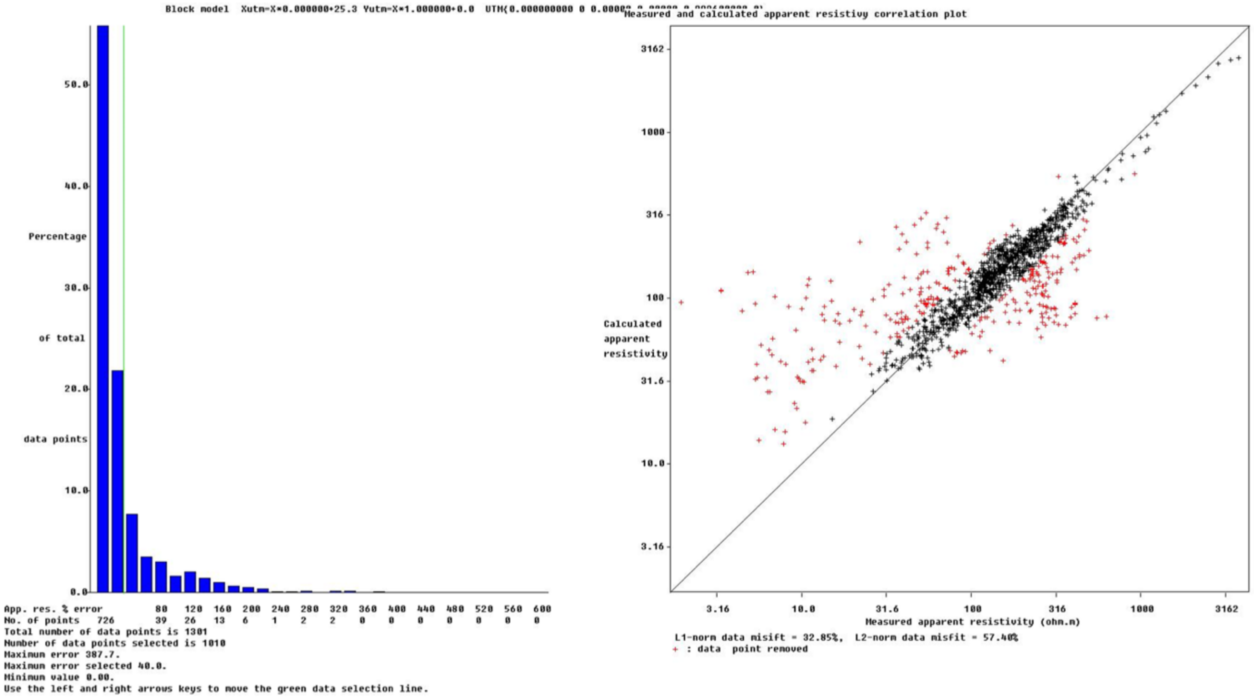

```
App. res. % error           80   120  160  200  240  280  320  360  400  440  480  520  560  600
No. of points   726         39   26   13   6    1    2    2    0    0    0    0    0    0    0
Total number of data points is 1301
Number of data points selected is 1010
Maximum error 387.7.
Maximum error selected 40.0.
Minimum value 0.00.
Use the left and right arrows keys to move the green data selection line.
```

Figure 5.42: *Automatic removal of outliers. Percentage of total number of data points (on left side) and (on right side) scatter plot between resistivity values (calculated vs measured).*

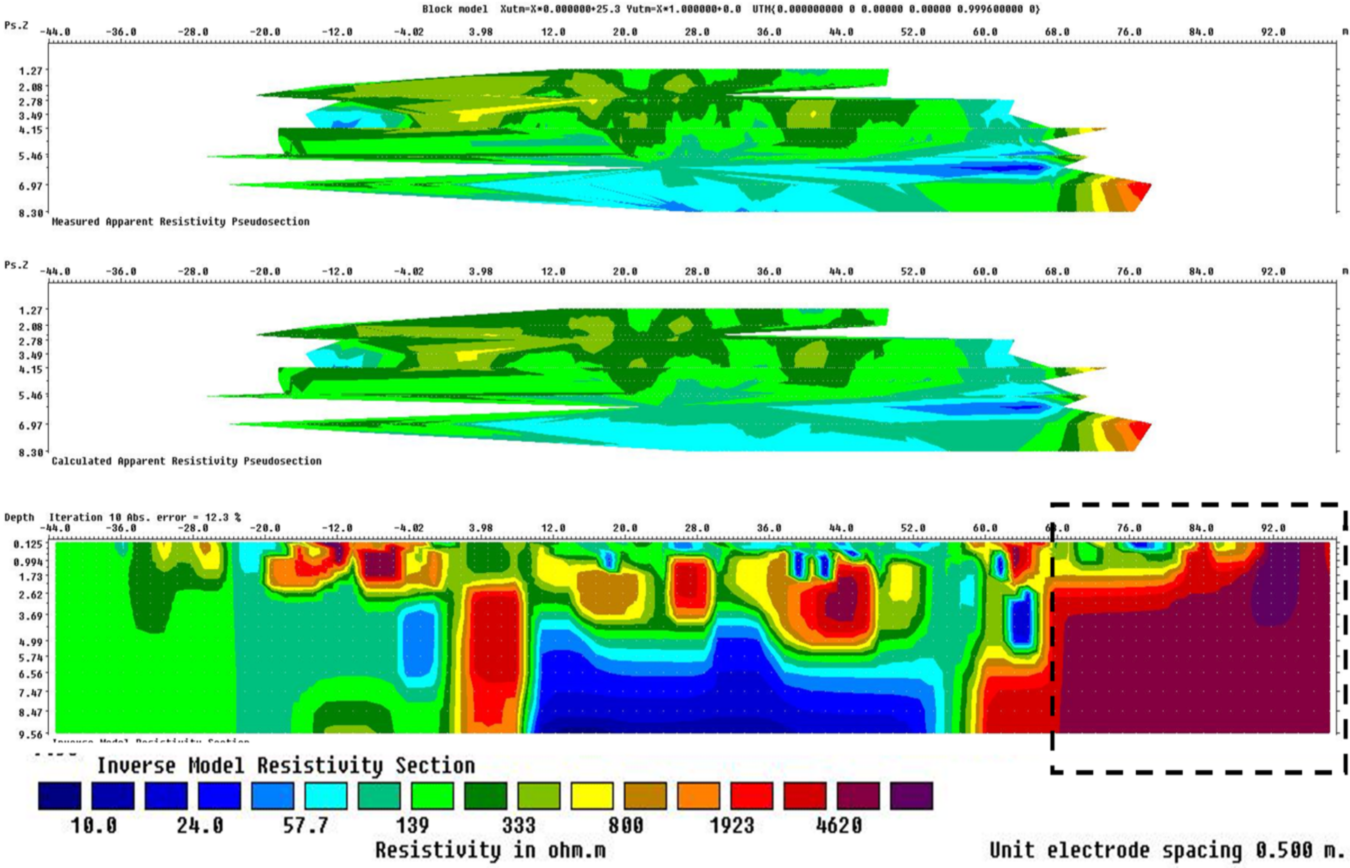

Figure 5.43: *Inversion result of dataset 1 automatic removal of outliers. The investigation depth is 9.56 m. Range of resisitivity is between 1 to 6000 Ωm. Black box is representing resistive part as the streamer was not completely spread due to the river.*

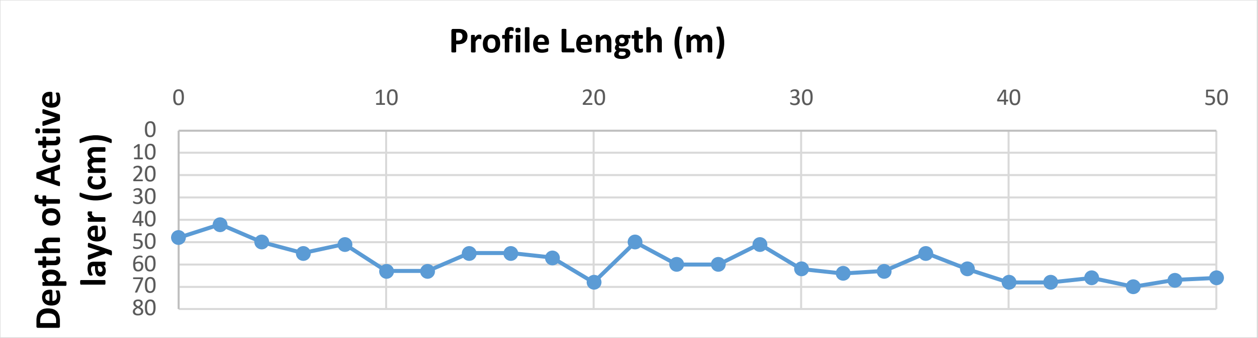

Figure 5.44: *Depth of active layer (in cm) is measured manually in July 2019 along the 50 m profile line in Adventdalen site. Average depth of active layer is 59 cm.*

5.2.2.4. Referenced Terrameter profile (16 m long)

The resistivity structure of the Adventdalen site had been monitored by (Oswald, 2009) using a Terrameter device in 2008. Figure 5.45, shows the inversion results obtained with DC2DINVRES software at the same position as our dataset 1. The Terrameter profile was only 16 m long and the depth of investigation is therefore lower than for dataset 1. The direction of their profile is from the river towards the road (NE to SW). We selected the inverted profile of month of July. The resistivities in upper soil in both profiles (i.e., A-2008-07-01 and A-2008-07-22) are ≤ 150 Ωm**.** The lower resistive part on right side of the both profiles might be an artifact due to inversion process (figure 5.45). The resistive top layer is active layer and the deep resistive part is frozen.

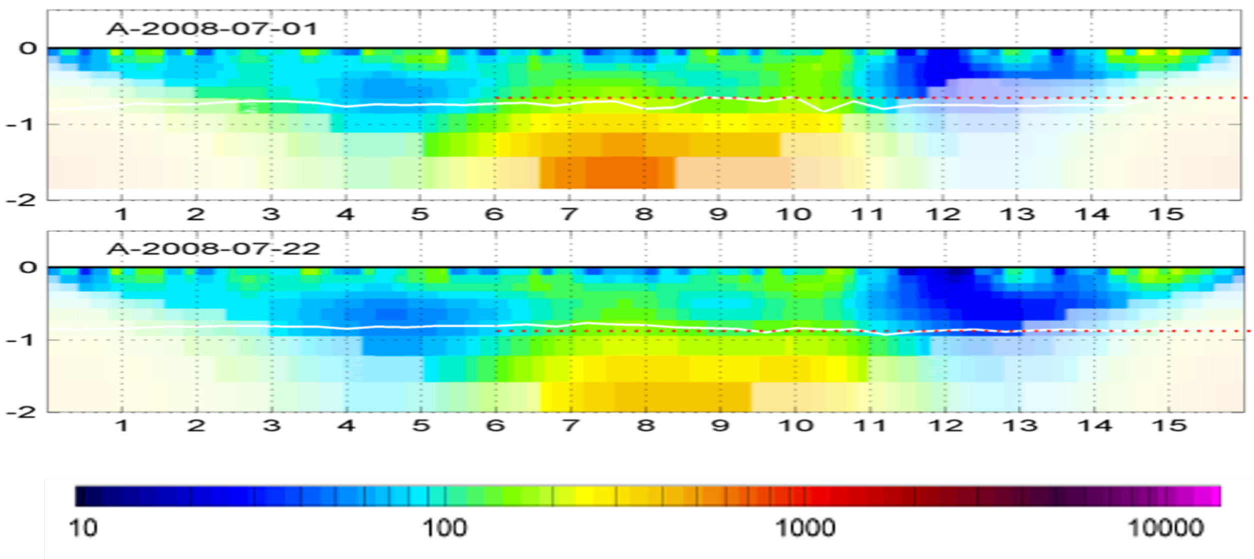

Figure 5.45: *Subsurface resistivity model of Adventdalen site for the month of July, 2008. Range of resistivity is displayed on color scale from 10 Ωm to 10 kΩm. Depth of active layer is done by manually and displayed as white line. Results are from (Oswald, 2009).*

5.2.3. Topography of the ice wedges in Adventdalen

The DEM (Digital Elevation Model) of Adventdalen site can be investigated with ArcMap software. The classification of pixels shows the shading effect of the topography. It can be seen that the ice wedges generates a trough in the topography (figure 5.46).

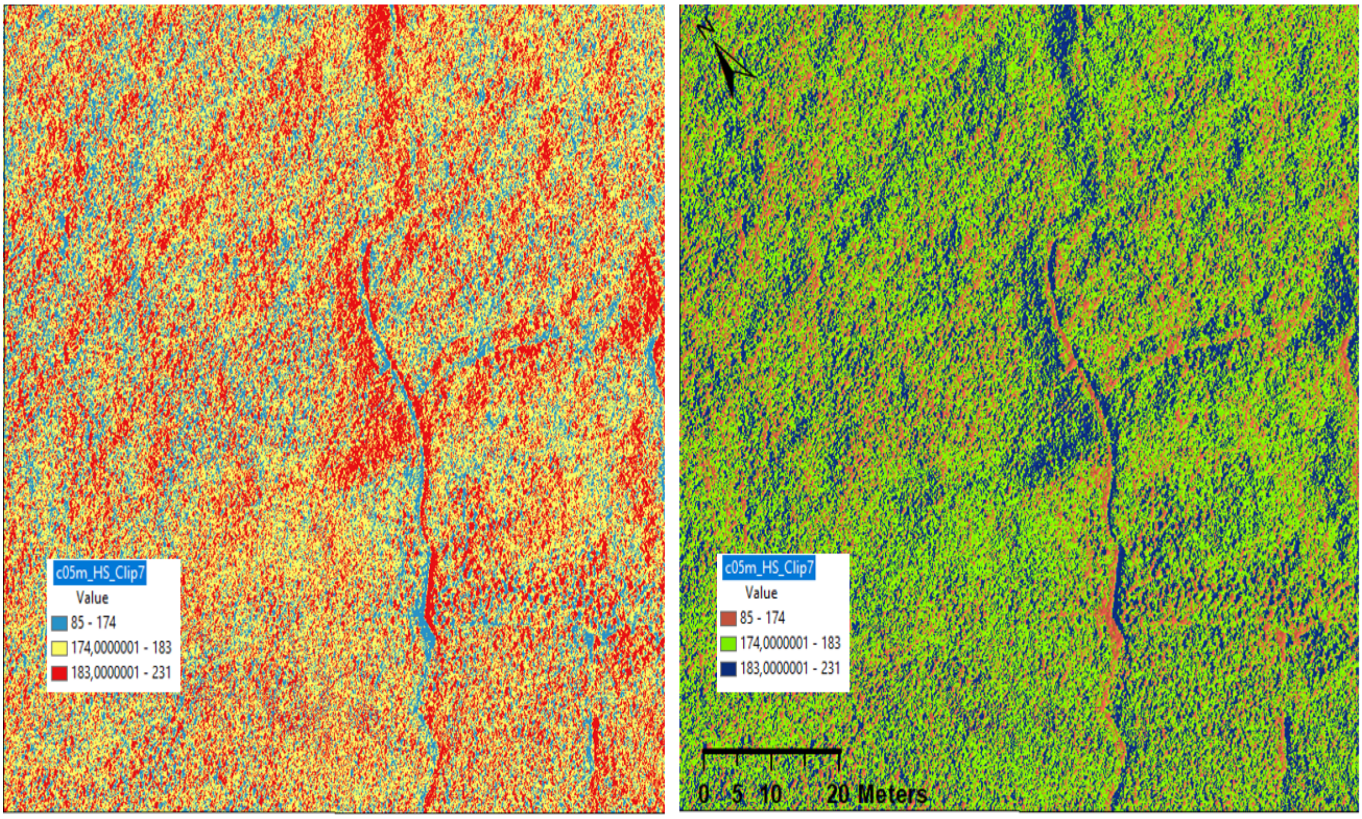

Figure 5.46: *DEM of Adventdalen site, classified with different values of pixels represents the shading effect on topography. On left figure (blue color in legend bar) and on right figure (red color in legend bar) are the smallest values of pixels. The geometry of the shades show that it is trough.*

6. Discussion

6.1. Performance of resistivity surveys in arctic environment

6.1.1. Terrameter and CCR profiles of UNIS East site

The resistivity models acquired by the two methods are quite similar but the Terrameter one is smoother and easier to interpret geologically.

The penetration depth along the CCR profile obtained by merging our three datasets (Dataset 1, dataset 4 and dataset 5) collected in July 2019 and inverted with Res2DInv software is 8.20

m (figure 5.19). The thickness of the conductive layer along the resistivity section varies between 0 to 2.7 m while the manual measurements of the thawed layer have an average of 35 cm (figure 5.20). During Summer season in September 2017, a Terrameter survey was conducting by NGI and NGTS. The penetration depth was much greater than for the CCR survey. The depth of active layer was measured manually and the average depth was recorded as 79 cm (figure 5.22). It is greater than 35 cm recorded in July 2019 during OhmMapper survey (figure 5.19). The two surveys illustrate that the depth of active layer varies in summer and in winter due to freeze and the thaw processes.

6.1.2. Terrameter and CCR profiles of Adventdalen site

Adventdalen is a flat area and no topographic corrections are applied during the processing. The UNISCALM site is optimal for using a CCR streamer as the vegetation is relatively sparse, the ground is flat and the field is far away from residential area.

At this site, we acquired 2 different types of OhmMapper surveys: a "map survey mode or 3-D survey" and a "simple survey or 2-D survey". Two map surveys were performed to acquire two different 3-D grids in two perpendicular directions. The investigation depth for the 3-D surveys are 2.94 and 2.40 m. The investigation depth of the 2-D profile is 9.56 m. The raw data of 3-D grids are less noisy and the inverted models have less RMS errors.

The inspection of the two 3-D grids show that the direction of the acquisition is important for detecting linear features in the geology.

Figure 5.35, elaborates the 3-D resistivity model of UNISCALM site. Transparency effect is used to interpret the features of the resistivity model. Resistive anomaly is not elaborated on the 3-D resistivity model as the movement of streamer was parallel to the direction of anomaly. The resistive anomaly (in black boxes) can easily be seen in 3-D grid (figure 5.39). The direction of survey was not parallel to the direction of anomaly. This resistive anomaly corresponds to ice wedge. Resistivity range for conductive layer is from 8 to 100 Ωm and for ice wedge is 1 kΩm for shallow 3-D grid (figure 5.39).

In the CCR model along 50 m long profile (figure 6.1), the conductive layer (resistivity range < 150 Ωm) corresponds to the active layer of permafrost. The thickness varies from 0 to 1.7 m while measuring manually the average of 59 cm is seen (figure 5.44). The depth of investigation for 50 m CCR profile up to 9.56 meters (figure 6.1).

In the Terrameter model (figure 5.45), the conductive layer near the surface also corresponds to the active layer of permafrost. The range of conductivity in active layer is up to 100 Ωm. The frozen part of the profile starts at 1 m depth and the resistivity is around 0.5 Ωm. The depth of investigation for 16 m ERT profile is up to 2 meters, which is much lower than for our CCR profile.

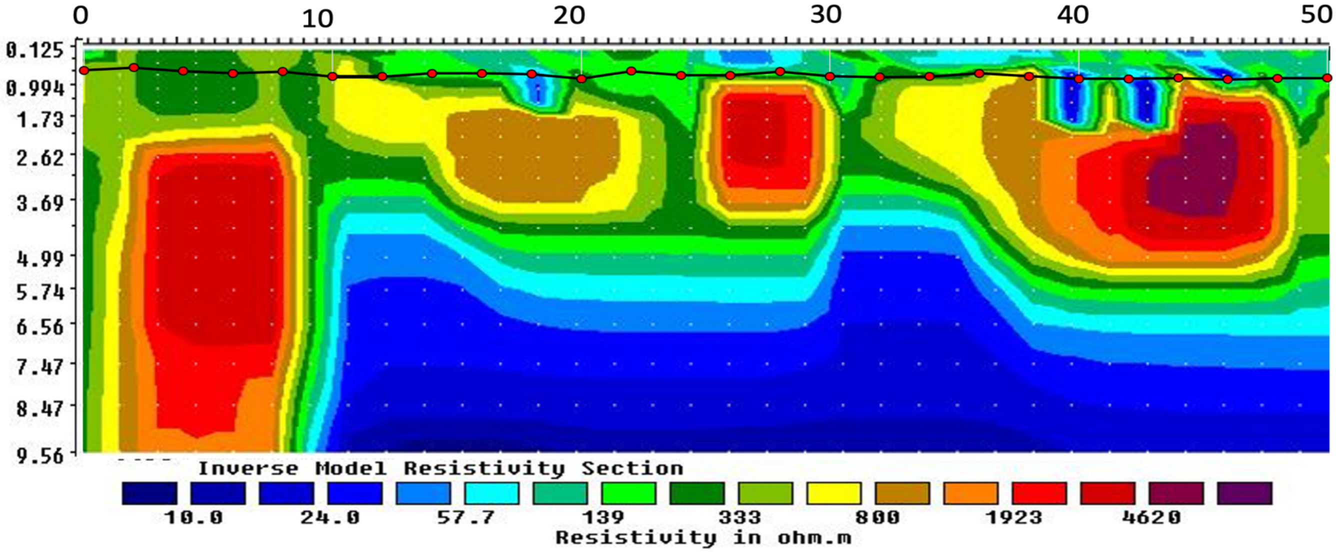

Figure 6.1: *OhmMapper 50 m long vertical profile with measurement of active layer in red dots. The measurement of active layer was done manually.*

6.2. Perspective about the climate change monitoring

It has been observed that the trend of active layer thickness in UNISCALM grid is increasing in last 10 years from 2000 to 2010 (figure 6.2). The active layer thickened from 74 cm to 110 cm between 2000 and 2010 (Christiansen et al. 2010). In summer of 2019, the thaw depth of UNISCALM grid was measured manually by UNIS research center and the range of thaw depth was between 48 to 76 cm (figure 6.3). Because of its geometrical scale, the UNISCALM grid does not detect any anomaly related to the ice wedges (Christiansen, 2005) that are observed on the DEM (figure 5.37) and on our 3D resistivity grids (figure 5.39).

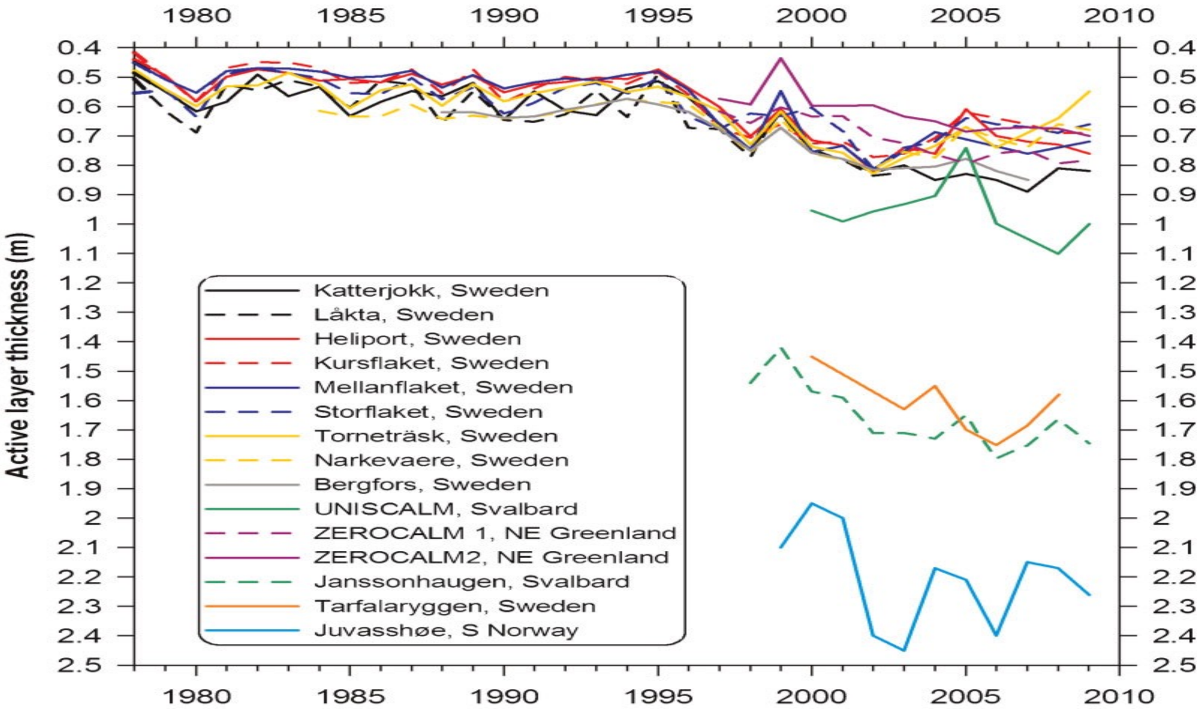

Figure 6.2: *Thickness of active layer measured at different active sites of in Nordic region. The Adventdalen UNISCALM grid is shown green (Christiansen et al. 2010).*

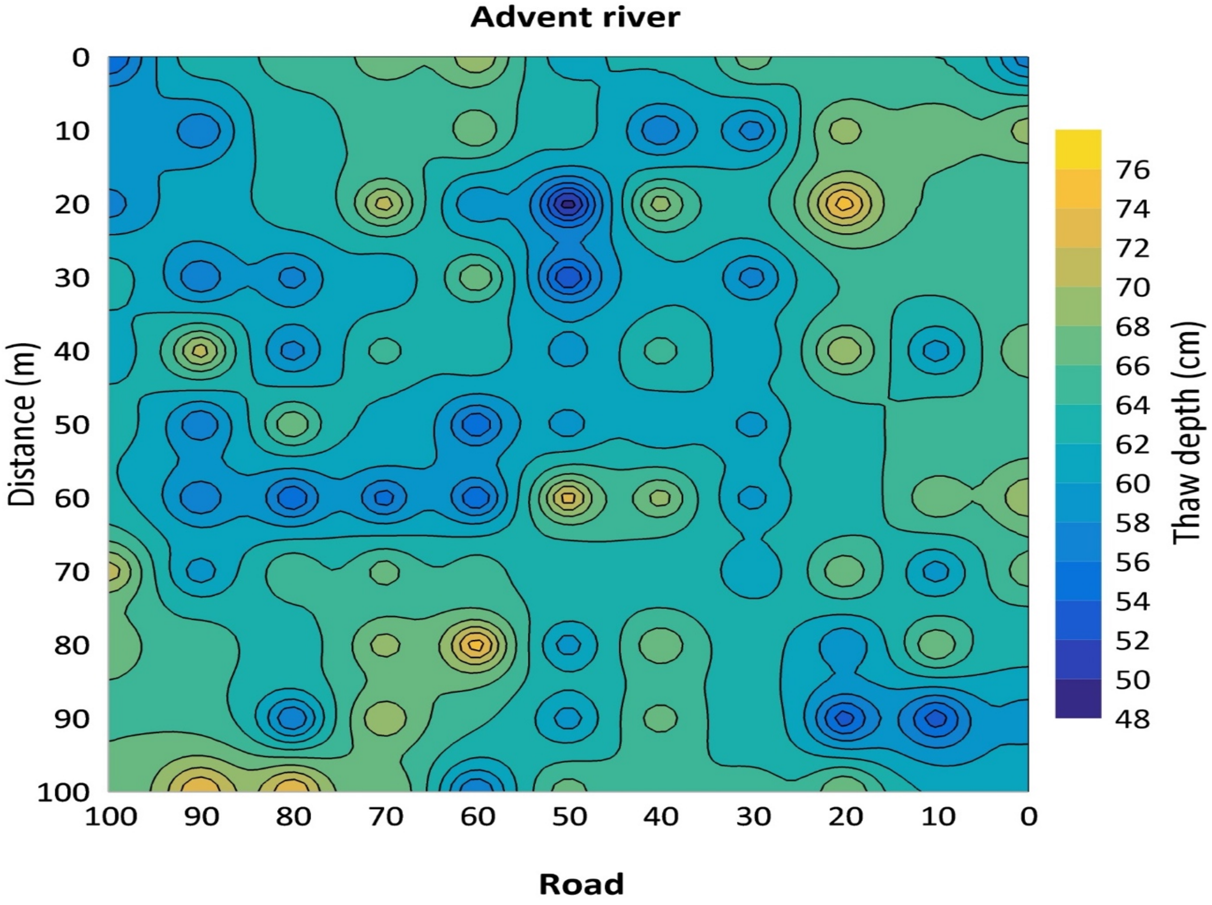

Figure 6.3: *Thaw depth of UNISCALM grid, Adventdalen site measured on June, 2019 by UNIS research center.*

6.3. Comparison between Terrameter and CCR techniques

Electrode-based ERT can be superior over CCR technique in terms of depth of investigation. The horizontal resolution is however higher in a CCR survey than in a Terrameter survey.

The models measured by a Terrameter are overall less noisy as compared with the data obtained with OhmMapper. The model quality of Terrameter is much better, as root mean square error percentage is just 3% while for OhmMapper, it goes up to 35% which is probably caused by shifts in the streamer during successive passes (figure 5.18).

Inversion models obtained from Terrameter and OhmMapper can image the subsurface and detect the conductive layer that corresponds to the active layer of the permafrost.

7. Conclusions

It is easy to tow the streamer of CCR in UNISCALM site as the condition of ground is flat with scattered vegetation and the site is relatively far away from the city noise. CCR method is useful surveying method which also used to map the thickness of active layer. This method is relatively easy to use as it can be used to acquire 2-D and 3-D resistivity profiles of the site. This method can also avoid the challenge due to electrical coupling between the electrodes and the ground in cold and resistive environments. CCR method has an advantage due to its non-invasive and non-destructive nature, compared to conventional ERT method that uses metallic electrodes to drive mechanical probing into the ground.

The horizontal resolution is higher in CCR survey due to the higher density of measurement points that makes resistivity model more difficult to interpret as compared with the resistivity model obtained from conventional survey. Hence for the vertical panel acquisition, the conventional ERT method looks more effective method to map the active layer of permafrost.

In the CCR method, the operator does not need to change the spacing between dipoles during acquisition and operator can easily acquire 3-D profile by walking along parallel (survey) lines. This method is therefore potentially useful for monitoring climate changes by regularly mapping changes in the active layer in a reference area.

8. References

Åkerman, H. J. (1992). "Hydrographic characteristics of the Strokdammane plain, west Spitsbergen, Svalbard." Geografiska Annaler: Series A, Physical Geography 74(2-3): 169-182.

Angelopoulos, M. C., et al. (2013). "The application of CCR and GPR to characterize ground ice conditions at Parsons Lake, Northwest Territories." Cold Regions Science and Technology 85: 22-33.

Arenson, L., et al. (2003). Shearing response of ice-rich rock glacier material. Eighth International Conference on Permafrost. AA Balkema, Zurich, Switzerland.

Brown, J. and V. E. Romanovsky (2008). "Report from the International Permafrost Association: State of permafrost in the first decade of the 21st century." Permafrost and Periglacial Processess. 19 (2): 255-260.

Calvert, H., et al. (2001). "Application of geophysical techniques for mapping ice-bearing sediments, Mackenzie Delta, Western Arctic, Canada. In *Conference on the Geophysical Detection of Subsurface Water on Mars* (p. 7041).

Calvert, H. T. (2002). Capacitive-coupled resistivity survey of ice-bearing sediments, Mackenzie Delta, Canada. SEG Technical Program Expanded Abstracts 2002, Society of Exploration Geophysicists**:** 696-698.

Chen, H. (2020). Capacitively-coupledresistivity methods and its application in near-surface geophysical prospecting (Doctoral dissertation).

Christensen, T. R., et al. (2004). "Thawing sub-arctic permafrost: Effects on vegetation and methane emissions." Geophysical Research Letters **31**(4).

Christiansen, H. H. (2005). "Thermal regime of ice-wedge cracking in Adventdalen, Svalbard." Permafrost and Periglacial Processes **16**(1): 87-98.

Christiansen, H. H., et al. (2010). "The thermal state of permafrost in the nordic area during the international polar year 2007–2009." Permafrost and Periglacial Processes **21**(2): 156-181.

Cohen, S. M. (2013). Geomorphological studies of a karst system in a permafrost environment at Linnédalen, western Spitsbergen (Master's thesis): 1-5.

Corner, G. D. (2006). "A transgressive-regressive model of fjord-valley fill: stratigraphy, facies and depositional controls". Society or sedimentary geology. 161-178.

Dallmann, W. K. (1999). Lithostratigraphic lexicon of Svalbard: review and recommendations for nomenclature use: Upper Palaeozoic to Quaternary bedrock, Norsk Polarinstitut.

De Pascale, G. P., et al. (2008). "Geophysical mapping of ground ice using a combination of capacitive coupled resistivity and ground-penetrating radar, Northwest Territories, Canada." Journal of Geophysical Research: Earth Surface **113**(F2).

Dionne, J.-C. (1996). "Ballantyne, CK et Harris, C.(1994). The Periglaciation of Great Britain. Cambridge University Press, x+ 330 p., 279 fig., 21 tabl., 22, 5× 28, 5 cm, cartonné. ISBN 0 521 32459 9." Géographie physique et Quaternaire **50**(2): 245-246.

Elvevold, S., Dallmann, W., & Blomeier, D. (2007). "Geology of Svalbard". Norwegian polar institute: 3-36.

Fortier, R., et al. (1994). "Effect of physical properties of frozen ground on electrical resistivity logging." Cold Regions Science and Technology **22**(4): 361-384.

Fortier, R. and C. Savard (2010). "Engineering geophysical investigation of permafrost conditions underneath airfield embankments in Northern Quebec (Canada)." Geo-2010. Confer. Proceed. Calgary: 1307-1316.

French, H. (2007). The periglacial environment. 2007, Chichester: John Wiley & Sons.

French, H. M. and O. Slaymaker (2011). Changing cold environments: a Canadian perspective, John Wiley & Sons.

French, H. M. and P. Williams (2007). The periglacial environment, Wiley Online Library.

Gilbert, G., Instanes, A., & Sinitsyn, A. (2020). "Factual Report-Permafrost Research Site." Norwegian Geotest Sites Project. 7-24.

Gilbert, G., et al. (2019). "Characterization of two sites for geotechnical testing in permafrost: Longyearbyen, Svalbard."

Gilbert, G. L. (2018). "Cryostratigraphy and sedimentology of high-Arctic fjord-valleys."

Gruber, S., et al. (2004). "Permafrost thaw and destabilization of Alpine rock walls in the hot summer of 2003." Geophysical Research Letters **31**(13).

Haeberli, W. and M. Beniston (1998). "Climate change and its impacts on glaciers and permafrost in the Alps." Ambio: 258-265.

Haeberli, W. and D. Vonder Mühll (1996). "On the characteristics and possible origins of ice in rock glacier permafrost." Zeitschrift für Geomorphologie. Supplementband(104): 43-57.

Hagen, J. O., et al. (2003). "Glaciers in Svalbard: mass balance, runoff and freshwater flux." Polar research **22**(2): 145-159.

Hagen, J. O., et al. (2003). "On the net mass balance of the glaciers and ice caps in Svalbard, Norwegian Arctic." Arctic, Antarctic, and Alpine Research **35**(2): 264-270.

Hauck, C. (2001). Geophysical methods for detecting permafrost in high mountains, (Doctoral dissertation, ETH Zurich). 91-109.

Hauck, C. (2002). "Frozen ground monitoring using DC resistivity tomography." Geophysical Research Letters **29**(21): 12-11-12-14.

Hauck, C., et al. (2004). "Geophysical surveys designed to delineate the altitudinal limit of mountain permafrost: an example from Jotunheimen, Norway." Permafrost and Periglacial Processes **15**(3): 191-205.

Hauck, C. and C. Kneisel (2006). "Application of capacitively-coupled and DC electrical resistivity imaging for mountain permafrost studies." Permafrost and Periglacial Processes **17**(2): 169-177.

Hauck, C. and C. Kneisel (2008). Applied geophysics in periglacial environments, Cambridge University Press.

Hilbich, C. (2009). Geophysical monitoring systems to assess and quantify ground ice evolution in mountain permafrost (Doctoral dissertation). 1-10.

Hilbich, C., et al. (2008). "Monitoring mountain permafrost evolution using electrical resistivity tomography: A 7-year study of seasonal, annual, and long-term variations at Schilthorn, Swiss Alps." Journal of Geophysical Research: Earth Surface 113(F1).

Hoekstra, P. (1973). Electromagnetic probing of permafrost. Proceedings of 2nd International Conference on Permafrost, Yakutsk, USSR, North American Contribution, National Academy of Science.

Humlum, O., et al. (2003). "Permafrost in Svalbard: a review of research history, climatic background and engineering challenges." Polar research 22(2): 191-215.

Ingeman-Nielsen, T. (2006). "Geophysical techniques applied to permafrost investigations in Greenland." Technical University of Denmark. 1-10.

Ingólfsson, Ó. (2011). "Fingerprints of Quaternary glaciations on Svalbard." Geological Society, London, Special Publications 354(1): 15-31.

Instanes, A. (2016). "Incorporating climate warming scenarios in coastal permafrost engineering design–Case studies from Svalbard and northwest Russia." Cold Regions Science and Technology **131**: 76-87.

Isaksen, K., et al. (2011). "Degrading mountain permafrost in southern Norway: spatial and temporal variability of mean ground temperatures, 1999–2009." Permafrost and Periglacial Processes **22**(4): 361-377.

King, M., et al. (1988). "Seismic and electrical properties of unconsolidated permafrost1." Geophysical Prospecting **36**(4): 349-364.

Kneisel, C. (2004). "New insights into mountain permafrost occurrence and characteristics in glacier forefields at high altitude through the application of 2D resistivity imaging." Permafrost and Periglacial Processes **15**(3): 221-227.

Kneisel, C. (2006). "Assessment of subsurface lithology in mountain environments using 2D resistivity imaging." Geomorphology **80**(1-2): 32-44.

Kneisel, C., et al. (2008). "Advances in geophysical methods for permafrost investigations." Permafrost and Periglacial Processes **19**(2): 157-178.

Kneisel, C., et al. (2000). "Permafrost below the timberline confirmed and characterized by geoelectrical resistivity measurements, Bever Valley, eastern Swiss Alps." Permafrost and Periglacial Processes **11**(4): 295-304.

Kneisel, C. and A. Kääb (2007). "Mountain permafrost dynamics within a recently exposed glacier forefield inferred by a combined geomorphological, geophysical and photogrammetrical approach." Earth Surface Processes and Landforms: The Journal of the British Geomorphological Research Group **32**(12): 1797-1810.

Kneisel, C., et al. (2007). "Hazard assessment of potential periglacial debris flows based on GIS-based spatial modelling and geophysical field surveys: a case study in the Swiss Alps." Permafrost and Periglacial Processes **18**(3): 259-268.

Kååb, A., Chiarle, M., Raup, B., & Schneider, C. (2007). Climate change impacts on mountain glaciers and permafrost. *Global and Planetary Change*, *56*(1-2), vii-ix.

Mangerud, J. and J. I. Svendsen (1992). "The last interglacial-glacial period on Spitsbergen, Svalbard." Quaternary Science Reviews **11**(6): 633-664.

Marescot, L., et al. (2003). "Assessing reliability of 2D resistivity imaging in mountain permafrost studies using the depth of investigation index method." Near Surface Geophysics **1**(2): 57-67.

Matsuoka, N. (1993). Critical polygon size for ice-wedge formation in Svalbard and Antarctica. Proceedings of the 6th International Conference on Permafrost, 1993, South China University of Technology Press.

Matsuoka, N., et al. (2018). "Ice-wedge polygon dynamics in Svalbard: Lessons from a decade of automated multi-sensor monitoring." Permafrost and Periglacial Processes **29**(3): 210-227.

Maurer, H. and C. Hauck (2007). "Geophysical imaging of alpine rock glaciers." Journal of Glaciology **53**(180): 110-120.

Mühll, D. V., et al. (2001). "New geophysical methods of investigating the nature and distribution of mountain permafrost with special reference to radiometry techniques." Permafrost and Periglacial Processes **12**(1): 27-38.

Murton, J. (2007). Ice wedges and ice wedge casts. W: SA Elias (red.), Encyclopedia of Quaternary Sciences, Elsevier.

Murton, J. (2013). "PERMAFROST AND PERIGLACIAL FEATURES| Ice Wedges and Ice-Wedge Casts.": 436-451.

Oswald, A. (2009). Monitoring active layer development and freeze-back using DC resistivity tomography: two field examples from Svalbard, Graz.

Reusch, H. (1901). "Nogle bidrag til forstaaelsen af, hvorledes Norges dale og fjelde er blevne til."

Romanovsky, V. E., et al. (2010). "Thermal state of permafrost in Russia." Permafrost and Periglacial Processes **21**(2): 136-155.

Romanovsky, V. E., et al. (2010). "Permafrost thermal state in the polar Northern Hemisphere during the international polar year 2007–2009: a synthesis." Permafrost and Periglacial Processes **21**(2): 106-116.

Scott, W., et al. (1990). "Geophysics in the study of permafrost." Geotechnical and environmental geophysics **1**: 355-384.

Shroder, J. F. (2013). "Treatise on geomorphology." Glacial and periglacial geomorphology **8**: 193-195.

Sørbel, L. and J. Tolgensbakk (2002). "Ice-wedge polygons and solifluction in the Adventdalen area, Spitsbergen, Svalbard." Norsk Geografisk Tidsskrift-Norwegian Journal of Geography **56**(2): 62-66.

Sørbel, L., et al. (2001). "Geomorphological and Quaternary geological map of Svalbard, 1/100.000." Geological map of Svalvard and Geomorphological and Quaternary geological map of Svalbard: 4-55.

Steel, R. J. and D. Worsley (1984). Svalbard's post-Caledonian strata—an atlas of sedimentational patterns and palaeogeographic evolution. Petroleum geology of the North European margin, Springer**:** 109-135.

Timofeev, V., et al. (1994). A new ground resistivity method for engineering and environmental geophysics. 7th EEGS Symposium on the Application of Geophysics to Engineering and Environmental Problems, European Association of Geoscientists & Engineers.

Vonder Mühll, D., et al. (2002). "Mapping of mountain permafrost using geophysical methods." Progress in Physical Geography **26**(4): 643-660.

Walker, J. P. and P. R. Houser (2002). "Evaluation of the OhmMapper instrument for soil moisture measurement." Soil Science Society of America Journal **66**(3): 728-734.

Washburn, A. L. (1980). Geocryology: a survey of periglacial processes and environments, Wiley.

Worsley, D. (1986). The geological history of Svalbard: evolution of an Arctic archipelago, Den norske stats oljeselskap as.

Worsley, D. (2008). "The post-Caledonian development of Svalbard and the western Barents Sea." Polar research **27**(3): 298-317.

Yoshikawa, K., et al. (2006). "Comparison of geophysical investigations for detection of massive ground ice (pingo ice)." Journal of Geophysical Research: Planets **111**(E6).

You, Y., et al. (2013). "Application of electrical resistivity tomography in investigating depth of permafrost base and permafrost structure in Tibetan Plateau." Cold Regions Science and Technology **87**: 19-26.